Swansea University
Prifysgol Abertawe

Bioinformatics investigation of the amyloid precursor protein and its interactions with presenilin-1 and acetylcholinesterase in early onset familial Alzheimer's disease

Joic Benjamin Majo Jacinto

Submitted September 2024

Swansea University

Submitted to Swansea University in fulfilment of the requirements for the Degree of MSc by Research

Abstract / Summary

Since the discovery of the amyloid precursor protein (APP) over 30 years ago, scientists have investigated its involvement in Alzheimer's disease (AD). They have also found specific cases where mutations in this gene led to the early onset familial form of AD (EOFAD). However, little attention has been paid to the structural mechanisms by which these EOFAD mutations trigger AD pathogenesis, probably due to the relatively small percentage of AD patients (<1%) that carry these missense mutations. By using bioinformatics tools (i.e. STRING, Reactome, UCSF Chimera, AlphaFold2, AlphaFold Server) and databases (i.e. ClinVar, UniProt, PDB), APP and the pathological consequences of EOFAD mutations were studied comprehensively. By exploring the network of proteins that APP physically or functionally interacts with, key interactors were identified. Presenilin-1 (PSEN1) is one of them. PSEN1 is part of the γ-secretase complex, involved in the amyloidogenic processing of APP, leading to the formation of Aβ peptides. Another interactor is the enzyme acetylcholinesterase (ACHE). Their interaction is less known, but they have been found to co-localise in neurons. ACHE is responsible for the hydrolysis and recycling of the neurotransmitter acetylcholine. Investigating the APP-PSEN1 and APP-ACHE complexes at the molecular level provides opportunities for identification of key binding amino acids – valuable information for understanding pathological mechanisms and discovering novel drug targets. In the context of EOFAD, some of these APP mutations might be closely involved with such amino acids or might influence important structural regions involved in their protein-protein interface. These findings highlight the importance of further investigating the structural intricacies of APP and its interactions, offering new avenues for understanding EOFAD pathogenesis and identifying potential therapeutic targets that could benefit both rare and common forms of AD.

Declarations

This work has not previously been accepted in substance for any degree and is not being concurrently submitted in candidature for any degree.

Signed..... [redacted] .....

Date.....29/09/2024.....

This thesis is the result of my own investigations, except where otherwise stated. Other sources are acknowledged by footnotes giving explicit references. A bibliography is appended.

Signed..... [redacted] .....

Date.....29/09/2024.....

I hereby give my consent for my work, if relevant and accepted, to be available for photocopying and for inter-library loans **after expiry of a bar on access approved by the University.**

Signed..... [redacted] .....

Date.....29/09/2024.....

The University's ethical procedures have been followed and, where appropriate, that ethical approval has been granted.

Signed..... [redacted] .....

Date.....29/09/2024.....

Table of Contents

Table of Figures

Table of Tables

Abbreviations

AChE	Acetylcholinesterase
AChEI	Acetylcholinesterase inhibitor
AD	Alzheimer's disease
ADAM10	Disintegrin and metalloproteinase domain-containing protein 10 / alpha-secretase
AI	Artificial intelligence
AICD	APP intracellular domain
APOE	Apolipoprotein E
APP	Amyloid precursor protein

Aβ	Amyloid beta
BACE1	Beta-secretase 1
BChE	Butylrylcholinesterase
C83	83-amino-acid C-terminal fragment
C99	99-amino-acid C-terminal fragment
CAA	Cerebral amyloid angiopathy
CHAT	Choline acetyltransferase
CHRNA7	Neuronal acetylcholine receptor subunit alpha-7
CMS	Congenital myasthenic syndromes
CNS	Central nervous system
COLQ	Acetylcholinesterase collagenic tail peptide
CSF	Cerebrospinal fluid
CuBD	Copper binding domain
DNA	Deoxyribonucleic acid
EOAD	Early onset Alzheimer's disease
EOFAD	Early onset familial Alzheimer's disease
GFLD	Growth factor-like domain
HB	Hydrogen bond
IDR	Intrinsic disordered region
ipTM	Interface predicted template modelling
JMR	Juxtamembrane region
KPI	Kunitz protease inhibitor
lDDT	Local distance difference test
LOAD	Late onset Alzheimer's disease
LTP	Long term potentiation
MCI	Mild cognitive impairment
MRI	Magnetic resonance imaging
NFT	Neurfibrillaty tangle
NMDA	N-methyl-D-aspartate
PDB	Protein data bank
PET	Position emission tomography
pLDDT	Per-residue local distance difference test
PPIs	Protein-protein interactions
PSEN1	Presinilin-1
PSEN2	Presinilin-2
pTM	Predicted template modelling
RMSD	Root mean square deviation
RNA	Ribonucleic acid
SDM	Structural distance measure
TBM	Template-based modelling
TMD	Transmembrane domain
UK	United Kingdom
US	United States
WT	Wild type

Acknowledgements

Firstly, I would like to thank Dr Jonathan Mullins for supporting me on this journey. Not only was he always happy to discuss any ideas or developments about the thesis, but his advice and kind words during stressful moments really lifted me up and motivated me to continue pursuing my goals.

Thank you Dr Karl Austin-Muttitt for always being happy to help and have a conversation, you are a wonderful person and scientist.

Thank you Dr Aled Lloyd, every day I saw you at the office, your passion and hard work deeply inspired me.

Thank you, my dear family, for always supporting me and caring for me.

Last but not least, thank you Mari, for your love, patience and for every morning that you woke up early to do breakfast after a long night writing this thesis. I adore you mi media naranja.

1 Introduction to Alzheimer's disease and amyloid precursor protein

1.1 Neurodegenerative conditions and their impact

The field of neurodegenerative diseases is vast and complex. Neurodegenerative diseases do not currently have a cure, their incidence and prevalence increase with age, and they represent an emerging threat to good-quality living (Duggan et al., 2020). These diseases are characterised by the progressive loss of neuronal cells, caused by different disorders of the nervous system. They can adversely affect basic abilities such as speech, movement, and balance, as well as advanced abilities such as organ function and cognition (Lamptey et al., 2022). Ultimately, these diseases impact the way people interact with their world and those who are part of it.

Among the diverse types of neurodegenerative diseases, there is a prominent type that affects the highest number of people around the globe and that has been thoroughly investigated over the last decades – this refers to Alzheimer's disease (AD)(Lamptey et al., 2022). Around 900,000 people suffer with AD in the United Kingdom (UK), and this figure is predicted to increase to 1.6 million by 2040 (Alzheimer's Society, 2023). This uprising trend is not exclusive of the UK, but it is one that applies globally (World Health Organization, 2021).

1.2 Alzheimer's disease and dementia

AD was first described in 1906 by a German physician named Alois Alzheimer’s (Neundörfer, 2003). Alzheimer studied the case of a cognitively impaired 50-year-old woman who died 5 years later due to “a peculiar severe disease process of the cerebral cortex” (Ramirez-Bermudez, 2012). In his histopathological examination he reported to have noted characteristic plaques and neurofibrillary tangles (Neundörfer, 2003). These pathological features became the defining characteristics of AD. Extracellular plaques on brains with AD are composed of a peptide named amyloid-beta (Aβ), which derives from a larger protein called amyloid precursor protein (APP) (Glenner & Wong, 1984; Coronel et al., 2018). Neurofibrillary tangles are intracellular accumulations of a protein named tau (Wood et al., 1986; Kosik et al., 1986). Tau is a stabilizing component of microtubules in healthy neurons, contributing to the integrity and smooth transport of metabolites and molecules inside neurons (Kosik et al., 1986). When hyperphosphorylation of tau occurs, these proteins aggregate together and form the characteristic toxic tangles commonly seen in AD, as well as in other tau-centred pathologies termed tauopathies (Ehrenberg et al., 2017; Crary et al., 2014). Furthermore, other pathological dysregulations and abnormalities in neuronal cell functioning exist and actively add complexity to the pathogenesis and dynamics of this neurodegenerative disease (Ferrari & Sorbi, 2021). Examples of additional hallmarks of AD

include loss of cholinergic neurons, oxidative stress, metal dyshomeostasis, neuroinflammation and cell cycle disruption (Bubley et al., 2023; Misrani et al., 2021; Zhang et al., 2023). The most relevant hallmarks will be briefly explored in this chapter.

Importantly, AD is also classed as a type of dementia and it is, in fact, the most common one being present in between 60-70% of all dementia cases (World Health Organisation & Alzheimer's Disease International, 2017). Dementia is an umbrella term used to describe a group of diseases that collectively impair memory, as well as other thinking abilities, which eventually lead to the inability to conduct daily activities. Multiple dementing disorders exist other than AD, examples include frontotemporal dementia, vascular dementia, Lewy-body dementia and limbic-predominant age-related TDP-43 Encephalopathy (LATE) – mixed forms of dementia also occur frequently (Schneider, 2022). According to the World Health Organization (2021), in 2019 there were 55.2 million people with dementia around the world, with an estimated global cost of 1.3 trillion US dollars. Furthermore, “Dementia and Alzheimer’s disease” was ranked the number one leading cause of death in England and Wales in 2022 (Office for National Statistics, 2023).

All this contextual information emphasises the paramount importance of the research that aims to understand AD and to find a cure for it. Therefore, in order to combat AD more effectively and to support with the battle against neurodegenerative diseases and dementia, improvements in diagnostics, drug therapies and disease management are urgently needed.

1.3 Early onset Alzheimer’s disease and genetic susceptibilities

One way to categorise AD is to use the age of onset. Using this metric, AD can be grouped into early onset AD (EOAD) and late onset AD (LOAD). Typically, EOAD (also known as young onset AD) refers to the manifestation of AD before the age of 65; contrasting with LOAD, which occurs after the age of 65 and is sometimes referred as classical AD since it is the most frequent form of the disease (Mendez, 2019). The percentage of EOAD cases is approximately 5.5% of all AD cases (Zhu et al., 2015).

Both EOAD’s and LOAD’s share the same pathophysiological hallmarks – amyloid plaques and neurofibrillary tangles – however, EOAD has some defining characteristics worth mentioning. For instance, there is a larger percentage of nonamnestic phenotypic variants in the EOAD population compared to the LOAD population (Mendez, 2019). These phenotypic variants don’t mainly impair memory, but other cognitive abilities such as speech, visual perception and behaviour. Furthermore, EOAD patients present more aggressive pathologies and increased mortality rates compared to LOAD patients (Wattmo & Wallin, 2017; Chang et al., 2017). Additionally, EOAD has a genetic susceptibility component, which translates to around 10 % of EOAD cases having an autosomal dominant familial AD mutation in one of the following genes: APP, PSEN1 or PSEN2 (Karch & Goate, 2015; Bekris et al., 2010). These category of EOAD cases will be referred as early onset familial AD (EOFAD) from now forward.

The *APP* gene, which encodes for the APP protein, is located on chromosome 21 and it was discovered by St George-Hyslop et al. (1987) while investigating the genetic cause of familial AD and its high prevalence in people with Down's syndrome (Wisniewski et al., 1985; Lai & Williams, 1989; Nurk et al., 2022). To date (June 2024), there are 555 genetic mutations in *APP* according to the ClinVar database (Landrum et al., 2014). Out of these, around 25 mutations in *APP* have been linked to the development of AD – these also include the *APP* duplication (TCW & Goate, 2016; Qing et al., 2019). These causal mutations have been found in 10-15% of EOFAD patients (Bekris et al., 2010; Guerreiro et al., 2012; Tanzi, 2012).

The *PSEN1* gene, which codes for the presenilin-1 protein (PSEN1 or PS1), is located on chromosome 14 and plays a critical role in the pathogenesis of EOFAD (Nurk et al., 2022). Mutations in *PSEN1* are a significant cause of EOFAD, accounting for approximately 20-60% of EOFAD cases (Bird, 2008; Tanzi, 2012; Theuns et al., 2000). The ClinVar database documents 531 genetic mutations in the PSEN1 gene (Landrum et al., 2014), underscoring its genetic variability and potential impact on disease progression. *PSEN1* encodes a component of the γ-secretase complex, which is essential for the proteolytic processing of APP into amyloid-β (Aβ) peptides. Mutations in *PSEN1* often lead to altered γ-secretase activity, resulting in an increased production of the pathogenic Aβ42 isoform, which is prone to aggregation and plaque formation in the brain (Kurth et al., 2023).

The *PSEN2* gene, which codes for the presenilin-2 protein (PSEN2 or PS2), is located on chromosome 1 and it also contributes to the genetic landscape of AD, although its impact is less pronounced than PSEN1 (Nurk et al., 2022). According to the ClinVar database, there are 313 genetic mutations identified in *PSEN2* (Landrum et al., 2014). These mutations account for less than 1% of autosomal dominant EOFAD cases (Bekris et al., 2010; Tanzi, 2012). Despite the lower prevalence, *PSEN2* mutations are crucial for understanding the genetic heterogeneity and complexity of EOFAD. Like *PSEN1*, *PSEN2* encodes a component of the γ-secretase complex and influences the production of Aβ peptides. Mutations in *PSEN2* can lead to similar pathogenic outcomes, including the dysregulation of Aβ peptide generation and subsequent amyloid plaque deposition

Finally, the apolipoprotein E (*APOE*) gene, which codes for the APOE protein, is located on chromosome 19 and it is one of the most well-established genetic risk factors for AD, although more commonly linked to LOAD (Nurk et al., 2022; Verghese et al., 2011). The APOE gene has three common alleles: ε2, ε3, and ε4, with the ε4 variant being strongly associated with an increased risk of developing AD (Verghese et al., 2011). The presence of one ε4 allele increases the risk of AD by about 2-3 times, while carrying two ε4 alleles can increase the risk by up to 12 times compared to those with the most common ε3/ε3 genotype (Troutwine et al., 2022). This risk is particularly pronounced for the amnestic phenotype of AD, which is characterised by a significant impairment in memory function. The *APOE* ε4 variant is more prevalent in the LOAD population, highlighting its role in the non-familial form of the disease (Corder et al., 1993; Liu et al., 2013). The mechanism by which *APOE* ε4 influences AD susceptibility is thought to involve the promotion of amyloid-β aggregation and deposition, disruption of lipid metabolism, and enhancement of

neuroinflammatory responses, all of which contribute to the pathophysiological processes underlying AD (Liu et al., 2013).

A number of additional AD susceptibility genes exist (e.g. *CLU, CR1, MAPT, TREM2, SORL1,* etc.). Numerous genome wide association studies (GWAS) aim to define these genes, and continuous research is necessary to understand their biological function and link to AD (Bellenguez et al., 2022; Wightman et al., 2021; Lambert et al., 2023).

1.4 The amyloid hypothesis and the role of amyloid precursor protein

The characteristic plaques seen by Alzheimer over 100 years ago, and present in the brains of AD patients, had Aβ as their principal component – this was first discovered by Glenner & Wong (1984). Since then, extensive of research has been conducted to investigate the amyloid cascade hypothesis, also termed amyloid hypothesis, initially formulated by Hardy & Higgins (1992), which proposes that Aβ aggregates are able to detrimentally interact with several metabolic and signalling pathways that eventually terminates in neurodegeneration and thus AD symptoms. Aβ is a proteolytic fragment of APP of varying length, with most common form existing as a 40 amino acid fragment and longer forms having 42 or 43 amino acids – these being more prone to oligomerise (Nhan et al., 2014; Sinha et al., 1999). The modern version of the amyloid hypothesis also considers soluble Aβ oligomers and other APP-derived fragments, and not just senile insoluble plaques, to have a relevant role in neurodegeneration and cognitive decline symptoms seen in AD (Lacor et al., 2007; Shankar et al., 2008; Jin et al., 2011; Nhan et al., 2014; Hampel et al., 2021; Zhang et al., 2023). Furthermore, there is a scientific perspective that minimises the effects of the amyloid hypothesis and attributes them to stochastic environmental factors and other genetic susceptibilities which are not related to Aβ processing or synthesis (Frisoni et al., 2022; Gouilly et al., 2023; van der Kant et al., 2019). Therefore, carefully investigating the contribution of Aβ and APP on the pathophysiology of AD can bring key insights to the understanding of AD pathogenesis and in the field of drug development.

APP is a transmembrane protein known for its significant role in the pathogenesis of AD and generation of Aβ. The gene encoding APP undergoes alternative splicing, resulting in several isoforms with distinct lengths and structures. The most prevalent isoforms of APP contain 770, 751, or 695 amino acid residues. The APP751 and APP695 isoforms arise from the exclusion of exons 7 and 8 during mRNA splicing (Chen et al., 2017; Zhao et al., 2015). These isoforms exhibit different expression patterns across various tissues (Min et al., 2017). For example, APP695 is predominantly expressed in neuronal cells, making it the principal isoform in the brain, while APP770 and APP751 are more commonly found in non-neuronal cells. This differential expression pattern indicates that APP serves diverse functional roles in different cellular contexts (Coronel et al., 2018).

Structurally, APP is a type I transmembrane protein featuring a large extracellular domain, a single transmembrane region (also known as transmembrane domain), and a short

intracellular domain (Kang et al., 1987; Dyrks et al., 1988). The extracellular domain contains several functional motifs, including heparin-binding domains, a metal-binding domain, and a Kunitz protease inhibitor (KPI) domain in some isoforms (Chen et al., 2017; Byun et al., 2023). These motifs facilitate interactions with extracellular matrix components and other cell surface proteins, implicating APP in cell adhesion, migration, and signalling pathways (Pfundstein et al., 2022). Functionally, APP is involved in synaptic formation and repair, neuronal growth, neuroprotection and some evidence suggest it could also act as an antimicrobial peptide (Turner et al., 2003; Priller et al., 2006; Wang et al., 2009; Bateman et al., 2022; Soscia et al., 2010). It is also processed by secretases through two main pathways: the non-amyloidogenic pathway, where cleavage by α-secretase prevents the formation of amyloid-β (Aβ) peptides, and the amyloidogenic pathway, where sequential cleavage by β-secretase and γ-secretase generates Aβ peptides (Haass et al., 2012; Chen et al., 2017). The accumulation of Aβ peptides, particularly Aβ42, is a hallmark of AD pathology, leading to the formation of amyloid plaques (Olsson et al., 2014). More on the amyloidogenic pathway will be discussed in Chapter 4 “APP processing by gamma-secretase”.

1.5 Other relevant pathophysiological contributors of Alzheimer's disease

Tau proteins, crucial for the stabilisation of microtubules in neurons, play a pivotal role in the pathophysiology of AD. As confirmed by Wang et al. (2003), Aβ peptides can initiate the pathological cascade by activating kinases, leading to the hyperphosphorylation of tau proteins. Normally, tau proteins maintain the structural integrity and proper function of microtubules, which are essential for intracellular transport (Kosik et al., 1986). However, when tau becomes hyperphosphorylated, it detaches from the microtubules, causing these structures to destabilise and disintegrate. This disruption impairs the microtubule network, hindering the transportation of essential nutrients and organelles along the axon, ultimately compromising neuronal function (Goedert et al., 1991; Rapoport et al., 2002).

The aggregation of hyperphosphorylated tau proteins into neurofibrillary tangles (NFTs) marks a critical event in AD progression. These tangles accumulate within neurons, exacerbating the impairment of intracellular transport and promoting neuronal dysfunction and death. The formation of NFTs is closely linked to the activation of apoptosis pathways, further contributing to neuronal loss observed in AD (Mandelkow et al., 2003). Given its central role in the pathophysiology of AD, tau protein and its post-translational modifications are key targets for therapeutic intervention, with strategies aimed at preventing tau hyperphosphorylation, promoting tau clearance, or stabilizing microtubules showing potential in slowing or halting disease progression (Zhang et al., 2004; Grüninger, 2015).

The cholinergic hypothesis, formulated over four decades ago, proposes that dysfunction of cholinergic neurons in the brain significantly contributes to the cognitive decline observed in aging and AD (Bartus et al., 1982). This hypothesis emerged from various observations including decreased acetylcholine bioavailability, disruptive processing and transport, and

decreased receptor expression (Davies & Maloney, 1976; Perry et al., 1977; Whitehouse et al., 1982). It is now known that cholinergic neurons situated on the basal forebrain and the excitatory neurotransmitter acetylcholine play and important role in memory and learning (Bekdash, 2021; Hu et al., 2016).

The cholinergic system includes key enzymes such as choline acetyltransferase (CHAT) – responsible for synthesizing acetylcholine from acetate and choline – and acetylcholinesterase (AChE), which breaks down acetylcholine in the synaptic cleft – leaving its products available for reuptake (Bekdash, 2021). In mice AD models, Aβ negatively impacted special memory, reduced the activity of CHAT and acetylcholine, and increased the activity of AChE (Semwal & Garabadu, 2020). Therapeutic strategies targeting the cholinergic system, such as AChE inhibitors (AChEIs), remain a cornerstone in AD treatment aiming to enhance acetylcholine levels and mitigate cognitive symptoms by compensating for the loss of cholinergic function. Despite the complexity and evolving understanding of AD pathology, cholinergic-based treatments continue to offer valuable insights into managing and potentially altering the disease course.

Finally, the glutamate neurotoxicity hypothesis is a significant concept in understanding the pathophysiology of AD. Glutamate, the most abundant excitatory neurotransmitter in the brain, is essential for synaptic transmission, learning, and memory formation (Mayer & Westbrook, 1987). Glutaminergic transmission operates through the α-amino-3-hydroxy-5-methyl-4-isoxazolpropionic acid (AMPA) and N-methyl-D-aspartate (NMDA) receptors (Gasiorowska et al., 2021). Activation of NMDA receptors is critical for synaptic plasticity and long-term potentiation (LTP). LTP is a process that strengthens synapses based on recent patterns of activity and is crucial for memory formation (Kemp & Bashir, 1999; Bliss & Cooke, 2011). However, in the context of AD, Aβ peptides stimulate the release of presynaptic glutamate by binding to α 7 nicotinic acetylcholine receptor (α7nAChR), thus disrupting normal glutamate regulation and leading to excessive glutamate levels in the synaptic cleft (Hascup & Hascup, 2016). This overstimulation of NMDA receptors results in prolonged calcium influx into neurons, also known as glutamate neurotoxicity. While calcium signalling is vital for normal cellular processes, its dysregulation triggers a cascade of detrimental events, including the activation of enzymes that degrade cell structures, the generation of reactive oxygen species, and ultimately, neuronal cell death (Nakamura & Lipton, 2010). NMDA receptor antagonists provide therapeutic potential for targeting this dysregulated pathway, one such example commonly prescribed for AD treatment in the drug memantine.

The cascade of effects that accumulation of Aβ plaques can have in the central nervous system (CNS) is vast, from hyperphosphorylation of tau to the malfunction of cholinergic and glutaminergic neurons. These have a synergic effect on neuronal communication, both in the cholinergic and glutaminergic systems, and can be especially detrimental as they lead to impaired memory formation and synaptic plasticity, including LTP, essential for learning and memory consolidation.

1.6 Diagnosis and treatment of early onset Alzheimer's disease

In addition to the pathophysiological context, it is crucial to address the importance of diagnosis in AD, especially in EOAD. The diagnosis of AD is a comprehensive process that involves clinical evaluations, cognitive testing, neuroimaging, and biomarker assessments. Clinicians begin with detailed medical histories and cognitive assessments using standardised tests, such as the Mini-Mental State Examination (MMSE) and the Montreal Cognitive Assessment (MoCA), to evaluate cognitive functions including memory, attention, language, and problem-solving (Wang et al., 2022). Advanced diagnostic tools include neuroimaging techniques like magnetic resonance imaging (MRI) and positron emission tomography (PET) scans. MRI reveals brain atrophy patterns typical of AD, particularly in the hippocampus, while PET scans assess metabolic activity and detect amyloid plaques and tau tangles using specific tracers (Živanović et al., 2023). Cerebrospinal fluid (CSF) analysis can also measure Aβ and tau levels, correlating with AD pathology (Hameed et al., 2020). Emerging blood tests for biomarkers such as plasma Aβ and tau are under development to offer less invasive diagnostic options (Mapstone et al., 2014; Karikari et al., 2020).

Mild cognitive impairment (MCI) represents a transitional stage between normal cognitive aging and dementia, including AD. Being able to detect MCI is crucial for early clinical intervention and could increase the efficiency of pharmacological treatments against the progression to early AD (Hane et al., 2017; Sperling et al., 2011). For that reason, advances in diagnostic methods and biomarker research that focus on effective and differential early diagnosis can potentially contribute to better therapeutic responses and management of AD.

AChEIs play a crucial role in the symptomatic treatment of AD by enhancing cholinergic neurotransmission. Donepezil, Rivastigmine, and Galantamine are prominent AChEIs used in AD treatment (Cummings et al., 2014; Gasiorowska et al., 2021). Donepezil selectively inhibits AChE in the CNS, thus increasing acetylcholine levels and improving cognitive function. Rivastigmine, on the other hand, inhibits both AChE and butyrylcholinesterase (BChE), with a notable effect in the cortex and hippocampus, areas critical for memory. This dual inhibition results in a more sustained increase in acetylcholine levels. Galantamine not only inhibits AChE but also acts as a positive allosteric modulator (PAM) at nicotinic receptors, enhancing the response of these receptors to acetylcholine, which may further boost cognitive functions (Opler et al., 2013; Kume & Takada-Takatori, 2018).

Memantine, an NMDA receptor antagonist, offers a different therapeutic approach by targeting the glutamatergic system and combating glutamate neurotoxicity (Areosa et al., 2005; Howard et al., 2012). Memantine functions by blocking these receptors, thus preventing the harmful influx of calcium while allowing normal synaptic transmission. This neuroprotective mechanism is significant in managing the symptoms of AD and slowing disease progression and has been proved to be particularly effective in combination with donepezil for mild to severe AD (Howard et al., 2012).

Additionally, ongoing developments on the field of disease-modifying immunotherapies promises new insights and solutions to treat AD. These therapies aim to target and clear Aβ

plaques and tau tangles, potentially altering the disease course and providing more profound benefits than symptomatic treatments alone (Vogt et al., 2023; Shi et al., 2022). Some examples include aducanumab, donanemab, and lecanemab. These are monoclonal antibodies that target Aβ plaques and can trigger an immune reaction to clear the Aβ deposits. This pharmaco-immune mechanism has been shown to slow down the progression of AD (i.e. cognitive decline) to different degrees of success (Sims et al., 2023; Swanson et al., 2021; Sevigny et al., 2016). Furthermore, amelioration of symptoms seems to be correlated with early administration of treatment, restating emphasis on early diagnosing (Golde & Levey, 2023).

Non-pharmacological approaches are also essential in managing AD, focusing on improving quality of life and maintaining cognitive function. Cognitive therapies, including memory training and mental exercises, can help slow cognitive decline (Epperly et al., 2017; Woods et al., 2012; Cui et al., 2018). Physical activity and regular exercise have been shown to have neuroprotective effects, potentially slowing the progression of AD symptoms (Sofi et al., 2010; Laver et al., 2016; Brown et al., 2012). Social engagement and activities that stimulate the brain, such as puzzles, reading, and social interactions, are equally important (Graff et al., 2006; Epperly et al., 2017). Finally, creating a supportive environment, with routines and modifications to reduce confusion and enhance safety, is crucial for individuals with AD. Thus, multi-faceted approaches in combination with pharmacological treatments, provide a holistic management strategy for AD.

1.7 Project objectives

In this project, the main aim is to investigate the molecular mechanisms underlying AD, specifically EOFAD, by focusing on APP's molecular structure and its interactions with γ-secretase and AChE. These objectives are designed to leverage bioinformatics and computational methods to explore the following project objectives:

- Study the protein network and dynamics of APP and identifying relevant proteins of interest.
- Obtain insights about the molecular structures of three groups of variants of APP (i.e. benign, early onset familial AD and cerebral amyloid angiopathy) using molecular modelling programmes.
- Analyse the molecular contacts between the each of the APP variants and γ-secretase using molecular modelling programmes.
- Construct a protein complex with a binding phase between AChE and APP, followed by the identification of pathological enhancements in their interaction, using molecular docking approaches.

2 General methods

2.1 Overview of methodological approach

An overview of the methodological workflow followed to research and obtain the subsequent results chapters can be seen below (**Figure 2.1**).

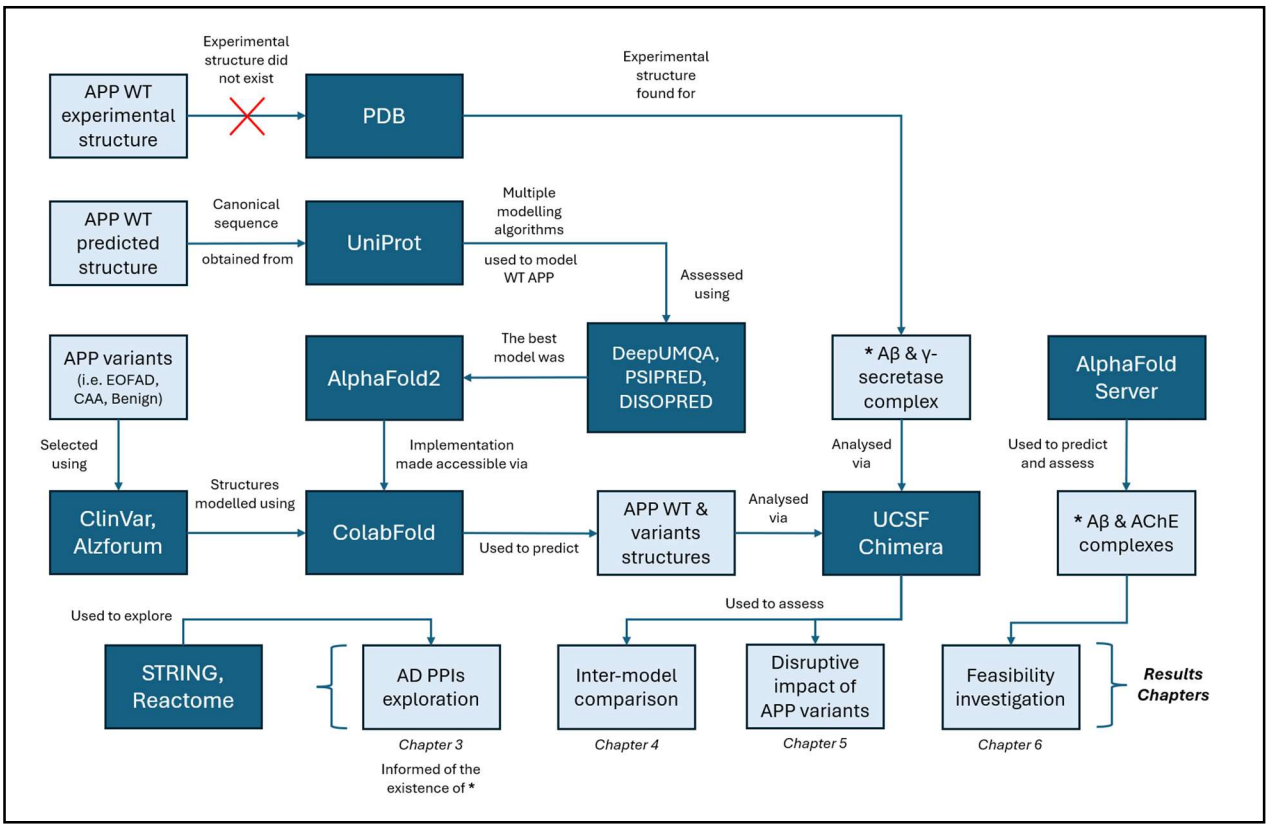

Figure 2.1 Overview of methodological workflow
Diagram displaying the methodological workflow followed during this thesis. Four results chapters were obtained by using diverse tools and pathways. Light blue boxes represent goals or actions accomplished. Dark blue boxes represent software, webtools or databases. Legend: amyloid β (Aβ), acetylcholinesterase (AChE), AD (Alzheimer's disease), amyloid precursor protein (APP), cerebral amyloid angiopathy (CAA), early onset familial Alzheimer's disease (EOFAD), protein data bank (PDB), protein-protein interactions (PPIs), wild type (WT).

2.2 Data sources

2.2.1 UniProt

The UniProt Knowledgebase (UniProtKB) was used throughout this project as the primary source for protein sequence and annotation data. UniProt is a freely accessible, comprehensive, and regularly updated repository that integrates curated (reviewed) and computationally annotated (unreviewed) protein entries (Bateman et al., 2022). It provides canonical sequences, isoforms, functional annotations, domain structures, and links to relevant literature and external resources.

For this project, UniProt (v2023_02) was employed to retrieve canonical protein sequences of APP and AChE alongside isoform information and annotated functional domains. Protein sequences were downloaded in FASTA format for subsequent structural modelling, alignment, and interaction studies. Data were accessed through the UniProt web interface (https://www.uniprot.org/). The canonical isoforms for APP and AChE were retrieved from the 'Sequence and Isoform' section (**Figure 2.2**). APP UniProt ID: P05067-1; AChE UniProt ID: P22303-1. UniProt was accessed up to August 2024.

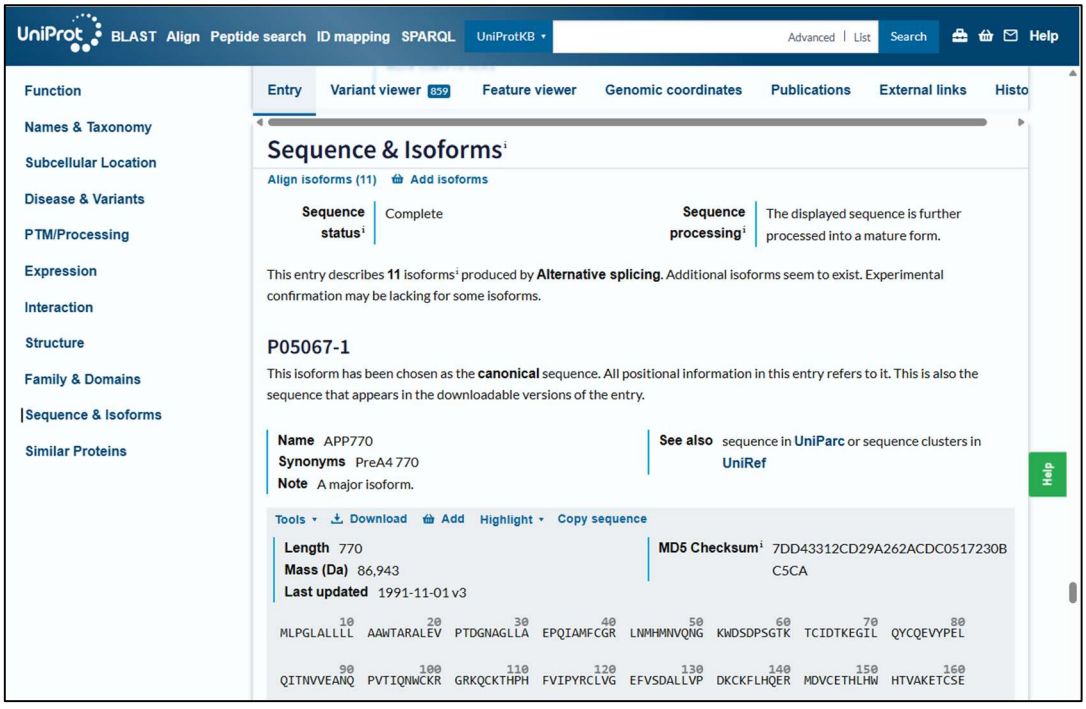

Figure 2.2 Sequence and Isoforms of human APP in UniProt.
UniProt web interface of the human APP, showing the 'Sequence & Isoforms' subsection and the UniProt ID for the canonical APP sequence chosen (P05067-1). Picture taken September 2025 (https://www.uniprot.org/uniprotkb/P05067/entry).

2.2.2 Protein Data Bank

The Protein Data Bank (PDB) was employed throughout this project as the primary repository for experimentally determined three-dimensional (3D) macromolecular structures. The PDB provides crystallographic, cryo-electron microscopy (cryo-EM), and nuclear magnetic resonance (NMR) models of proteins, nucleic acids, and complexes, offering a reliable foundation for structural bioinformatics investigations. In this research, the PDB was used to obtain reference structures of proteins of interest, including APP, PSEN1 and AChE. These experimentally validated structures provided critical benchmarks for comparison with *in silico* predicted models generated using ColabFold or AlphaFold3, and enabled the assessment of variant effects, domain orientations, and protein–protein interactions in the context of AD. Data were accessed through the PDB web interface up to June 2024 (https://www.rcsb.org/) (Berman, 2000).

2.2.3 ClinVar

ClinVar was used as a primary resource to obtain curated information on genetic variants in the *APP* gene and their clinical interpretations. This database integrates submissions from multiple expert panels, research groups, and clinical laboratories, providing a consensus classification of variants into categories such as pathogenic, likely pathogenic, benign, and variants of uncertain significance. For this project, ClinVar was consulted to identify the connections between *APP* sequence variants and AD, CAA or benign phenotypes, allowing to stratify mutations by clinical relevance and identification of mutated amino acids (**Figure 2.3**). Data were accessed through the ClinVar web interface up to November 2023 (https://www.ncbi.nlm.nih.gov/clinvar/) (Landrum et al., 2014).

2.2.4 Alzforum

Alzforum is an open-access information platform founded in 1996 with the goal of accelerating research into AD and related disorders. In addition to news and research pdates, Alzforum hosts a curated *mutations database*, which catalogues reported variants in key AD-associated genes, including APP, PSEN1, and PSEN2. Each entry links genetic variants – including clear display of the affected amino acids – with their associated clinical and neuropathological features, as well as experimental findings regarding functional effects such as altered amyloid-β (Aβ) processing.

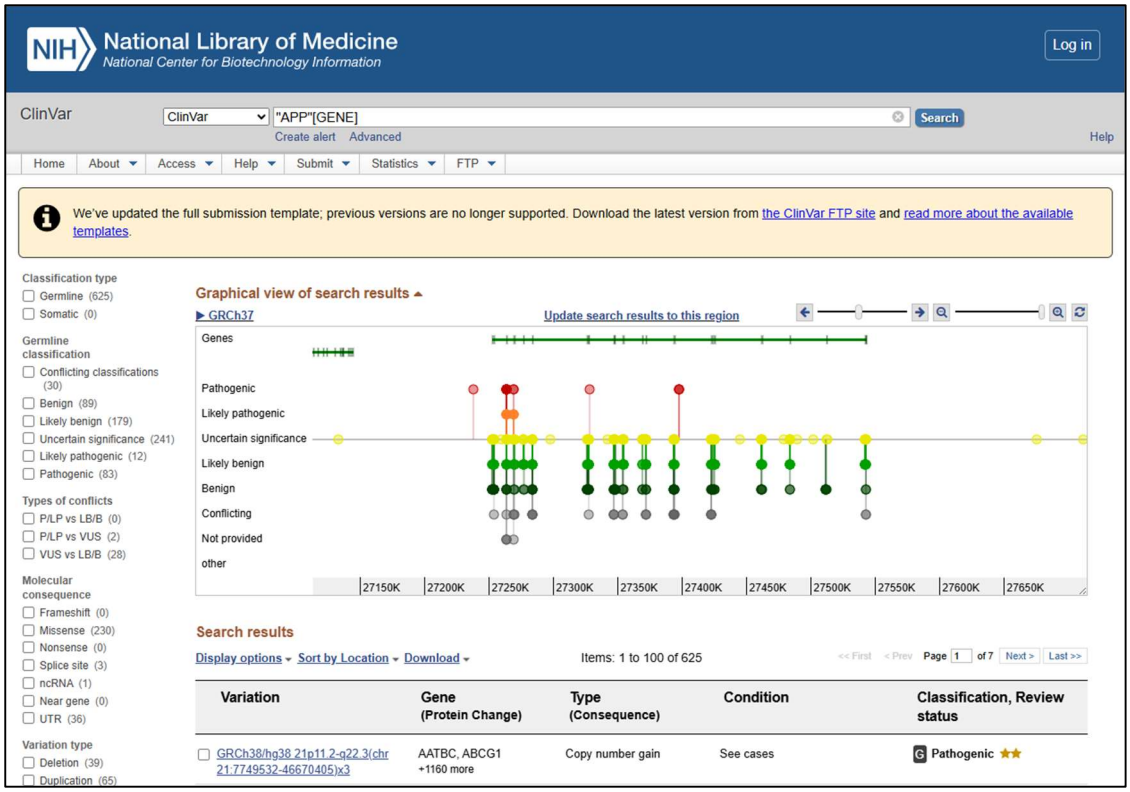

Figure 2.3 Genetic variations of the *APP* gene in ClinVar.
ClinVar web interface of the human APP gene, showing a 'Graphical view of search results' in the form of an interactive mutations map. On this map mutations can be explored along the length of the *APP* gene and information regarding pathogenicity can be accessed. A table with equivalent results appears below the genetic map. Picture taken September 2025 (https://www.ncbi.nlm.nih.gov/clinvar/?term=%22APP%22%5BGENE%5D&redir=gene).

The APP section of the Alzforum mutations database was particularly relevant, as it distinguished between pathogenic mutations associated with early onset familial Alzheimer's disease (EOFAD), those associated with cerebral amyloid angiopathy (CAA), and benign variants. Out of 71 missense mutations listed in the ALZFORUM mutations database (n.d.), 21 of them (29.6%) were selected and classified into one of three groups (i.e. EOFAD, CAA, benign) (see **2.6**).

The database also reports functional data such as the Aβ40/Aβ42 ratio and cites the original publications for each mutation, allowing for cross-verification with the primary literature (*APP | ALZFORUM*, n.d.) (**Figure 2.4**). This resource therefore complemented ClinVar by providing mechanistic insights into the biochemical and pathological consequences of specific variants, as well as clear clinical categorisation. The APP mutation database was accessed through the Alzforum web interface up to May 2024 (https://www.alzforum.org/mutations/ app).

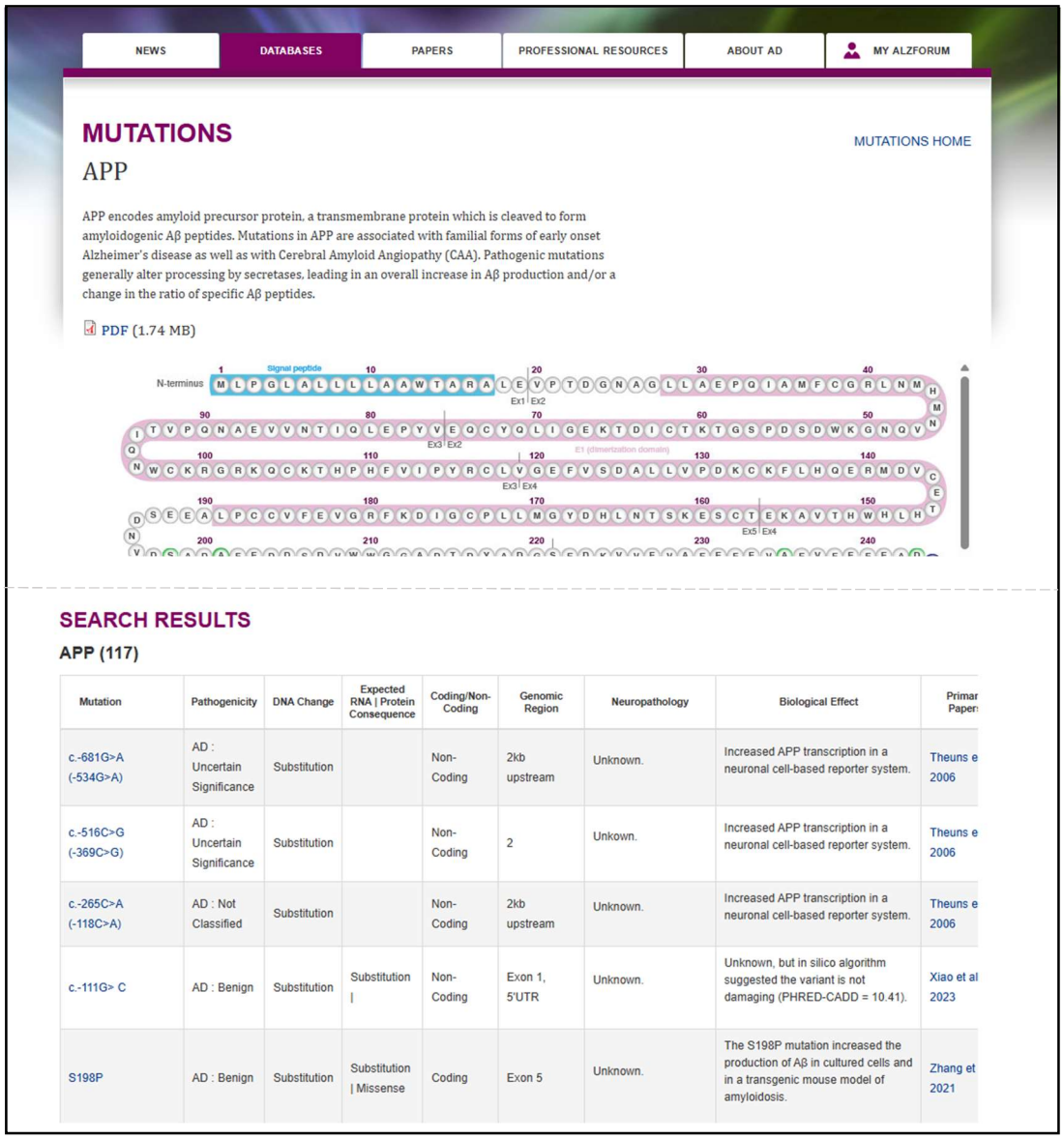

Mutation	Pathogenicity	DNA Change	Expected RNA | Protein Consequence	Coding/Non-Coding	Genomic Region	Neuropathology	Biological Effect	Primar Paper
c.-681G>A (-534G>A)	AD : Uncertain Significance	Substitution		Non-Coding	2kb upstream	Unknown.	Increased APP transcription in a neuronal cell-based reporter system.	Theuns e 2006
c.-516C>G (-369C>G)	AD : Uncertain Significance	Substitution		Non-Coding	2	Unkown.	Increased APP transcription in a neuronal cell-based reporter system.	Theuns e 2006
c.-265C>A (-118C>A)	AD : Not Classified	Substitution		Non-Coding	2kb upstream	Unknown.	Increased APP transcription in a neuronal cell-based reporter system.	Theuns e 2006
c.-111G> C	AD : Benign	Substitution	Substitution |	Non-Coding	Exon 1, 5'UTR	Unknown.	Unknown, but in silico algorithm suggested the variant is not damaging (PHRED-CADD = 10.41).	Xiao et al 2023
S198P	AD : Benign	Substitution	Substitution | Missense	Coding	Exon 5	Unknown.	The S198P mutation increased the production of Aβ in cultured cells and in a transgenic mouse model of amyloidosis.	Zhang et 2021

Figure 2.4 Alzforum's APP mutations database.
Alzforums's web interface of the APP mutations database. At the top, introductory information about APP and the mutations table accompanied by a schematic map of APP amino acid structure including key domains and point mutations. At the bottom, the mutations table is displayed. Relevant columns for this study included: 'Mutation', 'Pathogenicity', 'Biological Effect' and 'Primary Papers'. Picture taken September 2025 (https://www.alzforum.org/mutations/app).

2.2.5 DrugBank

DrugBank is a freely accessible bioinformatics and cheminformatics database that integrates detailed drug-related information with corresponding molecular targets. It provides comprehensive data on chemical properties, pharmacology, mechanisms of action, and clinical use, alongside sequence, structure, and pathway information for drug–target interactions. This resource was consulted to identify the pharmacological targets of currently approved AD medications. This information was accessed through the Drugbank web interface (**Figure 2.5**) (https://go.drugbank.com/) (v5.1.10) (Wishart et al., 2018). DrugBank was last accessed in October 2023.

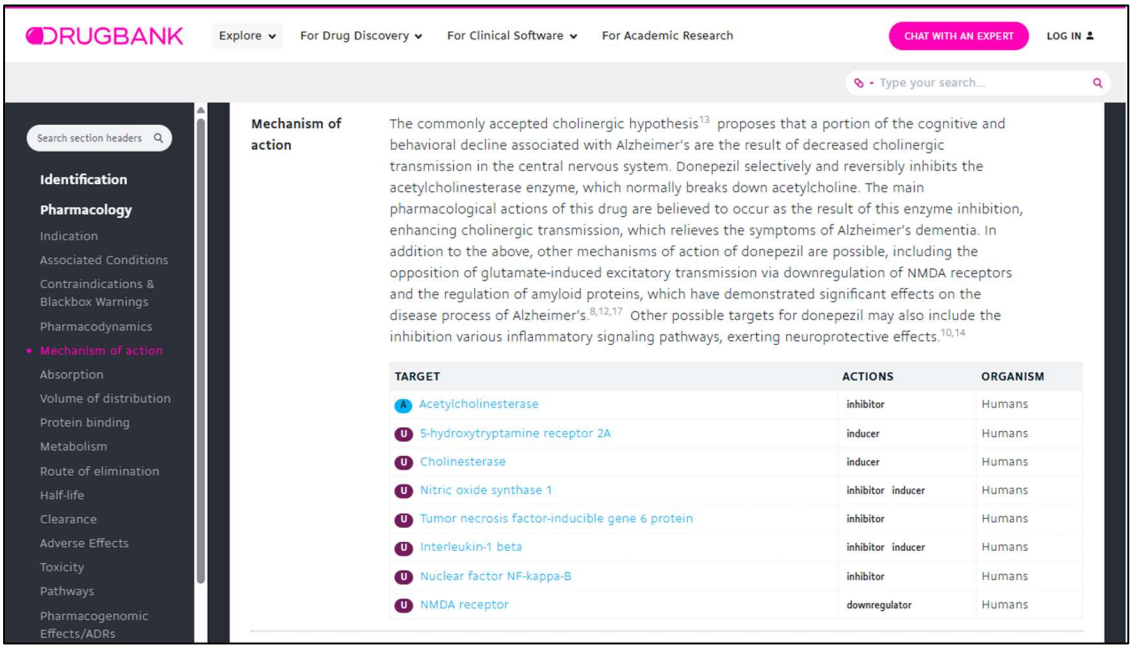

Figure 2.5 'Mechanism of action' information of donepezil in Drugbank.
Drugbank web interface of the AD drug donepezil (Drugbank ID: DB00843), showing the 'Mechanism of action' section which contains the drug target information displayed as a table. Under the 'target' column, an 'A' label indicated pharmacologically active targets which were included in this study; a 'U' label indicated targets with an unknown pharmacological effect – these were not included. Picture taken September 2025 (https://go.drugbank.com/drugs/DB00843).

2.3 Protein networks and pathways analysis

2.3.1 STRING database

The Search Tool for the Retrieval of Interacting Genes/Proteins (STRING) database was used to investigate a selection of protein–protein interactions (PPIs) relevant to AD. STRING is a

comprehensive platform that integrates experimental data, computational prediction methods, and public text collections to provide insights into both physical and functional protein associations. It compiles interaction evidence from multiple sources, including:

- Experimental data (e.g., high-throughput interaction screens)
- Computational predictions (e.g., genomic neighbourhood, gene fusion, and co-occurrence)
- Conserved co-expression patterns
- Text-mining from scientific literature
- Curated knowledge from existing databases

STRING's scoring system provides a confidence measure for each reported interaction, facilitating the differentiation between high-confidence and low-confidence associations. This tool was chosen for its broad coverage (encompassing millions of proteins across numerous species) and its capacity to generate visual interaction networks, making it highly suitable for identifying candidate protein networks involved in AD pathogenesis. Protein networks were generated through the STRING web interface (https://string-db.org/) (v12.0) (Szklarczyk et al., 2022). The STRING database was last accessed in December 2023.

2.3.2 Reactome

Reactome is an open-source, manually curated, and peer-reviewed biological pathway database that provides bioinformatics tools for the visualization, interpretation, and analysis of molecular pathways. The resource organizes biological knowledge into reactions and pathways spanning intermediary metabolism, signalling, transcriptional regulation, apoptosis, and disease processes. Each entry is linked to the primary literature and reviewed by experts, ensuring reliability and reproducibility.

A central feature of Reactome is the Pathway Browser, which provides an interactive environment to explore pathway hierarchies and to visualise detailed Pathway Diagrams (**Figure 2.6**). Pathway Diagrams represent biological processes as interconnected molecular events ("reactions"), with explicit spatial context across cellular compartments (e.g., extracellular space, plasma membrane, endosomes, or cytosol). Molecules and complexes are colour-coded by type (e.g., proteins, small molecules, sets, or complexes), and reactions are depicted with inputs, outputs, catalysts, and regulators. Special symbols indicate modifications such as phosphorylation, while disease processes are highlighted with red borders and connectors.

In this project, Reactome (v86) was used to contextualise AD-related proteins in their biological pathways, particularly focusing on APP processing and the metabolic role of AChE. Data were accessed through the Reactome web interface (https://reactome.org/) (Milacic et al., 2023). The Reactome database was last accessed in December 2023.

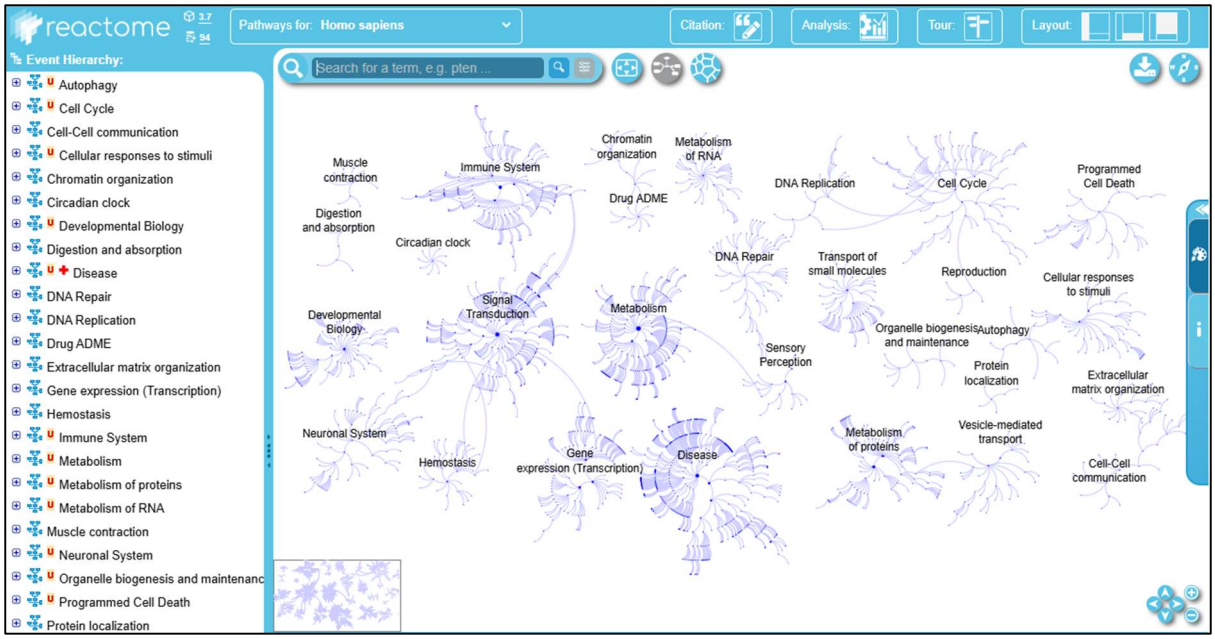

Figure 2.6 Reactome Pathway Browser.
Reactome web interface of the 'Pathway Browser' tool, showing the interactive map of the different pathways available in its database. Picture taken September 2025 (https://reactome.org/PathwayBrowser/).

2.4 Structural prediction and quality assessment

2.4.1 AlphaFold2/ColabFold

AlphaFold2 (Jumper et al., 2021) was employed to retrieve the three-dimensional structure of APP WT (https://alphafold.ebi.ac.uk/) (AlphaFold ID: AF-P05067-F1-v4). This system uses deep learning models trained on the Protein Data Bank (PDB) to infer residue–residue contacts and predict accurate structural conformations. Confidence metrics provided by AlphaFold2 include:

- pLDDT (per-residue confidence score, 0–100)
- pTM (predicted template modelling score, confidence in global fold)
- PAE (predicted aligned error, reliability of domain placement)

ColabFold (Mirdita et al., 2022) was used as an accessible implementation of AlphaFold2 to model APP WT and their selected variants (see **2.6** & **4.2.1**). It integrates with the MMseqs2 homology search pipeline to accelerate multiple sequence alignment (MSA) generation. ColabFold enables large-scale predictions via Google Colaboratory and supports both single-chain and multimer predictions. AlphaFold2 and ColabFold were accessed up to March 2024.

For this project, APP's canonical amino acid sequence was retrieved from UniProt (see **2.2.1**) and the sequences of its variants were curated integrating the information from ClinVar and Alzforum (see **2.2.3** and **2.2.4**) . Sequences were input in FASTA format, and models were

generated using the default ColabFold notebook (https://colab.research.google.com/github/sokrypton/ColabFold/blob/main/AlphaFold2.ipynb). Unless otherwise stated, five ranked models were produced per sequence, and the top-ranked model was selected based on average pLDDT and visual inspection.

2.4.2 AlphaFold Server

The AlphaFold Server (https://alphafoldserver.com/) was used to predict multimeric protein complexes involving APP and AChE. The server is powered by AlphaFold3, which extends the AlphaFold2 framework to model not only proteins but also protein–protein, protein–ligand, and protein–nucleic acid complexes with improved accuracy (Abramson et al., 2024). Compared to AlphaFold2, AlphaFold3 incorporates architectural improvements such as more efficient sequence–structure processing and the use of a diffusion-based approach, which together enable more reliable predictions of complex biomolecular assemblies.

Predicted protein complexes models reported the following metrics:

- Per-residue local Distance Difference Test (pLDDT) – representing a per-residue confidence score from 0 to 100. Provided by AlphaFold Server.
- Predicted template modelling (pTM) score – reflecting global fold accuracy, going from 0 to 1. Provided by AlphaFold Server.
- Interface predicted template modelling (ipTM) score – assessing confidence in subunit orientation within a complex, going from 0 to 1. Provided by AlphaFold Server.

For this project, a model confidence score was computed based on the reported metrics by the AlphaFold Server, this was done in order to assess the feasibility and quality of the different APP-AChE complexes (see **6.2.1**). The AlphaFold Sever was accessed up to August 2024.

2.4.3 DeepUMQA

DeepUMQA is a web-based deep learning tool for assessing the quality of protein structures, both for single proteins and complexes (Guo et al., 2022)(http://zhanglab-bioinf.com/DeepUMQA/). It evaluates how closely a predicted model matches realistic structural features by analysing residue–residue distances, contact patterns, and local accuracy scores. For monomeric proteins, DeepUMQA uses information from the sequence, structural templates, and predicted features to provide a residue-level confidence score, i.e. pLDDT. For protein complexes, it also assesses the accuracy of interactions between subunits. This makes it particularly suitable for evaluating models where both intra- and inter-molecular features are important.

In this project, DeepUMQA (v3) was used to compare different monomeric structural predictions of the canonical APP (generated by different modelling algorithms) ensuring that downstream analyses were based on the models with the highest structural reliability (see **4.2.1**). DeepUMQA was last accessed in February 2024.

2.4.4 PSIPRED & DISOPRED

PSIPRED and DISOPRED are computational tools developed by the UCL Bioinformatics Group for predicting secondary structure elements and intrinsically disordered regions (IDRs), respectively (Buchan et al., 2024; Jones & Cozzetto, 2014). They can both be accessed through the 'PSIPRED Workbench' (https://bioinf.cs.ucl.ac.uk/psipred/).

PSIPRED predicts secondary structure using position-specific scoring matrices derived from PSI-BLAST (Altschul et al., 1997), analysed through a neural network. The latest version (PSIPRED 4.0) incorporates deeper neural network architectures and an extended input window, improving prediction accuracy. Output includes graphical and textual representations of predicted α-helices, β-strands, and coil regions, together with residue-specific confidence scores.

DISOPRED identifies disordered regions within protein sequences, which often contribute to structural flexibility and dynamic biological roles. The updated version (DISOPRED 3) improves the sensitivity and specificity of disorder prediction and includes modules for identifying protein-binding sites within IDRs.

In this study, both PSIPRED (v4.0) and DISOPRED (v3) were used as complementary tools for structural evaluation of the top three highest scored canonical APP structures, by DeepUMQA (see **Table 4.1**). PSIPRED and DISOPRED combined evaluation helped selecting the most reliable APP model in terms of its secondary structure, emphasising on the accurate placement of IDRs (see **4.2.1**). The 'PSIPRED Workbench' was last accessed in February 2024.

2.5 Structural manipulation and visualisation

2.5.1 UCSF Chimera

UCSF Chimera (v1.17.1) is a comprehensive program for the visualisation and interactive analysis of molecular structures and associated data. It supports a wide range of formats (e.g., PDB, MOL2, SDF) and provides tools for examining atomic structures, density maps, supramolecular assemblies, docking results, and conformational ensembles (Pettersen et al., 2004).

The program offers a wide range of capabilities relevant to structural bioinformatics, including:

- 3D visualisation and annotation of protein structures
- Superimposition of multiple models to assess structural similarity
- Measurement of distances, angles, and torsional parameters
- Analysis of hydrophobic, polar, and electrostatic interactions using tools such as the *Find Clashes/Contacts* module
- Preparation of publication-quality figures with flexible colour schemes, labelling, and rendering styles

In this study, UCSF Chimera was employed across multiple contexts: to visualise structural models of APP and its variants (see **4.2.1**), to assess APP–γ-secretase interactions (see **5.2.1**), and to characterise APP–AChE complexes (see **6.2.1**). Its versatility made it an essential tool for evaluating predicted structures and PPIs in AD research. UCSF Chimera was accessed up to September 2024. The software can be downloaded through: https://www.cgl.ucsf.edu/chimera/

2.6 Variant classification

Thorough research was necessary in order to stratify APP variants into appropriate and clinically reliable categories. Individual APP variants were examined aiming to understand the link between a missense mutation and its consequent disease phenotype. The following groups were defined:

- Early onset familial AD (EOFAD)
- Cerebral amyloid angiopathy (CAA)
- Benign

The EOFAD or CAA groups were chosen as multiple mentions of point mutations in APP leading to the development of these diseases were found in the literature (Mullan et al., 1992; Kumar-Singh, 2000; Pasalar et al., 2002; Eckman et al., 1997; Ancolio et al., 1999; Murrell et al., 2000; Naruse et al., 1991; Chartier-Harlin et al., 1991; Murrell et al., 1991; Kwok et al., 2000; Theuns et al., 2006; Levy et al., 1990; Bugiani et al., 2010; Hardy & Higgins, 1992; Obici et al., 2005). Causal mutations in APP leading to LOAD were not as clearly identified, which is in line with an inconsistent pattern of inheritance reported by Bertram & Tazi (2005), thus a LOAD group was not formed. Finally, APP benign variants were found as part of clinical studies or scientific publications and were selected for having no apparent AD-related symptoms on patients that were older than 65 years old (Sassi et al., 2014; Nicolas et al., 2015; Sala Frigerio et al., 2015; Jonsson et al., 2012). These variant classifications were used in **Chapters 4** & **5**. The full list of mutations and their categories are shown in **Table 2.1**.

APP variant	Category	Reference
K670N+M671L	EOFAD	Mullan et al., 1992
T714I	EOFAD	Kumar-Singh, 2000
T714A	EOFAD	Pasalar et al., 2002
V715M	EOFAD	Ancolio et al., 1999
I716V	EOFAD	Eckman et al., 1997
V717L	EOFAD	Murrell et al., 2000
V717I	EOFAD	Naruse et al., 1991
V717G	EOFAD	Chartier-Harlin et al., 1991
V717F	EOFAD	Murrell et al., 1991
L723P	EOFAD	Kwok et al., 2000
K724N	EOFAD	Theuns et al., 2006
E693Q	CAA	Levy et al., 1990
E693K	CAA	Bugiani et al., 2010
D694N	CAA	Grabowski et al., 2001
L705V	CAA	Obici et al., 2005
A201V	Benign	Sassi et al., 2014
A235V	Benign	Nicolas et al., 2015
A479S	Benign	Sala Frigerio et al., 2015
V562I	Benign	Sassi et al., 2014
E599K	Benign	Sassi et al., 2014
A673T	Benign*	Jonsson et al., 2012

Table 2.1 APP variants and their categories.
Table showing APP missense mutations, also referred as variants, and their respective category. Two pathological categories were defined: early onset familial AD (EOAFD) (green) and cerebral amyloid angiopathy (CAA) (yellow). The final category corresponds to 'Benign' (blue) cases where there was no sign of pathological impact emerging from mutations in the APP gene. Numerous studies found in the literature corroborate all these cases – these can be found under the 'Reference' column. *The A673T variant is considered to be a protective variant as seen in multiple studies – it could be classed as a 'super' benign.

2.7 Statistical framework

Statistical analysis was employed to compare structural and interaction-based measurements across different groups of APP protein models, namely EOFAD, CAA and benign variants. Outliers within each group were first identified using Tukey's fences (k = 1.5) and evaluated for potential influence on group distributions. Group-level comparisons were then performed using one-way analysis of variance (ANOVA). When the assumptions of ANOVA, such as normally distributed data, were not satisfied, the non-parametric Kruskal–

Wallis test was applied as an alternative. Normality of the datasets was assessed using the Shapiro–Wilk test.

Where significant group differences were detected, post-hoc pairwise comparisons were conducted. For ANOVA, Tukey's Honest Significant Difference (HSD) test was applied, whereas for Kruskal–Wallis results, pairwise Mann–Whitney U tests with Bonferroni correction were used to adjust for multiple testing ($\alpha = 0.017$ for three group comparisons). In addition to p-values, effect sizes were calculated to assess the magnitude of observed differences: η^2 (eta-squared) was reported for ANOVA and Kruskal–Wallis tests, and r values were reported for pairwise non-parametric comparisons. Where appropriate, descriptive statistics such as medians and interquartile ranges (IQR) were also provided to aid interpretation.

This statistical framework was applied consistently across analyses, whether comparing structural distances, secondary structure features, or contact/clash profiles from protein–protein interaction models. Statistical significance was defined at the threshold of $p < 0.05$, with adjusted thresholds applied in the context of multiple comparisons. Data handling and distribution was carried out using Microsoft Excel 2021 and statistical tests were performed using the Statistics Kingdom platform (https://www.statskingdom.com/).

3 Protein network analysis

3.1 Introduction

3.1.1 Protein selection reasoning

There are multiple proteins involved in the complex pathophysiology of AD. Interestingly, there seems to be a myriad number of effects which arise from the accumulation or overproduction of Aβ peptides (Chen et al., 2017). For this reason, studying APP and its protein interactors has been a priority to scientists for decades and is one of this chapter's main goals.

As previously seen, *APP, PSEN1* and *PSEN2* can carry autosomal-dominant mutations which lead to the development of AD, specifically EOFAD. These genes have been a therapeutical target for years, and various types of inhibitors and monoclonal antibodies therapies have been developed considering their mechanism of action and role in the processing of APP to Aβ. In addition, the gene *BACE1* also plays a crucial role in the amyloidogenic pathway of APP (see **1.4**). *BACE1* codes for the BACE1 protein which acts as the first secretase (i.e. β-secretase) that cleaves APP in order to produce Aβ peptides. The second secretase in the amyloidogenic pathway is γ-secretase, a protein complex containing the protein presenilin (coded by the *PSEN1* or *PSEN2* genes) which is key to carry out γ-secretase's proteolytic activity (Coronel et al., 2018; Chen et al., 2017). Thus, the proteins expressed from these genes (i.e. *BACE1, PSEN1*, *PSEN2*), integral for the amyloidogenic pathway of APP, will be included in the exploratory search of AD protein-protein interactions (PPIs).

Other relevant proteins to include would be those that have been long targeted by common AD medication. As explained before (see **1.6**), AChEIs such as donepezil are prescribed to increase acetylcholine levels in the brain by reversibly inhibiting the enzyme AChE. (Cavalcante et al., 2020). AChEIs can have additional secondary target proteins. In the case of rivastigmine, it also binds and inhibits butyrylcholinesterase (BChE), an enzyme which performs a similar role to AChE (Cavalcante et al., 2020; Wishart et al., 2018). Additionally, galantamine also acts as a positive allosteric modulator (PAM) at nicotinic cholinergic receptors, specifically binding to neuronal acetylcholine receptor subunit alpha-7 (CHRNA7), which strengthens the communication between cholinergic neurons (Cavalcante et al., 2020; Wishart et al., 2018). Furthermore, memantine blocks the excessive glutaminergic activity of NMDA receptors and reduces neurotoxic calcium influx into neurons. The NMDA receptor protein is an heterotetramer composed of a combination of protein subunits, including: GRIN1, GRIN2A, GRIN2B, GRIN2C, GRIN2D, GRIN3A, and GRIN3B (Yamamoto et al., 2015).

By considering the proteins involved in the amyloidogenic processing of APP and the ones targeted by common AD medication, PPIs can be used to elucidate potential relationships and networks of interest.

3.1.2 Aims

Using PPI and protein pathways databases, I aim to examine the associations and interactors of the following proteins of interest – in order to identify potential novel links between the main secretases involved in the amyloidogenic processing of APP and the proteins targeted by common AD drugs: APP, PSEN1, PSEN2, BACE1, AChE, BChE, CHRNA7, GRIN1, GRIN2A, GRIN2B, GRIN2C, GRIN2D, GRIN3A, and GRIN3B.

3.2 Specific methods

3.2.1 Selection of pharmacologically targeted proteins

DrugBank (v5.1.10) (see **2.2.5**) was queried to identify the primary protein targets of the four commonly prescribed AD medications: donepezil (DrugBank ID: DB00843), galantamine (DrugBank ID: DB00674), rivastigmine (DrugBank ID: DB00989), and memantine (DrugBank ID: DB01043)(Wishart et al., 2018). For each drug, the 'Mechanisms of action' section was consulted to capture only pharmacologically active targets (see **Figure 2.5**).

3.2.2 Generation of protein-protein interaction networks

PPI networks of the defined proteins of interest (i.e. APP, PSEN1, PSEN2, BACE1, AChE, BChE, CHRNA7, GRIN1, GRIN2A, GRIN2B, GRIN2C, GRIN2D, GRIN3A, and GRIN3B) were generated using the STRING database (v12.0) (see **3.1.1**, **2.3.1**) (Szklarczyk et al., 2022).

Two main search functions within the STRING database were used to explore different aspects of APP-related protein connectivity. First, the 'Multiple Proteins' search was used to investigate potential interaction networks among a predefined set of proteins. This functionality was used to expand the PPI network of the selected proteins involved in the APP amyloidogenic pathway (i.e. APP, BACE1, PSEN1, PSEN2), to explore the interconnectivity of commonly drug-targeted proteins in AD (i.e. AChE, BChE, CHRNA7, GRIN1, GRIN2A, GRIN2B, GRIN2C, GRIN2D, GRIN3A, and GRIN3B), and to uncover any potential associations or pathways between these two groups of proteins. Second, the 'Single Protein' search was employed to visualise the immediate interaction network surrounding a single query protein. This approach was useful to contextualise the biological environment of APP and AChE within their respective cellular processes.

Homo sapiens was the default selected organism in all searches. Each of the searches outputted a PPI network interactive graph. Each of these proteins (also known as nodes), were displayed as circular shapes in a network connected by lines (also known as edges) – see **Figure 3.3** for an example. The 'Basic Settings' for both search functions were set-up as

displayed in **Figure 3.1**, unless stated otherwise. The 'Advanced Settings' were kept as default.

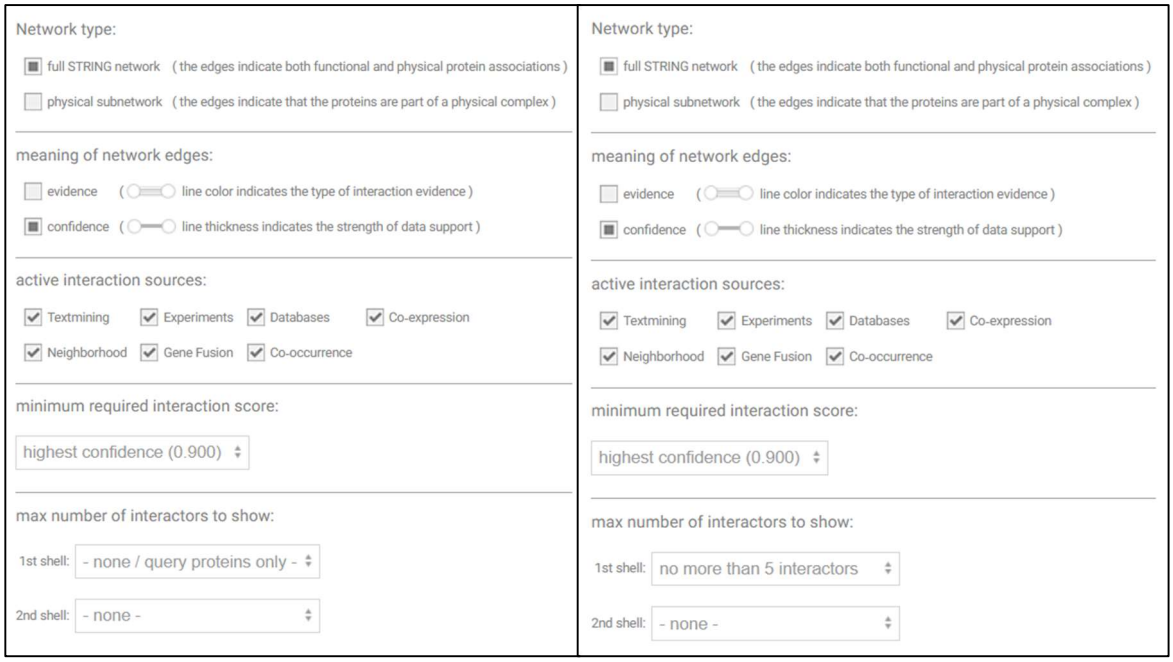

Figure 3.1 'Basic Settings' of the 'Multiple Proteins' (left) and 'Single Protein' (right) search methods.
The two search methods used were adjusted to show a combined confidence score as edges with a high confidence threshold. Unless stated otherwise, the default 'max number of interactions to show' was used (none for 'Multiple Proteins' and no more than 10 interactions for 'Single Protein').

The 'confidence' configuration was used for the edges as it combines the information from all the interaction sources (see **2.3.1**) and displays it as a single line with varying thickness – proportional to the combined confidence score. This score ranges from 0 to 1, 1 being the maximum score, and it allows for filtering of results showing only those edges (interactions) above a certain threshold. For all the networks, the minimum required interaction score (threshold) was set to 0.900. This high threshold exclusively displayed the edges with the highest level of confidence.

The 'Network Stats' tab (under 'Analysis') outputted informative values (i.e. 'average node degree', 'average local clustering coefficient', 'expected number of edges' and 'PPI enrichment p-value') for each PPI network. The 'average node degree' represented the average number of interactions above the confidence threshold that each protein (or node) in the network had. The 'average local clustering coefficient' measured the connectivity between all the proteins in the network – from 0 (lowest) to 1 (highest). The 'expected number of edges' computed a predicted value for the number of edges in a randomly selected set of proteins – this refers to the selection of proteins inputted in the 'Multiple Proteins' search function. Finally, the 'PPI enrichment p-value' acted as a measure of

statistical significance for randomly selected proteins in PPI networks, hence only providing value to the 'Multiple Protein' search function and not to the 'Single Protein' one (nodes and edges in this search function are non-randomly generated by STRING). For a network to significantly have more interactions than expected, the PPI enrichment p-value would fall below 0.05.

Networks were downloaded in high-resolution image format for inclusion in this thesis, and STRING-provided enrichment analyses (pathways, biological processes, molecular functions) were examined where relevant.

3.2.3 Protein pathways visualisation

To investigate the biological context in which the previous PPI networks occurred (see **3.1.1** & **3.2.2**), the Reactome database (v86) was consulted (see **2.3.2**) (Milacic et al., 2023). The 'Pathway Browser' was employed to query a selection of proteins of interest and obtain relevant proteins pathways (i.e. pathway diagrams).

Pathway diagrams displayed the following:

- Interactors as colour-coded ovals or boxes:
    - Green boxes = proteins
    - Green ovals = small molecules
    - Blue boxes with cut corners = complexes (i.e. proteins and/or other molecules) that are bound in a multimolecular entity
    - Blue boxes with double boundaries = sets of proteins/small molecules that are functionally equivalent
    - Purple boxes = pharmacological agents
- Physiological compartments (e.g. extracellular, plasma membrane, cytosol, endosomes) as orange rectangles with double boundaries.
- Directionality of reactions as arrows, with their ends marking catalysts (circles), activators (triangles) or inhibitors (T-shapes).
- Reactions as central nodes connected to input, output, and catalyst molecules – relevant subtypes included:
    - Open squares = 'transition'
    - Solid circles = 'association'
    - Double-bordered circles = 'dissociation'
    - A square with two slashes = 'omitted process'
- Multiple molecules (n >1) of the same type in a reaction as numbered boxes.
- Disease-associated processes as red-bordered shapes and arrows.

Two pathway diagrams were selected for investigation: the 'amyloid fibre formation' (Reactome ID: R-HSA-977225), and the 'AcCho is hydrolyzed to Cho and acetate by ACHE' (Reactome ID: R-HSA-372519).

3.3 Results

3.3.1 Key protein networks

The 'Multiple proteins' search function was used to investigate potential functional or physical interactions within a selected set of proteins – this method outputted the networks in **Figure 3.2**, **Figure 3.3** and **Figure 3.4**. The 'Single Protein by Name' search function was used to uncover high-confidence interactors of APP and AChE – two key proteins that play a central role in previously defined sets of proteins of interest (see **3.1.1**). This method outputted the networks in **Figure 3.6** and **Figure 3.5**.

A set of proteins involved in the amyloidogenic pathway of APP (i.e. BACE1, PSEN1 and PSEN2) were investigated (**Figure 3.2**). The network outputted by STRING was expanded to show additional proteins from the four inputted – and so the 'max number of interactors' was set to 'no more than 5 interactors' (see **Figure 3.1**). There were a total of 9 nodes and 25 edges in this network The average node degree was 5.56, and the average local clustering coefficient was 0.884. The expected number of edges was 0 and the PPI enrichment p-value was < 1.0e-16 – significantly low as expected by the expansion of the 'max number of interactors'. Closely interconnected subsets can be observed between proteins that are part of the γ-secretase complex (i.e. APH1A, APH1B, NCSTN, PSENEN, PSEN1, PSEN2). ADAM10, which constitutes the α-secretase, and BACE1, the constituent of β-secretase, also connect with various other proteins in the network.

Figure 3.3 displays the network of pharmacologically targeted proteins in AD (i.e. AChE, BChE, CHRNA7, GRIN1, GRIN2A, GRIN2B, GRIN2C, GRIN2D, GRIN3A, GRIN3B). In this network, some proteins were left isolated – not connected to any other protein. The total number of nodes and edges were 10 and 21 respectively. The average node degree was 4.2, and the average local clustering coefficient was 0.7. The expected number of edges was 0 and the PPI enrichment p-value was < 1.0e-16. This indicated that the connected proteins were biologically/functionally related. In this case, the interconnected proteins were all part of the same receptor (i.e. NMDA receptor) and so a significant PPI enrichment p-value was expected.

The combination of all the inputted proteins involved in the previous two networks (**Figure 3.2** and **Figure 3.3**) led to the outputted network shown in **Figure 3.4**. The total number of nodes and edges were 14 and 28 respectively. Similarly to their individual PPI networks, two local clusters emerged from this network. The average node degree was 4, and the average local clustering coefficient was 0.821. The expected number of edges as 0 and the PPI enrichment p-value is < 1.0e-16 indicating functional/physical associations between connected nodes. A couple of proteins did not associate with any of the two clusters.

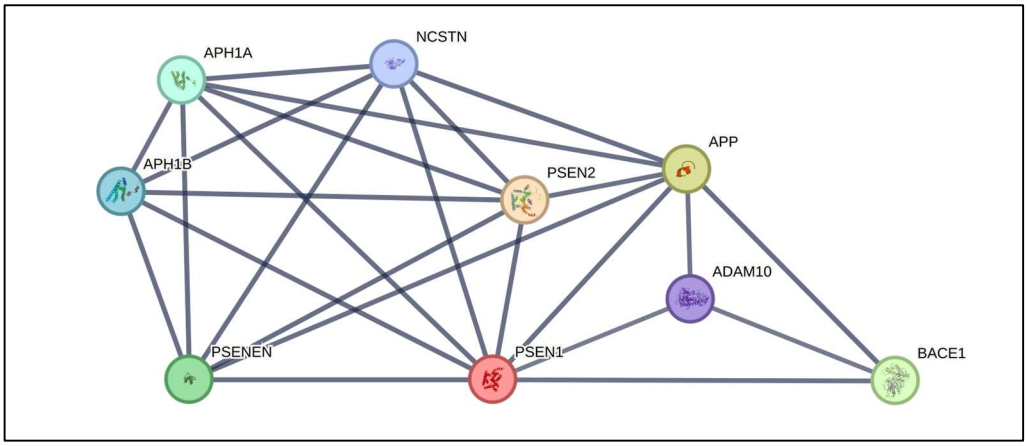

Figure 3.3 APP and protein components of secretases.
Diagram showing the network of APP alongside multiple protein components of secretases involved in the amyloidogenic and non-amyloidogenic processing of APP.
Legend: Disintegrin and metalloproteinase domain-containing protein 10 (ADAM10), gamma-secretase subunit APH-1A (APH1A), gamma-secretase subunit APH-1B (APH1B), amyloid precursor protein (APP), β-secretase 1 (BACE10), nicastrin (NCSTN), presenilin 1 (PSEN1), presenilin 2 (PSEN2), gamma-secretase subunit PEN-2 (PSENEN).

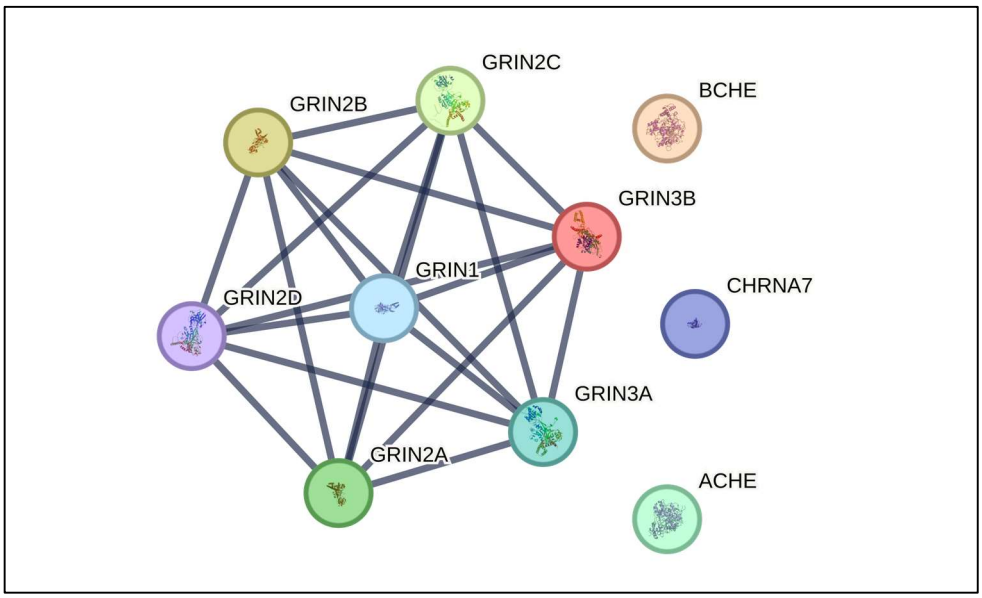

Figure 3.2 Proteins that are pharmacologically targeted in AD treatment.
Diagram illustrating multiple proteins which are targeted by different AD drugs such as donepezil, rivastigmine, galantamine and memantine. The local cluster corresponds to proteins which form the ionotropic glutamate NMDA receptor. Legend: Acetylcholinesterase (ACHE), butylcholinesterase (BCHE), neuronal acetylcholine receptor subunit α-7 (CHRNA7), glutamate receptor ionotropic NMDA type subunit 1/2A/2B/2C/ 2D/3A/3B (GRIN1, GRIN2A, GRIN2B, GRIN2C, GRIN2D, GRIN3A, GRIN3B).

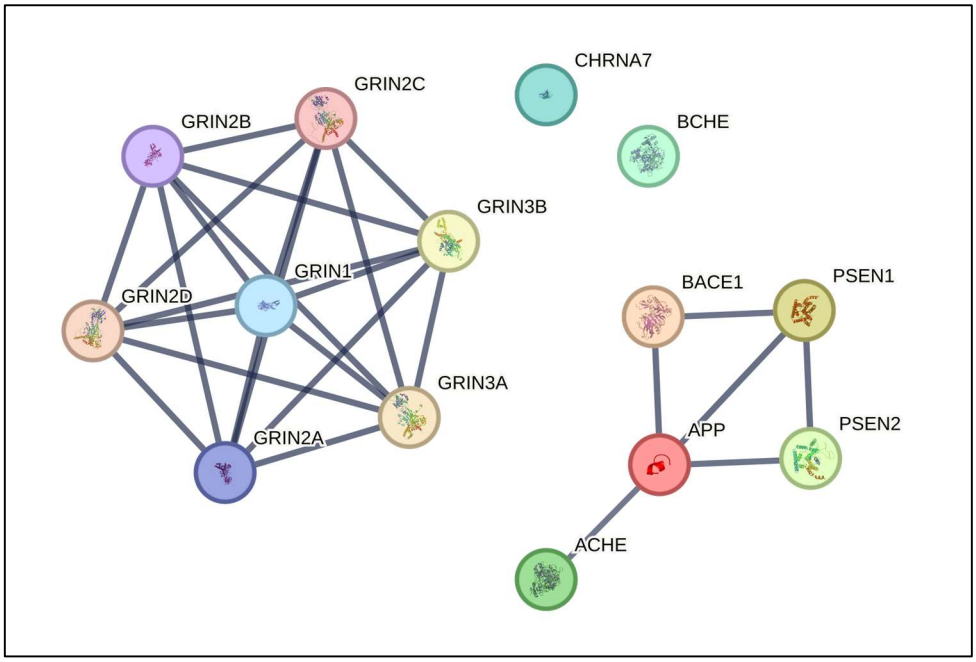

Figure 3.4 Proteins that are pharmacologically targeted in AD treatment in combination with APP amyloidogenic pathway proteins.
Diagram combining the inputted proteins of interest from the previous two networks (**Figure 3.3** & **Figure 3.2**). Two local clusters emerge, one corresponding to the subunits of the ionotropic glutamate NMDA receptor, and the other one including APP and secretase components from the amyloidogenic pathway – with the insightful addition of AChE. Legend: Acetylcholinesterase (ACHE), apolipoprotein E (APOE), amyloid precursor protein (APP), butylcholinesterase (BCHE), neuronal acetylcholine receptor subunit α-7 (CHRNA7), G protein-regulated inducer of neurite outgrowth 1 (GRIN1), N-methyl D-aspartate receptor subtype 2A/2B/2C/2D/3A/3B (GRIN2A, GRIN2B, GRIN2C, GRIN2D, GRIN3A, GRIN3B), presenilin 1 (PSEN1), presenilin 2 (PSEN2).

Figure 3.5 displays the network outputted by the 'Single Protein' search of AChE. The connection between APP and AChE, firstly uncovered in **Figure 3.4**, appeared again in this network. There contained 6 nodes and 8 edges, the average node degree is 2.67, and the average local clustering coefficient is 0.883. The expected number of edges is 5 and the PPI enrichment p-value is 0.135 (not informative for 'Single Protein' searches).

Finally, **Figure 3.6** shows the 'Single Protein' network of APP. BACE1 and PSEN1 were the only protein interactors of APP that were previously inputted in other networks. There were a total of 6 nodes and 8 edges in the network. The average node degree is 2.67, and the average local clustering coefficient is 0.772. The expected number of edges is 5 and the PPI enrichment p-value is 0.139 (not informative for 'Single Protein' searches).

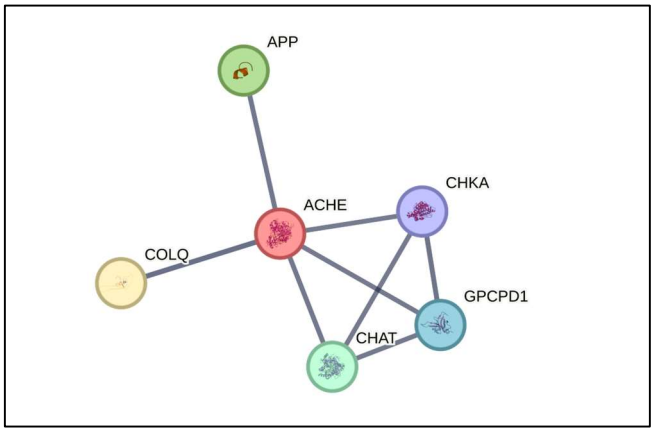

Figure 3.5 AChE single protein network.
Diagram showing the local network of AChE. The interaction between AChE and APP is shown – which will be explored later in **Chapter 6**. Legend: Acetylcholinesterase (ACHE), amyloid precursor protein (APP), choline O-acetyltransferase (CHAT), choline kinase α (CHKA), acetylcholinesterase collagenic tail peptide (COLQ), glycerophosphocholine phosphodiesterase (GPCPD1) (Szklarczyk et al., 2022).

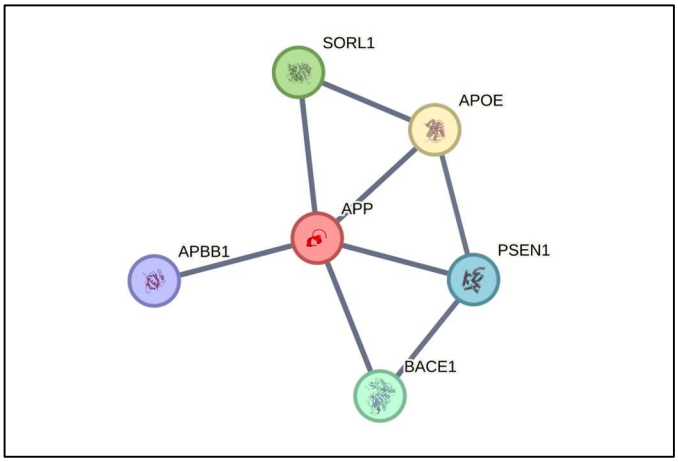

Figure 3.6 APP single protein network.
Diagram showing the local network of APP. Legend: Amyloid β precursor protein binding family B member 1(APBB1), apolipoprotein E (APOE), amyloid precursor protein (APP), β-secretase 1 (BACE10), presenilin 1 (PSEN1), sortilin-related receptor (SORL1).

3.3.2 Insightful pathways

The 'Pathway Browser' was used to investigate the biological context of some of the PPI networks previously obtained (see **3.3.1**) with special attention around two central proteins: APP, AChE. This led to the exploration of the 'amyloid fibre formation' (Jupe, 2010) and the 'AcCho is hydrolyzed to Cho and acetate by ACHE' (Mahajan, 2008) pathway diagrams (see **3.2.3**).

Both **Figure 3.7**and **Figure 3.8** show sections of the 'amyloid fibre formation' pathway diagram but focus on distinct biological processes. **Figure 3.7** displays APP processing by secretases within a cell. Important secretases (i.e. 'ADAM10:Zn^{2+}:TSPANs' complex, BACE1 and gamma-secretase complex) are located in the plasma membrane or in an endosomal membrane (orange rectangles with double boundaries). These enzymes act as catalysts (circle-ending arrows) and allow for the transition of their respective reactions (open squares). Different peptide products of APP are released in the endosome, with some functional equivalent peptides (blue boxes with double boundaries) moving to the plasma membrane before leaving the cell.

Figure 3.8 shows the pathogenic pathway (red-coloured arrows and shapes) that the APP peptides that left the cell (i.e. APP(672-713), APP(672-711)) take in order to become amyloid fibrils. Initially, these peptides that left the cell act as 'amyloid fibril monomers' which then transition (open square) to pathogenic 'amyloid fibril main peptide chains'. These chains associate (solid circle) with other molecules extracellularly yielding 'amyloid fibrils' which embed in the plasma membrane of the cell.

Finally, **Figure 3.9** shows the 'AcCho is hydrolyzed to Cho and acetate by ACHE' pathway diagram. The 'Cholinesterase' equivalent of AChE acts as a catalyst to transition the reaction from acetylcholine (and water) to choline and acetate. ACHEIs associate with AChE to form the 'ACHE:ACHEIs' complex thereby inhibiting AChE's catalytic ability.

3.4 Discussion

3.4.1 Cliques within PPI networks

By exploring the STRING database, I aimed to define the interactions between the main proteins involved in the amyloidogenic pathway and the proteins targeted in the symptomatic treatment of AD. Additionally, some of the PPI networks explored provided insightful information in the form of subnetworks or clusters, specifically the existence of closely interconnected clusters known as cliques. A clique is an undirected (edges with no orientation) subnetwork or cluster in which every two distinct nodes in the clique are adjacent (Alba, 1973). For instance, in a 4-node clique, each node would have 3 edges

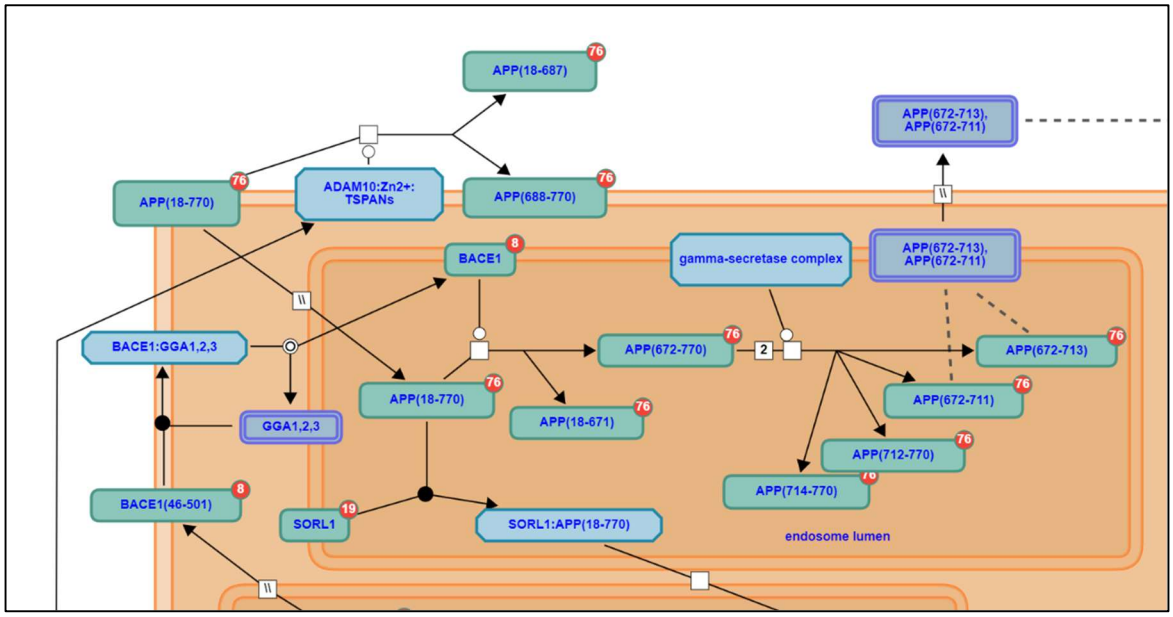

Figure 3.7 Amyloid fibre formation – processing by secretases.
Diagram showing the processing of APP (APP(18-770), top left) by different secretases (Jupe, 2010). APP can be processed by an α-secretase complex (ADAM10:Zn^{2+}:TSPANs) at the plasma membrane or it can be internalised via an endosome. Two important secretases (BACE1 and gamma-secretase complex) are in the endosomal membrane. Processing by these enzymes leads the APP peptide down the amyloidogenic pathway – where pathological fibres can potential be formed. Alternatively, another enzyme in the endosomal membrane (SORL1) can form a complex with APP (SORL1:APP(18-770)) and allow for the transport of APP to a different cellular location – away from the amyloidogenic processing.

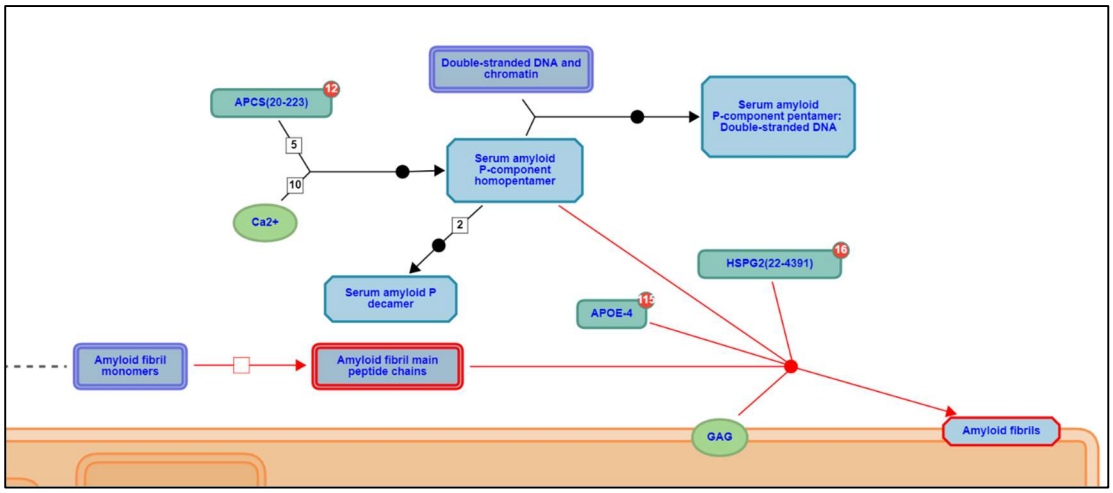

Figure 3.8 Amyloid fibre formation – amyloid fibrils pathological aggregation.
Diagram showing the pathogenic conversion (red-coloured arrows and shapes) of amyloid fibril monomers (previously APP(672-713), APP(672-711 in **Figure 3.7**) to amyloid fibrils in the plasma membrane (bottom right). After the transition from amyloid fibril monomers to amyloid fibril main peptide chains, different proteins (e.g. APOE-4, HSPG(22-4391)) and small molecules (GAG) associate to form the final amyloid fibrils.

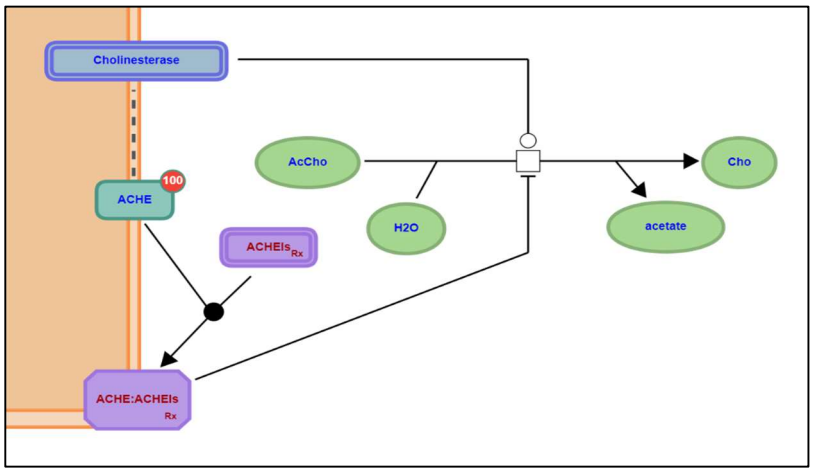

Figure 3.9 Acetylcholine (ACh) is hydrolysed to choline (Cho) and acetate by acetylcholinesterase (AChE).
Cholinesterase (AChE equivalent) catalyses the hydrolysis breakdown (open square) of acetylcholine (AcCho). This reaction can be inhibited by the association of ACHEIs with AChE forming a non-functional complex (Mahajan, 2008).

connecting it to the other nodes in the clique – an example of this can be seen in **Figure 3.3**, a 4-node clique is formed between APP, BACE1, PSEN1 and PSEN2. Cliques are signs of close interconnectivity, and in the protein network context, they can represent specific pathways or reactions. For this analysis, 3-node cliques were not highlighted since they lacked enough contextual information to assess their pathways.

Figure 3.3 explored the proteins involved in APP processing, both amyloidogenic and non-amyloidogenic pathways. By inputting the PSEN1, PSEN2, APP and BACE1 genes, the STRING database generated a greater network which included other proteins that were part of the γ-secretase complex (i.e. PSENEN, APH1A, APH1B, NCSTN) and α-secretase (i.e. ADAM10), picturing a wholistic APP processing network. A high average local clustering coefficient (i.e. 0.884) suggested close interconnection between multiple proteins. The 4-node clique involving APP, PSEN1, ADAM10 and BACE1 integrated APP's main secretases. Another important clique was the one formed by PSEN1-PSEN2-NCSTN-APH1A-APH1B-PSENEN, which contained the subunits of the γ-secretase complex, a critical enzyme in the amyloidogenic pathway of APP.

By inputting the proteins targeted by symptomatic AD drugs (i.e. donepezil, galantamine, rivastigmine and memantine) **Figure 3.2** showed some close interconnectivity. This PPI network had a low PPI enrichment p-value (< 1.0e-16), indicating potential interactions, but it was most likely driven by the GRIN-proteins clique (i.e. GRIN1, GRN2A, GRIN2B, GRIN2C, GRIN2D, GRIN3A, GRIN3B). All these proteins are subunits of the same receptor (NMDA ionotropic glutamate receptor) and so they will all interact physically and functionally with each other. The other proteins in this network (i.e. CHRNA7, AChE and BChE) did not have a

connection and thus STRING database considered them not to be biologically or functionally linked to any of the inputted proteins (at a high level of confidence).

Figure 3.4 encompassed all the previously inputted proteins from the networks in **Figure 3.3** and **Figure 3.2**. In this PPI network, two local clusters were formed. One corresponding to the GRIN-proteins clique, and the other one connecting APP, PSEN1, PSEN2, BACE1 and AChE. The connections of this latter cluster were similar than in **Figure 3.3** (a 4-node clique between APP-PSEN1-PSEN2-BACE1), but with the additional APP-AChE connection. This connection is the first one that linked 'pharmacologically AD-targeted proteins' to 'amyloidogenic APP processing proteins' – an insightful novel connection which is further explored in **Chapter 5**. Overall, this PPI network had high metrics including an average local clustering coefficient of 0.821 and a PPI enrichment p-value is < 1.0e-16 indicating functional and physical associations between proteins – specially within clusters.

The AChE single protein network (**Figure 3.6**) showed many functionally associated proteins of AChE. Amongst these, a 4-node clique formed by AChE-CHAT-GPCPD1-CHKA can be observed. The proteins in this 4-node clique include AChE, choline O-acetyltransferase (CHAT), glycerophosphocholine phosphodiesterase (GPCPD1) and choline kinase α (CHKA) and they play a role in glycerophospholipid biosynthesis (Williams, 2011). Additionally, two individual independent connections were formed with AChE, i.e. AChE-COLQ, AChE-APP. COLQ, which stands for AChE collagenic tail peptide, is a collagen protein that binds AChE and anchors it at the basal lamina of neuromuscular junctions, allowing the appropriate functioning of AChE at the synaptic cleft (Karmouch et al., 2020). Finally, the APP-AChE connection appeared again, highlighting their functional association and potential shared role in AD pathophysiology – or at least in the cholinergic degeneration aspect of AD.

Figure 3.5 showed the single protein network of APP. This network included proteins such as the amyloid-beta A4 precursor protein-binding family B member 1 (APBB1) and the sortilin-related receptor (SORL1), in addition to the previously seen BACE1, PSEN1 and APOE. APBB1 is involved in the transcriptional signalling of APP and its action can be inhibited in AD (Minopoli et al., 2012; Zhou et al., 2009; McLoughlin & Miller, 2008). SORL1 is involved in APP intracellular trafficking and has links to familial forms of AD increased AD susceptibility (Hung et al., 2021; Fazeli et al., 2024; Rovelet-Lecrux et al., 2021). No 4-node cliques were found in this network, suggesting these proteins partake in different cellular processes with APP as the epicentre.

3.4.2 Pathway highlights

Figure 3.7 and **Figure 3.8** showed an important process, the formation of Aβ fibrils. It is the accumulation of these fibrils that form the extracellular characteristic plaques seen in AD (Glenner & Wong, 1984). The ability to see the key interactors within the pathway provides great insight into the pathogenesis and pathophysiology of the disease. As previously stated, there are numerous counts of familial forms of AD (Bekris et al., 2010). Some of these, have mutations on enzymes/peptides involved in the processing of APP (i.e. PSEN1, PSEN2) or on

APP itself. Understanding the dysfunction of certain key players on this process, can lead to useful discoveries such as the characterisation of pathological mechanisms (e.g. tau hyperphosphorylation, disrupted paired cholinergic communication). This adds opportunities for pharmacological intervention, specifically intervention at the amyloidogenic pathway. Numerous attempts to attenuate the amyloidogenic process have been tested, such as inhibitors of the BACE1 enzyme. However, BACE1 therapies have not been successful so far due to undesired side effects, i.e. neuroinflammation (Das & Yan, 2019).

Furthermore, these figures provided information about additional components of Aβ fibrils such as serum amyloid P-component (SAP) homopentamer, apolipoprotein E isoform 4 (APOE-4), basement membrane-specific heparan sulphate proteoglycan core protein (HSPG2) and glycosaminoglycan (GAG) (Alexandrescu, 2005; Jupe, 2010). APOE has been previously discussed as a gene whose isoform 4 (APOE-4) increases the risk of developing late onset AD (Bekris et al., 2010).

Figure 3.9 explored the role of cholinesterases in hydrolysing acetylcholine into choline and acetate. In the Reactome interactive platform, two cholinesterase candidates could be revealed, these were AChE and BChE (Mahajan, 2008). These proteins have the ability to perform the same function although AChE has a faster rate of acetylcholine catalysis compared to BCHE (Weinstock & Groner, 2008). In this figure, AChE is located on the extracellular side of the plasma membrane, and it can act as an oligomeric ectoenzyme – forming monomers, dimers or tetramers (Velan et al., 1991). Additionally, the inhibitory action of AChEIs can be appreciated. These pharmacological agents (e.g. donepezil) can bind AChE and form reversible complexes, disrupting the hydrolysis of acetylcholine and increasing its bioavailability.

3.4.3 Limitations and future steps

Although the STRING and Reactome databases incorporate vast amounts of data and curated connections from very well-established databases (e.g. PubMed, BioGRID, KEGG, etc.), they are not perfect and cannot picture the complete and dynamic landscape of protein interactions and pathways. However, they do present a unique and simplified attempt to display the biological functioning of certain proteins and the networks they form.

Navigating Reactome's pathways can make it difficult to create a holistic picture of the function of a protein, as there can be several pathways that involve on individual protein. Furthermore, focusing on one single pathway can create an oversimplified view of a protein's metabolic role. Thus, it is necessary to explore the recent literature and the sources provided in each of the pathways to verify the biological roles of a protein. The same applies to the interaction information provided by STRING, as some of this can be outdated and more accurate mechanisms might have been recently uncovered.

Finally, future steps that build on the findings of this chapter include the exploration of the interactions between APP and γ-secretase, and APP and AChE. By using structural bioinformatics tools, future chapters will explore these interactions and their binding interfaces, and when appropriate, the disruptive effect of EOFAD mutations on APP.

4 Structural modelling of APP and its variants

4.1 Introduction

4.1.1 Protein folding and modelling algorithms

Protein folding is a fundamental process by which a linear chain of amino acids, synthesised by a ribosome, transforms into a functional three-dimensional structure. The transition from an unstable random coil to an ordered structure, known as the protein's native state, is driven by interactions among amino acids and is crucial for the protein's biological function (Nelson & Cox, 2013). The regulation of this process is complex, involving thermodynamic minimum energy states, help from molecular chaperons and protein quality checks – all of which had to undergo strong evolutionary influences (Díaz-Villanueva et al., 2015).

The 'protein folding problem' refers to the scientific difficulty in accurately predicting a protein's native structure from its sequence (Dill & MacCallum, 2012; Nassar et al., 2021). This challenge stemmed from the work by John Kendrew and Max Perutz, 1962 Nobel laureates in physiology/medicine, who respectively discovered the structure of the globular proteins myoglobin and haemoglobin (Kendrew et al., 1958; Perutz et al., 1960). Their work started the race for protein prediction despite apparent challenges. One of these, was highlighted by the Levinthal's paradox, which suggests that it would take an astronomical amount of time for a protein to sample all possible conformations (Levinthal, 1968). Despite this, thanks to Anfinsen's experiments (by which he received the 1972 Nobel Prize in Chemistry), it is known that a protein's native three-dimensional structure is determined by its one-dimensional amino acid sequence. This inspired the quest for biomathematical and computational methods to predict protein structures accurately (Anfinsen, 1973; Pauwels et al., 2007; Gambardella et al., 2022).

Bioinformatic modelling methods are generally categorised into template-based modelling (TBM) and template-free or *ab initio* approaches (Pearce et al., 2022). TBM relies on the availability of homologous structures in the PDB to guide the modelling process. The accuracy of TBM is highly dependent on the similarity between the target protein and the template, as well as the precision of the alignment between them. When homologous templates are available, TBM can produce highly accurate models. However, its utility is limited for proteins that lack similar structures in the PDB, necessitating alternative methods (Pearce et al., 2022). By contrast, a*b initio* modelling, or template-free modelling, addresses this limitation by not relying on pre-existing templates. Instead, it uses advanced energy functions and extensive conformational sampling techniques to predict protein structures from scratch (Pearce et al., 2022). Historically, the performance of *ab initio* methods has lagged behind TBM due to challenges in accurately simulating the protein folding process and the complexity of the energy landscapes involved. However, advancements in deep learning have revolutionised ab initio structure prediction, improving the prediction of

spatial restraints from sequence data, leading to more accurate contact and distance maps. These maps provide detailed spatial information that enhances the folding simulations, even for proteins lacking homologous templates. Despite these advancements, ab initio methods still face challenges, including lengthy simulation times and the need for extensive computational resources, particularly for larger proteins (Pearce et al., 2022).

AlphaFold2 is a template-free breakthrough AI system developed by DeepMind and it has demonstrated unprecedented accuracy in predicting protein structures in recent years (Jumper et al., 2021). Since its participation in CASP14 (Critical Assessment of Techniques for Protein Structure Prediction) in December 2020, AlphaFold2 revolutionised modelling algorithms, achieving a structure prediction accuracy far superior to any other method before and influencing other labs and teams around the globe (Callaway, 2020; Kryshtafovych et al., 2023). AlphaFold2 trains its neural network by providing the protein structures held in the PDB which allows the creation of multiple sequence alignments (MSA) that consider the evolutionary changes of protein relatives. This allows AlphaFold2 to do particularly well in predicting single protein chains, even the ones containing intrinsic disordered regions (IDRs). However, due to the lack of data about the structural impact of point mutations, AlphaFold can struggle in predicting these as well as proteins with few close relatives – also known as “orphan” proteins (Jumper et al., 2021). Despite these challenges, enhancements in training data and the incorporation of missense variant categorisation algorithms can improve AlphaFold2 to a newer more powerful version, furthering the understanding of protein folding and stability, particularly in the context of pathological missense mutations.

While correct folding is essential to ensure protein functionality, misfolding can lead to inactive proteins or, worse, proteins with toxic effects. This is the case of amyloids, which are proteins that when misfolded form insoluble amyloid fibrils. When these fibrils aggregate and form amyloid deposits, they can trigger pathological effects – typically referred as amyloidosis (Nelson & Cox, 2013; Chiti & Dobson, 2006; Nassar et al., 2021). Amyloids are linked to more than forty different human disorders (Graña-Montes & Ventura, 2015). Some of these include notorious neurodegenerative diseases, such as AD and Parkinson’s disease (Parakh & Atkin, 2016; Graña-Montes & Ventura, 2015).

Therefore, understanding what drives the formation of amyloids becomes highly relevant in the context of AD pathogenesis. This knowledge can provide insights into the mechanisms underlying AD and could open doors for the development of therapeutic strategies.

4.1.2 APP domains and mutations

APP is a 770 amino acid type-I transmembrane protein characterised by several conserved and characteristic regions that play crucial roles in its function and processing. The most notable regions include the E1 and E2 dimerisation domains, the Kunitz-type protease inhibitor (KPI) domain, and the YENPTY motif (Muller & Zheng, 2011; Chen et al., 2017).

The E1 dimerisation domain is located at the N-terminus between amino acids 28-189, and it comprises the growth factor-like domain (GFLD) and the copper-binding domain (CuBD). The GFLD is involved in neurite outgrowth and heparin binding, while the CuBD binds copper and zinc ions, essential for APP's biochemical activities. Following the E1 dimerisation domain, the KPI domain can be located between amino acids 291-341 and it is known for conferring protease inhibition. The E2 dimerisation domain (from amino acid 374-581), positioned between the KPI domain and the transmembrane region, is highly glycosylated and it participates in heparin binding, facilitating dimerisation and signal transduction. The C-terminal cytoplasmic tail, containing the YENPTY motif (from amino acid 757-762), is implicated in intracellular signalling pathways and interacts with multiple proteins, influencing APP's role in cellular functions such as transcription and synaptic formation (Muller & Zheng, 2011; Chen et al., 2017; APP|ALZFORUM, n.d.; Bateman et al., 2022).

Mutations in APP are predominantly located near the secretases' cleavage sites or within the transmembrane domain (TMD) from amino acid 699 to 725, particularly in exons 16 and 17. These mutations are significant because they directly impact the production and aggregation of Aβ peptides, a hallmark of AD. For instance, the "Swedish" mutations (K670N and M671L) (Mullan et al., 1992) and the "London" mutation (V717I) (Naruse et al., 1991) are well-documented for their role in increasing Aβ production, leading to EOFAD. The majority of pathogenic mutations cluster around the Aβ motif (form amino acid 672-720) (APP|ALZFORUM, n.d.; Kakuda et al., 2006), enhancing the proteolytic processing by β- and γ-secretases, which increases the generation of amyloidogenic Aβ42 peptides. These peptides aggregate to form fibrils and eventually plaques, contributing to the neurodegenerative processes observed in AD. Furthermore, familial mutations in *APP* gene have been linked to an additional pathology in the central nervous system (CNS) named cerebral amyloid angiopathy (CAA) (Sellal et al., 2016). In CAA, amyloid aggregates infiltrate the blood vessels of the brain and cause vascular disease, also referred as angiopathy, which can lead to haemorrhagic strokes as well as dementia (Kuhn & Sharman, 2022). CAA mutations also accelerate the formation of Aβ, although these mutations are mostly located in between secretases binding sites, further up from the Aβ motif (Biffi & Greenberg, 2011). An example would be the Dutch mutation (E693Q) (Levy et al., 1990), which is the most common cause of familial CAA (Maat-Schieman et al., 2005).

Understanding the structural implications of missense mutations in APP is crucial as they provide insights into the molecular mechanisms driving AD pathogenesis and offer potential targets for therapeutic intervention. To assess the structural three-dimensional impact, the selection of an appropriate protein structure predictive algorithm is required, followed by the quantitative bioinformatics analysis.

4.1.3 Aims

I aim to assess and select the best performing 3D modelling algorithm and use it to generate disease and healthy variant models of APP (see **2.6**). This will serve to compare APP's

structural changes at specific regions, and to inform of any potential disruptive events in APP's binding interfaces, across EOFAD, CAA and benign variant groups.

This analysis aims to provide new insights into EOFAD variants which could inform about pathological mechanisms and pharmacological protein targets

4.2 Specific methods

4.2.1 APP model assessment and selection

Multiple protein modelling algorithms were used to model the APP wild type (WT) – as no experimental structures were available in the PDB (**Figure 2.1**). These modelling algorithms were selected from the Critical Assessment of Structure Prediction 15th edition (CASP15) (Kryshtafovych et al., 2023) 'Regular targets' rankings which list the best performing teams in predicting single proteins structures and domains. From this list the following open-source algorithms were chosen: AlphaFold2, I-TASSER, IntFOLD7, trRosetta, trRosettaX, ReFOLD and SWISS-MODEL (Jumper et al., 2021; Baek et al., 2021; McGuffin et al., 2019; Yang et al., 2020; Wang et al., 2022; Waterhouse et al., 2018). The process to determine the most appropriate algorithm to model APP WT and selected variants was aided using DeepUMQA (Guo et al., 2022) – which computed lDDT scores – and the 'PSIPRED Workbench' (Buchan et al., 2024) – which predicted secondary structures and disordered regions (see **2.4.3** and **2.4.4**).

DeepUMQA (v3) allowed for the computation of per-residue lDDT by assessing interface residues accuracy (Guo et al., 2022) (see **2.4.3**). The lDDT measures obtained from DeepUMQA suggested that the three most accurate APP WT models were trRosetta, SWISS-MODEL and AlphaFold2 (**Table 4.1**). According to DeepUMQA quality scores, an lDDT score of 50 corresponds to an average quality model, and the top three APP WT models could be considered of medium/average quality.

To further evaluate the structural quality of the top three APP770 models (generated by trRosetta, SWISS-MODEL, and AlphaFold2) identified by DeepUMQA, secondary structure and disorder predictions were obtained using the PSIPRED and DISOPRED algorithms via the 'PSIPRED Workbench' (Buchan et al., 2024) (see **2.4.4**). PSIPRED (v4.0) was used to predict the distribution of α-helices, β-strands, and coil regions along the APP770 sequence (UniProt ID: P05067-1) (**Figure 4.1**), while DISOPRED (v3) identified intrinsically disordered regions (IDRs) and protein-binding disordered segments (Wright & Dyson, 1999; Chakrabarti & Chakravarty, 2022; Jamecna & Antonny, 2021) (**Figure 4.2**). The predicted structural features were compared against the corresponding regions in each model to assess secondary structure agreement and the placement of structured elements within IDRs. Qualitative inspection revealed that the trRosetta model deviated substantially from PSIPRED and DISOPRED predictions, showing multiple secondary structures embedded within disordered regions. Quantitative comparison confirmed this discrepancy, leading to the exclusion of the

trRosetta model from further analyses. Between the remaining two models, the SWISS-MODEL structure contained 52 amino acids with secondary structure elements located within IDRs, whereas the AlphaFold2 model showed only 38 such residues (**Figure 4.3**). Based on this improved agreement with predicted disorder regions and secondary structure patterns, the AlphaFold2 model was selected as the most accurate representation of the APP770 canonical structure for subsequent variant modelling and comparative analyses.

ColabFold (Mirdita et al., 2022), an open-source and searching-optimized algorithm, was used as an accessible implementation of AlphaFold2 to model APP WT (APP770) and the selected list of APP variants (see **2.4.1** & **2.6**).

Protein modelling algorithm	lDDT score
trRosetta	55.81
SWISS-MODEL	52.09
AlphaFold2	48.30
IntFOLD7	46.62
ReFOLD	46.61
I-TASSER	38.94
trRosettaX	31.46

Table 4.1 DeepUMQA lDDT scores. Table showing the lDDT (local Distance Difference Test) scores computed by DeepUMQA (Guo et al., 2022). The score ranges from 0 to 100, with a score of 50 considered to be an average quality model. The top three protein modelling algorithms are highlight in green.

4.2.2 Structural comparison tools

Predicted APP770 models and their variants (EOFAD, CAA, and benign) generated by ColabFold were imported into UCSF Chimera (v1.17.1) in '.pdb' format for structural inspection and comparative analysis (Pettersen et al., 2004) (see **2.5.1**). Chimera was used to visualise protein 3D models, measure structural features, and assess conformational variation across APP domains. Two key functionalities – 'Matchmaker' and 'Match→Align' – were employed for structural alignment and comparison, where each APP variant in **Table 2.1** was superimposed to the APP WT. 'Matchmaker' performed pairwise sequence alignment followed by structure-based superimposition, whereas 'Match→Align' generated structural alignments from the superimposed models obtained in the previous step.

'Matchmaker' calculated root mean square deviation (RMSD) across all superimposed α-carbons atom pairs (global RMSD). It also pruned all α-carbon pairs that are above 2.0 Å (default value) reporting the remaining the number α-carbon pairs below this threshold (atom pairs <2.0 Å). It also provided a sequence alignment score, which combines scores for residue similarity, secondary structure matching and gap penalties.

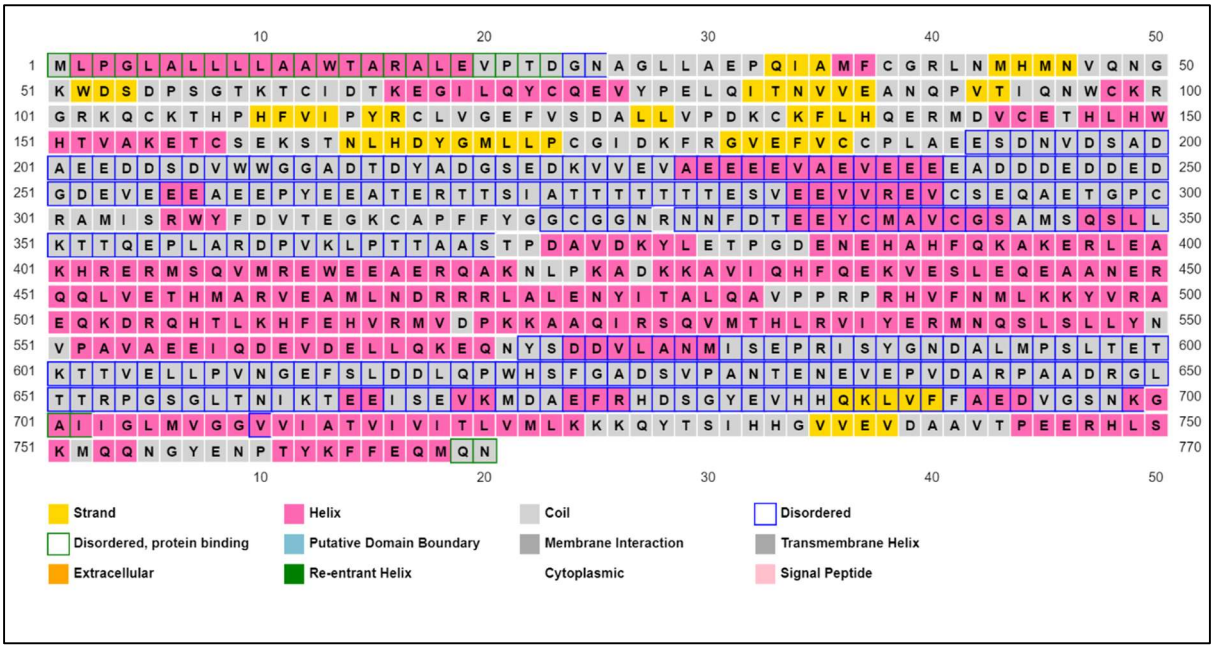

Figure 4.1 PSIPRED & DISOPRED analysis of APP amino acid sequence.
Figure showing the output of the PSIPRED and DISOPREAD algorithms which predict secondary structures and intrinsic disordered regions (IDRs) respectively. This prediction of the 770 amino acid APP isoform was used to compare and select the best APP model. The legend shows the secondary predictions and IDRs in different filling and border colours. There is some overlapping between the algorithms' output, however where IDRs prediction overweight secondary structure predictions (i.e. helices or strands).

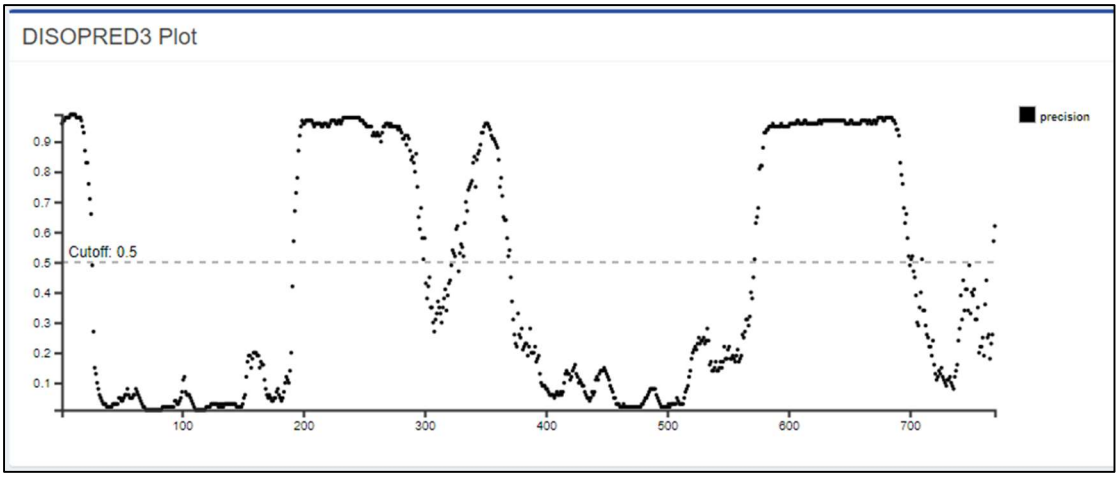

Figure 4.2 Intrinsic disordered region predictions of APP by DISOPRED.
Graph illustrating the prediction by DISOPRED of intrinsic disordered regions (IDRs) in the APP amino acid sequence (x-axis). On the y-axis the metric of precision can be seen. With a cutoff at 0.5, this score sets the limit where higher scored amino acids are labelled as intrinsically disordered.

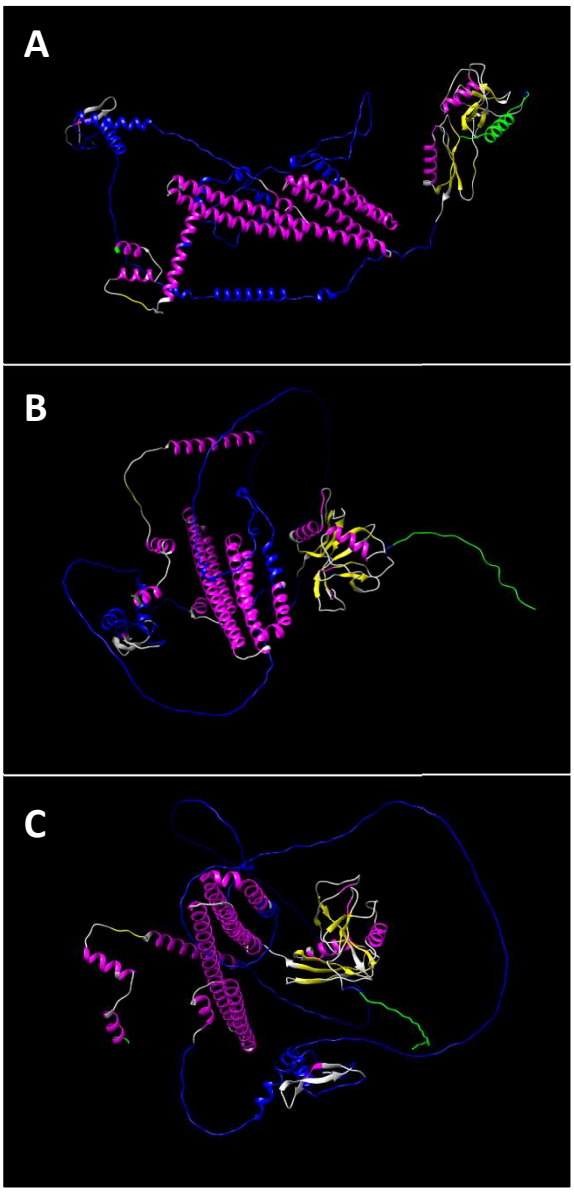

Figure 4.3 APP models incorporating PSIPRED and DISOPRED predictions.
Diagram showing the three best performing models of APP coloured according to PSIPRED and DISOPRED output (see **4.2.1**): trRosetta (A), SWISS-MODEL (B), AlphaFold2 (C). The secondary structure prediction is depicted in pink for α-helices, yellow for β-strands and grey for coil regions. Overlapping these colours, intrinsic disordered regions (IDRs) prediction are depicted in blue, except protein-binding IDRs which are shown in green. IDRs colours supersede helices and strands (pink and yellow), as within IDRs there cannot be a determined secondary structure. The worse model is at the top and the best one is at bottom.

'Match→Align' reports an 'overall RMSD' restricted to structurally aligned α-carbon pairs within 5.0 Å (atom pairs <5.0 Å). Furthermore, it outputted metrics such as the Structural Distance Measure (SDM) (from 'Match→Align'), which quantifies dissimilarity based on α-carbon spatial positions independently of sequence alignment (Johnson et al., 1990), and the Q-score (from 'Match→Align'), which integrates RMSD and alignment length to provide a normalised similarity index ranging from 0 (no similarity) to 1 (identical structures) (Krissinel & Henrick, 2004).

The output metrics provided by 'Match→Align' were not when global RMSD values (from 'Matchmaker') were below 2.0 Å for all variant comparisons, as its higher distance threshold (<5.0 Å) would yield redundant results without adding analytical value. When the 'Match→Align' tool was applied, the sequence alignment score was excluded from analysis, as it primarily reflects residue correspondence (sequence similarity) rather than structural deviation. Metrics such as SDM and Q-score were more informative for assessing three-dimensional structural similarity and conformational changes and were therefore prioritised. RMSD values below 2.0 Å were considered indicative of high structural similarity (Castro-Alvarez et al., 2017). These combined metrics provided complementary quantitative evidence to identify structural deviations among EOFAD, CAA, and benign APP variants.

To assess the conformational changes of individual domains, atoms where highlighted using the 'selection'. Domain annotations were obtained from UniProt/'Family & Domains' (UniProt ID: P05067) (see **2.2.1**) and from Alzforum APP scheme (under 'Mutations databse', see **2.2.4**) (**(page** 115) Figure S9.1). All other atoms (not part of a domain) were removed using the 'deletion' tool. Isolating domains in this manner allowed for the calculation of localised output metrics by 'Matchmaker' and 'Match→Align'. This process was repeated for each of the domains and for each of the APP models (WT and variants).

4.2.3 Statistical analysis

Statistical analysis was employed to compare structural domains across APP WT and APP variant (see **Table 2.1**) following the defined statistical framework in **2.7.**

4.3 Results

4.3.1 APP full structure comparison

First, comparisons between the full-length (770 amino acid) structures of each APP variant and the APP WT were performed (**Table 4.2, Figure 4.4A**). Differences in the averages between groups for each column in the table were assessed (one-way ANOVA/Kruskal-Wallis). No significant differences were found; however, a few outliers were present on the

data, specifically in the number of ‘atom pairs <2.0 Å’, in the SDM and ‘overall RMSD’ (Tukey’s fences, k=1.5).

Additionally, using the ‘Match->Align’ interactive sequence window, aligned amino acids were identified the two APP structures being compared. This allowed for the identification of aligned domains between the full-length structures. Most variants had a major alignment with APP WT at the E2 domain. Only a few variants contained a major alignment in the E1 domain (marked ‘*’ in **Table 4.2**). The A673T variant had an alignment in both E1 and E2 domains (marked ‘**’ in **Table 4.2**).

4.3.2 E1 domain comparison

Table 4.3 focuses on the E1 dimerisation domain of APP, ranging from amino acid 28 to 189 – 162 amino acids long (**Figure 4.4B**). Statistical differences between the averages of groups in each column were calculated. No statistically significant differences were found (one-way ANOVA/Kruskal-Wallis). However, a few outliers were present in the data, specifically in the ‘global RMSD’ and ‘sequence alignment score’ columns (Tukey’s fences, k=1.5). These outliers occurred in variants from the EOFAD group. The number ‘atom pairs <2.0 Å’ were 162 for most of the variants.

4.3.3 KPI domain comparison

Table 4.4 focuses on the KPI domain of APP, ranging from amino acid 291 to 341 – 51 amino acids long (**Figure 4.4C**). No statistically significant differences between the groups were found (one-way ANOVA/Kruskal-Wallis). However, a few outliers were present on the data, specifically in the ‘global RMSD’ column (Tukey’s fences, k=1.5). These outliers occurred in variants from the EOFAD group. The number ‘atom pairs <2.0 Å’ was consistently 51 across all the variants.

4.3.4 E2 domain comparison

Table 4.5 focuses on the E2 dimerisation domain of APP, ranging from amino acid 374 to 581 – 208 amino acids long (**Figure 4.4D**). No statistically significant differences between the groups were found (one-way ANOVA/Kruskal-Wallis). However, one outlier was identified in the EOFAD group under the ‘global RMSD’ column (Tukey’s fences, k=1.5). The number of ‘atom pairs <2.0 Å’ showed consistency alternating between 207 and 208 in almost all cases.

		MatchMaker		Match -> Align			
Variant	Type	Atom pairs <2.0 Å	Global RMSD (Å)	Atom pairs <5.0 Å	SDM score	Q-score	Overall RMSD (Å)
I716V	EOFAD	220	34.719	282	61.5	0.107	1.525
K670N_M671L	EOFAD	213	38.718	261	63.7	0.092	1.483
K724N	EOFAD	215	31.862	258	59.0	0.095	1.290
L723P	EOFAD	203	36.347	261	58.6	0.097	1.290
T714A*	EOFAD	163	33.744	292	74.5	0.096	2.107
T714I	EOFAD	207	36.283	260	62.3	0.093	1.426
V715M*	EOFAD	156	29.329	279	71.1	0.094	1.881
V717F	EOFAD	219	34.439	276	60.4	0.104	1.449
V717G	EOFAD	216	30.736	265	61.8	0.096	1.435
V717I	EOFAD	217	34.508	267	59.4	0.100	1.356
V717L	EOFAD	199	35.026	282	65.3	0.102	1.673
D694N	CAA	218	35.533	267	60.2	0.099	1.386
E693K	CAA	214	39.470	243	57.5	0.087	1.148
E693Q	CAA	213	31.613	280	66.1	0.100	1.694
L705V	CAA	211	29.719	279	64.7	0.101	1.630
A201V*	Benign	158	34.195	260	72.8	0.083	1.821
A235V	Benign	214	30.955	287	66.2	0.104	1.742
A479S	Benign	201	39.142	251	62.9	0.087	1.394
A673T**	Benign	198	28.618	295	66.7	0.108	1.811
E599K	Benign	211	27.674	272	65.7	0.096	1.627
V562I	Benign	202	39.336	272	61.0	0.101	1.448

Table 4.2 APP full structure comparison: APP WT vs EOFAD, CAA and benign variants.
Table containing data outputs of the 'Matchmaker' and 'Match->Align' functionalities, which were applied to compare the full-length (770 amino acids) APP WT against each superimposed individual variant (full-length structures) (see **4.2.2**). Most superimposed structures aligned well at the E2 domain of APP, except those with the '*' which aligned well at the E1 domain instead. Structures with '**' aligned well at both E1 and E2 domains. Variants belonged to one of the following groups: EOFAD (green), CAA (yellow) or benign (blue) (see **2.6**). Group averages were compared between groups (one-way ANOVA/Kruskal-Wallis) for each column with numerical data. No significant differences between the groups' averages were found, but some outliers were identified (Tukey's fences, k=1.5) (orange).

		MatchMaker		
Variant	Type	Atom pairs <2.0 Å	Global RMSD (Å)	Sequence alignment score
I716V	EOFAD	162	0.211	876.0
K670N_M671L	EOFAD	162	0.210	876.0
K724N	EOFAD	162	0.172	876.0
L723P	EOFAD	162	0.201	876.0
T714A	EOFAD	162	0.389	868.8
T714I	EOFAD	162	0.292	872.4
V715M	EOFAD	160	0.626	868.8
V717F	EOFAD	162	0.220	876.0
V717G	EOFAD	162	0.197	876.0
V717I	EOFAD	162	0.168	876.0
V717L	EOFAD	162	0.159	876.0
D694N	CAA	162	0.159	876.0
E693K	CAA	162	0.222	876.0
E693Q	CAA	162	0.226	876.0
L705V	CAA	160	0.609	872.4
A201V	Benign	162	0.390	868.8
A235V	Benign	162	0.346	872.4
A479S	Benign	162	0.213	876.0
A673T	Benign	162	0.395	872.4
E599K	Benign	162	0.154	876.0
V562I	Benign	162	0.195	876.0

Table 4.3 APP E1 dimerasation domain comparison: APP WT vs EOFAD, CAA and benign variants.

Table containing data outputs of the 'Matchmaker' functionality, which were applied to analyse conformational changes in the E1 dimerasation domain of APP (from amino acid 28 to 189). For each variant, this domain was superimposed with the equivalent domain in the APP WT (see **4.2.2**). Variants belonged to one of the following groups: EOFAD (green), CAA (yellow) or benign (blue) (see **2.6**). Group averages were compared between groups (one-way ANOVA/Kruskal-Wallis) for each column with numerical data. No significant differences between the groups' averages were found, but some outliers were identified (Tukey's fences, k=1.5) (orange).

		MatchMaker		
Variant	Type	Atom pairs <2.0 Å	Global RMSD (Å)	Sequence alignment score
I716V	EOFAD	51	0.087	284.5
K670N_M671L	EOFAD	51	0.046	284.5
K724N	EOFAD	51	0.056	284.5
L723P	EOFAD	51	0.066	284.5
T714A	EOFAD	51	0.170	284.5
T714I	EOFAD	51	0.071	284.5
V715M	EOFAD	51	0.139	284.5
V717F	EOFAD	51	0.056	284.5
V717G	EOFAD	51	0.053	284.5
V717I	EOFAD	51	0.071	284.5
V717L	EOFAD	51	0.047	284.5
D694N	CAA	51	0.089	284.5
E693K	CAA	51	0.047	284.5
E693Q	CAA	51	0.049	284.5
L705V	CAA	51	0.173	284.5
A201V	Benign	51	0.177	284.5
A235V	Benign	51	0.193	284.5
A479S	Benign	51	0.053	284.5
A673T	Benign	51	0.161	284.5
E599K	Benign	51	0.057	284.5
V562I	Benign	51	0.071	284.5

Table 4.4 APP KPI domain comparison: APP WT vs EOFAD, CAA and benign variants.
Table containing data outputs of the 'Matchmaker' functionality, which were applied to analyse conformational changes in the KPI domain of APP (from amino acid 291 to 341). For each variant, this domain was superimposed with the equivalent domain in the APP WT (see **4.2.2**). Variants belonged to one of the following groups: EOFAD (green), CAA (yellow) or benign (blue) (see **2.6**). Group averages were compared between groups (one-way ANOVA/Kruskal-Wallis) for each column with numerical data. No significant differences between the groups' averages were found, but some outliers were identified (Tukey's fences, k=1.5) (orange).

		MatchMaker		
Variant	Type	Atom pairs <2.0 Å	Global RMSD (Å)	Sequence alignment score
I716V	EOFAD	207	0.308	1105.5
K670N_M671L	EOFAD	207	0.301	1105.5
K724N	EOFAD	208	0.371	1105.5
L723P	EOFAD	207	0.389	1105.5
T714A	EOFAD	208	0.469	1105.5
T714I	EOFAD	207	0.280	1105.5
V715M	EOFAD	207	0.598	1105.5
V717F	EOFAD	208	0.348	1105.5
V717G	EOFAD	207	0.350	1105.5
V717I	EOFAD	207	0.387	1105.5
V717L	EOFAD	207	0.360	1105.5
D694N	CAA	207	0.331	1105.5
E693K	CAA	208	0.254	1105.5
E693Q	CAA	207	0.334	1105.5
L705V	CAA	208	0.436	1105.5
A201V	Benign	208	0.516	1105.5
A235V	Benign	208	0.497	1105.5
A479S	Benign	207	0.409	1103.4
A673T	Benign	205	0.706	1098.3
E599K	Benign	207	0.301	1105.5
V562I	Benign	207	0.377	1104.8

Table 4.5 APP E2 dimerasation domain comparison: APP WT vs EOFAD, CAA and benign variants.

Table containing data outputs of the 'Matchmaker' functionality, which were applied to analyse conformational changes in the E1 dimerasation domain of APP (from amino acid 374 to 581). For each variant, this domain was superimposed with the equivalent domain in the APP WT (see **4.2.2**). Variants belonged to one of the following groups: EOFAD (green), CAA (yellow) or benign (blue) (see **2.6**). Group averages were compared between groups (one-way ANOVA/Kruskal-Wallis) for each column with numerical data. No significant differences between the groups' averages were found (one-way ANOVA/Kruskal-Wallis). Additionally, one outlier was identified (Tukey's fences, k=1.5) (orange).

4.3.5 Aβ peptide comparison

Table 4.6 focuses on the Aβ49 peptide of APP, ranging from amino acid 672 to 720 – 49 amino acids long (**Figure 4.4E**). No statistically significant differences between the groups were found; however, the 'Q-score' column came close (one way ANOVA, p=0.065). After adjusting for multiple comparisons, no pair of groups came close to statistical significance (Tukey HSD, Bonferroni-adjusted α=0.017; EOFAD-CAA: p=0.990; EOFAD-benign: p=0.073; CAA-benign: p=0.146). Finally, a few outliers were present on the data, specifically in the 'global RMSD' and 'SDM score' columns (Tukey's fences, k=1.5). These outliers occurred in variants from the EOFAD group.

4.3.6 TMD comparison

Table 4.7 focuses on the TMD of APP, ranging from amino acid 699 to 725 – 27 amino acids long (**Figure 4.4F**). No statistically significant differences between the groups were found. The the 'sequence alignment score' column could not be compared across groups as only the EOFAD group showed some variation across variants. Additionally, a few outliers were present on the data, specifically in the 'global RMSD' and 'sequence alignment score' columns (Tukey's fences, k=1.5). These outliers occurred in variants from the EOFAD group. The number 'atom pairs <2.0 Å' was consistently 27 across all the variants.

4.4 Discussion

4.4.1 Structural analysis of APP regions

As seen in **Figure 4.4**, multiple superimposed regions of APP (and the full-length structure) were analysed. The main objective of this chapter was to identify structural differences between pathological APP variants (i.e. EOFAD and CAA) and benign APP variants (and APP WT) that could inform of distinct pathological mechanisms in APP-involving diseases. All variants were individually superimposed against the WT structure, and multiple metrics were outputted and assessed (see **4.2.2**).

Table 4.2 provided a first insight into full length structural analysis of APP (**Figure 4.4A**). There were no significant differences between the groups' metrics, but some curious outputs were obtained. Using the 'Match->Align' function allowed to locate the physically close (<0.5 Å) aligned amino acids pairs were located. Interestingly, most close alignments took place around the E2 dimerisation domain (amino acids 374-581). This could suggest that the E2 dimerisation domain plays an important structural and possibly functional role in the stability of APP, as the superimposition of the structures (variant + WT) relied constantly

		MatchMaker		Match -> Align			
Variant	Type	Atom pairs <2.0 Å	Global RMSD (Å)	Atom pairs <5.0 Å	SDM score	Q-score	Overall RMSD (Å)
I716V	EOFAD	25	18.338	32	33.4	0.361	1.281
K670N_M671L	EOFAD	11	15.881	25	64.6	0.163	2.318
K724N	EOFAD	28	12.796	35	32.0	0.425	1.344
L723P	EOFAD	22	16.905	32	47.4	0.297	1.979
T714A	EOFAD	8	15.914	16	90.8	0.064	2.447
T714I	EOFAD	24	17.205	27	41.3	0.251	1.378
V715M	EOFAD	17	18.275	24	36.6	0.217	0.976
V717F	EOFAD	17	4.903	38	53.4	0.339	2.641
V717G	EOFAD	25	12.746	28	29.5	0.300	0.898
V717I	EOFAD	23	15.077	26	35.7	0.250	1.061
V717L	EOFAD	24	4.914	38	47.7	0.379	2.302
D694N	CAA	26	7.778	28	38.0	0.276	1.287
E693K	CAA	24	20.681	29	36.4	0.297	1.269
E693Q	CAA	23	5.516	35	44.8	0.353	2.002
L705V	CAA	20	24.190	23	30.9	0.210	0.671
A201V	Benign	14	13.777	21	70.3	0.120	2.186
A235V	Benign	13	12.388	25	45.1	0.213	1.415
A479S	Benign	12	11.157	21	70.4	0.120	2.189
A673T	Benign	21	21.742	23	30.8	0.210	0.664
E599K	Benign	6	26.960	20	87.6	0.087	2.858
V562I	Benign	24	27.878	27	34.3	0.270	1.058

Table 4.6 APP's Aβ49 peptide comparison: APP WT vs EOFAD, CAA and benign variants.
Table containing data outputs of the 'Matchmaker' and 'Match->Align' functionalities, which were applied to analyse conformational changes in the Aβ49 peptide of APP (from amino acid 672 to 720). For each variant, this region was superimposed with the equivalent region in the APP WT (see **4.2.2**). Variants belonged to one of the following groups: EOFAD (green), CAA (yellow) or benign (blue) (see **2.6**). Group averages were compared between groups (one-way ANOVA/Kruskal-Wallis) for each column with numerical data. No significant differences between the groups' averages were found (one-way ANOVA/Kruskal-Wallis), although the 'Q-score' column was close (one-way ANOVA, p=0.065) After post-hoc testing, no pair of groups came close to statistical significance for this column (Tukey HSD, Bonferroni-adjusted α=0.05, EOFAD-CAA: p=0.990; EOFAD-benign: p=0.073; CAA-benign: p=0.146). Additionally, some outliers were identified (Tukey's fences, k=1.5) (orange).

		MatchMaker		
Variant	Type	Atom pairs (<2.0 Å)	Global RMSD (Å)	Sequence alignment score
I716V	EOFAD	27	0.325	132.8
K670N_M671L	EOFAD	27	0.178	133.5
K724N	EOFAD	27	0.235	130.0
L723P	EOFAD	24	1.553	117.8
T714A	EOFAD	27	0.692	130.0
T714I	EOFAD	27	0.446	129.3
V715M	EOFAD	27	0.442	131.4
V717F	EOFAD	27	0.321	130.0
V717G	EOFAD	27	0.186	128.6
V717I	EOFAD	27	0.330	132.8
V717L	EOFAD	27	0.252	131.4
D694N	CAA	27	0.255	133.5
E693K	CAA	27	0.228	133.5
E693Q	CAA	27	0.312	133.5
L705V	CAA	27	0.617	131.4
A201V	Benign	27	0.409	133.5
A235V	Benign	27	0.771	133.5
A479S	Benign	27	0.155	133.5
A673T	Benign	27	0.564	133.5
E599K	Benign	27	0.545	133.5
V562I	Benign	27	0.204	133.5

Table 4.7 APP's TMD comparison: APP WT vs EOFAD, CAA and benign variants.
Table containing data outputs of the 'Matchmaker' functionality, which were applied to analyse conformational changes in the APP's TMD of APP (from amino acid 699 to 725). For each variant, this region was superimposed with the equivalent region in the APP WT (see **4.2.2**). Variants belonged to one of the following groups: EOFAD (green), CAA (yellow) or benign (blue) (see **2.6**). Group averages were compared between groups (one-way ANOVA/Kruskal-Wallis) for each column with numerical data. No significant differences between the groups' averages were found (one-way ANOVA/Kruskal-Wallis). Additionally, one outlier was identified (Tukey's fences, k=1.5) (orange).

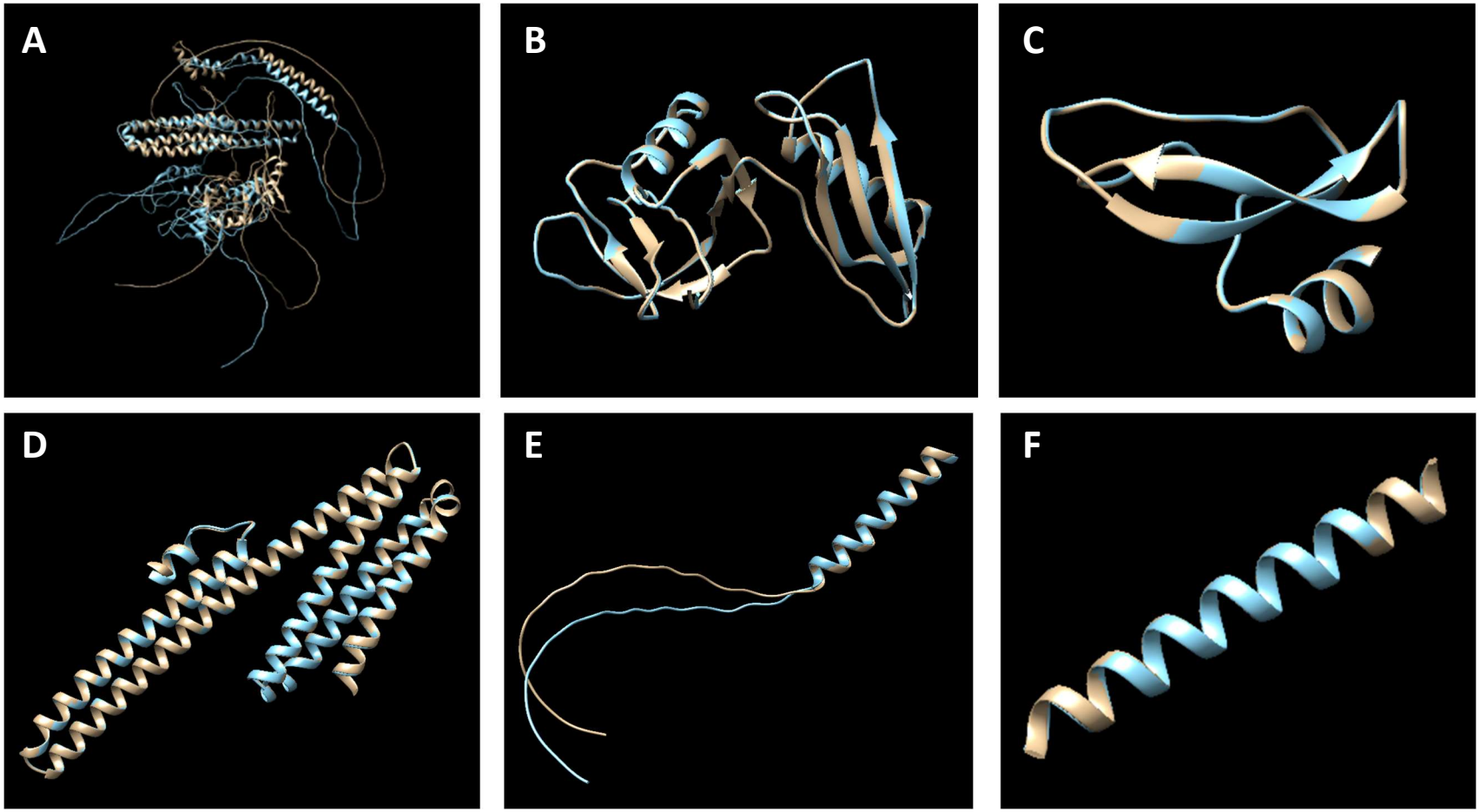

Figure 4.4 Superimposed APP structures and domains studied.
Figure showing APP's wild type model (light orange) aligned with the CAA variant of APP D694N (light blue) across multiple regions of interest. This process (wild type against variant) was repeated for all 21 APP variants. To superimpose structures, the 'Matchmaker' tool was used. Legend: A) Full APP structure (770 amino acids), B) E1 dimerisation domain (from amino acid 28 to 189), C) Kunitz protease inhibitor (KPI) domain (from amino acid 291 to 341), D) E2 dimerisation domain (from amino acid 374 to 581), E) Aβ49 peptide (from amino acid 672 to 720), F) TMD (from amino acid 699 to 725).

on that domain. This is supported by the fact that the E2 domain is conserved across homologs from the same family (Muller & Zheng, 2011). However, in some instances the E1 domain was the one preferred by the superimposition algorithm. This was the case for T714A (EOFAD), V715M (EOFAD) and A201V (benign). The A673T mutant, considered a protective variant, displayed both the E1 and E2 dimerisation domains as close alignments (<0.5 Å) – being the only variant to do so (Guyon et al., 2020). This highlights the ability of the A673T variant in maintaining both domains structurally close to the WT, despite having a mutation within the Aβ peptide range – usually associated with pathogenicity. The rest of the cases with a major alignment in the E1 dimerisation domain (i.e. T714A, V715M and A201V), were outliers on at least one column, suggesting the difference in the alignment of the structures might have impacted all other metrics. Curiously, this was not the case for A673T, which seemed to be within the normal range of the column measurements (Tukey's fences, k=1.5).

When isolating the E1 dimerisation domain (**Table 4.3**, **Figure 4.4B**), the T714A (EOFAD) and V715M (EOFAD) variants were outliers under the 'global RMSD' and 'sequence alignment score' columns (Tukey's fences, k=1.5). This meant that these variants were less aligned with the WT compared to the other variants in the EOFAD group. Even though they stood out on the EOFAD group, it might not translate to being different than the values from the benign group. In fact, some variants in the benign group had equivalently high 'global RMSD' values and low 'sequence alignment scores' – except for V715M whose 'global RMSD' value still stood out above the benign variants.

T714A and V715M variants produced a similar output on the KPI domain – this time being outliers under the 'global RMSD' column only (Tukey's fences, k=1.5) (**Table 4.4**, **Figure 4.4C**). In an almost identical way, these outliers stood out in the EOFAD group but are not higher than some 'global RMSD' values under the benign group.

The V715M variant was the only outlier under the 'global RMSD' column (Tukey's fences, k=1.5) in **Table 4.5** – corresponding to the E2 dimerisation domain region (**Figure 4.4D**) with a value of 0.598 Å. The recurrent theme of standing out under the EOFAD group but being of 'normal' range for the benign group was true again in this case. The A673T benign variant was of particular interest, as this one had a 'global RMSD' value of 0.706 Å. These values are not high or troublesome as the range for being structurally different is usually 2.0 Å (Castro-Alvarez et al., 2017). However, it still raises some questions regarding the context of the superimpositions of the benign group compared to the EOFAD one.

In **Table 4.6**, which represent the Aβ49 peptide (**Figure 4.4E**), T714A was an outlier under the 'SDM score' column and the EOFAD mutations V717L and V717F were outliers under the 'global RMSD' column. The 'SDM score' is related to phylogenetic and structural identities, and the T714A stands out amongst the EOFAD mutations for having a higher (worse) score (Johnson et al., 1990). Importantly, this variant also had relatively fewer 'atom pairs aligned', which suggests a comparatively poor alignment. Curiously, the V717L and V717F EOFAD variants stood out for having a lower 'global RMSD' than the rest of variants (4.914 Å and 4.903 Å respectively) even amongst benign and CAA groups. They also had the most 'atom pairs aligned' suggesting these EOFAD variants were particularly well aligned with the WT

Aβ49 peptide. Furthermore, the difference in the averages between the EOFAD and benign groups was close to being statistically significant for the 'atom pairs aligned' and 'Q-score' columns (Tukey HSD, Bonferroni-adjusted α=0.017; 'atom pairs aligned': p=0.087; 'Q-score': p=0.073). The EOFAD mutations appeared to get a higher number of 'atom pairs aligned' which influenced the 'Q-score' outputs (Krissinel & Henrick, 2004). It is interesting to see the EOFAD mutations better aligning with the WT Aβ49 peptide, as almost all these variants had their missense mutations within this specific region (670-720), which theoretically would cause worse alignments.

Finally, in **Table 4.7**, corresponding to the TMD (**Figure 4.4F**), the L723P (EOFAD) variant was an outlier under the 'global RMSD' and 'sequence alignment score' columns. This variant stands out for having a lower number of 'atom pairs <2.0 Å' compared to all other consistent variants. This variant followed the 'normal' rationale of having a missense mutation within a studied region, that later leads to fewer atoms pairs, a higher 'global RMSD' and a lower 'sequence alignment score'. Its 'global RMSD' value is significantly higher than all other variants in other groups, suggesting the leucine to proline change is quite disruptive in the structure of the TMD of APP.

The EOFAD variants T714A and V715M seemed to recurrently be outliers in the EOFAD group. Firstly, the impact of a missense mutation threonine to alanine (T714A) could be very detrimental for the protein function and stability. Threonine contains a hydroxyl group and is therefore able to make hydrogen bonds (HBs), an alanine substitute instead would lose this ability as this one lacks a functional group (Shen & Sergi, 2021). This means that the protein region would become more hydrophobic and could have an impact on the region structure and any interactions that take place there (Dyson et al., 2006). For instance, some crucial amyloidogenic cleavages of APP take place on the Aβ49 (position 670 to 720) peptide region, and progressively – in a tripeptide style – it catches up to position 714-715, where a secretase cuts the peptide at this position to form Aβ43. This peptide is the predecessor of Aβ40, and perhaps a mutation at position 714 or 715 could stop further processing, leaving Aβ43 as the final product or, at least, increasing its production rate. Aβ43 is toxic, and like Aβ42, is very likely to form fibrils and later plaques (Saito et al., 2011). Based on this reasoning, a missense mutation valine to methionine at position 715 (V715M) could be equally problematic. Methionine has a longer side chain compared to valine due to the sulphur atom and its methyl group, making methionine bulkier. This steric change can lead to slower chemical reactions – such as the mentioned secretase processing – also known as steric hindrance. It is worth considering that these missense mutations occur within the TMD of APP, which is a flexible but tightly packed helical region (Barrett et al., 2012). This means that changes in hydrophobicity and conformation can have an impact on APP transport and processing.

4.4.2 Limitations and future steps

One of the main limitations is maintaining a high accuracy across all protein models. An AlphaFold2-based method was chosen, ColabFold, to model 21 APP mutants and a WT protein. According to Magana and Kovalevskiy (2024), AlphaFold2 can struggle to predict the structures of proteins with point mutations due to the lack of training data. However, based on an accuracy assessment study by Akdel et al. (2022), for regions with high level of confidence (pLDDT > 0.9) AlphaFold2 produces stability change predictions comparable to experimental models. In the APP models, these regions of high confidence do exist, e.g. the E1 and E2 dimerisation domains, the KPI domain and the TMD. This improved accuracy on high confidence regions can explain why some EOFAD variants had higher numbers of 'atom pairs <5.0 Å ' aligned compared to benign variants, as many EOFAD mutations occur at the TMD (a region of high confidence) contrasting with some benign mutations which are found within IDRs. Additionally, Magana and Kovalevskiy (2024) stated that AlphaFold2 can have a lack of orientation for transmembrane regions. In this chapter, the TMD was studied in isolation (see **4.3.6**) apart from the initial whole protein analysis (see **4.3.1**). Hence, a dynamic study within a membrane was not performed.

Lastly, AlphaFold2 and ColabFold did well in predicting the location of IDRs, as corroborated by Tunyasuvunakool et al. (2021) – regardless of ColabFold having less computational power than AlphaFold2. Thus, AlphaFold2-based algorithms were considered to be accurate protein folding predictors, which can be useful to predict changes in structure stability caused by point mutations in high confidence models.

Another limitation involves low statistical power of the analyses due to small sample sizes. To address this, one potential improvement would be to unify the EOFAD and CAA groups into a single 'pathological group,' as both represent disease-associated variants. This would yield a larger combined sample size and increase the power of the analysis. Additionally, by increasing the number of benign samples to match the pathological group, aiming for two groups of approximately 15 samples each, the tests would be more balanced, potentially allowing for more robust and reliable statistical comparisons. This approach would help mitigate the limitations posed by small sample sizes, though it would require careful consideration of whether the EOFAD and CAA variants can be appropriately combined into a single category.

Considering the findings in this chapter, the next step would be to explore these mutations in a PPI context. In the following chapters, the APP-PSEN1 and APP-AChE interactions will be explored.

5 APP processing by γ-secretase

5.1 Introduction

5.1.1 APP proteolytic processing and mechanisms of γ-secretase cleavage

The amyloidogenic pathway of APP processing is a critical mechanism underlying the pathogenesis of AD. APP can be proteolytically processed by multiple secretases at various critical sites, initiating pathways that have vastly different outcomes (Coronel et al., 2018; Chasseigneaux & Allinquant, 2011) **Figure 5.1**).

In the amyloidogenic pathway, cleavage by β-secretase occurs at the juxtamembrane region (JMR), which is situated between the E2 and the transmembrane domain (TMD), and it produces a soluble APP fragment (sAPPβ) and a membrane-tethered 99-amino-acid C-terminal fragment (C99) (Chen et al., 2017). Following this, the γ-secretase complex mediates further intramembrane proteolysis at multiple sites. This sequential cleavage primarily occurs at the ε-cleavage sites, specifically after Leu49 or Thr48, producing Aβ49 or Aβ48 and the APP intracellular domain (AICD) which can act as a transcription factor (Chow et al., 2009; Bukhari et al., 2017; APP|ALZFORUM, n.d.). These initial Aβ products are further trimmed in increments of three amino acids to generate shorter Aβ peptides: Aβ49 → Aβ46 → Aβ43 → Aβ40; and Aβ48 → Aβ45 → Aβ42. The main amyloid species formed through these pathways are Aβ40 and Aβ42, which are predominant in amyloid plaques found in AD patients' brains (Hur, 2022). Notably, alternative minor pathways can also generate other Aβ species such as Aβ38, which can originate from Aβ42 or Aβ43, highlighting the complexity of γ-secretase activity (Olsson et al., 2014). The mechanism of γ-secretase cleavage involves specific interactions within its active site, where there are three S' pockets ready to accommodate the substrate in a tripeptide style, at positions P1', P2', and P3' (Bolduc et al., 2016) (**Figure 5.2**). The structure-function relationship within these S' pockets dictate the cleavage pattern and efficiency, influenced by the lipid environment of the membrane and the presence of cholesterol, which can modulate enzyme activity.

On the other hand, the non-amyloidogenic pathway is initiated by α-secretase cleavage within the Aβ sequence, which prevents the formation of amyloidogenic peptides. Cleavage by α-secretase releases a soluble APP fragment (sAPPα) and leaves behind an 83-amino-acid C-terminal fragment (C83) that is further processed by γ-secretase to produce the non-toxic P3 peptide and the AICD which, in this pathway, gets rapidly degraded (Bukhari et al., 2017; Chen et al., 2017) (**Figure 5.1**). The differential processing by α- and β-secretases is influenced by the conformational flexibility and trafficking of APP within the cellular environment (van der Kant & Goldstein, 2015).

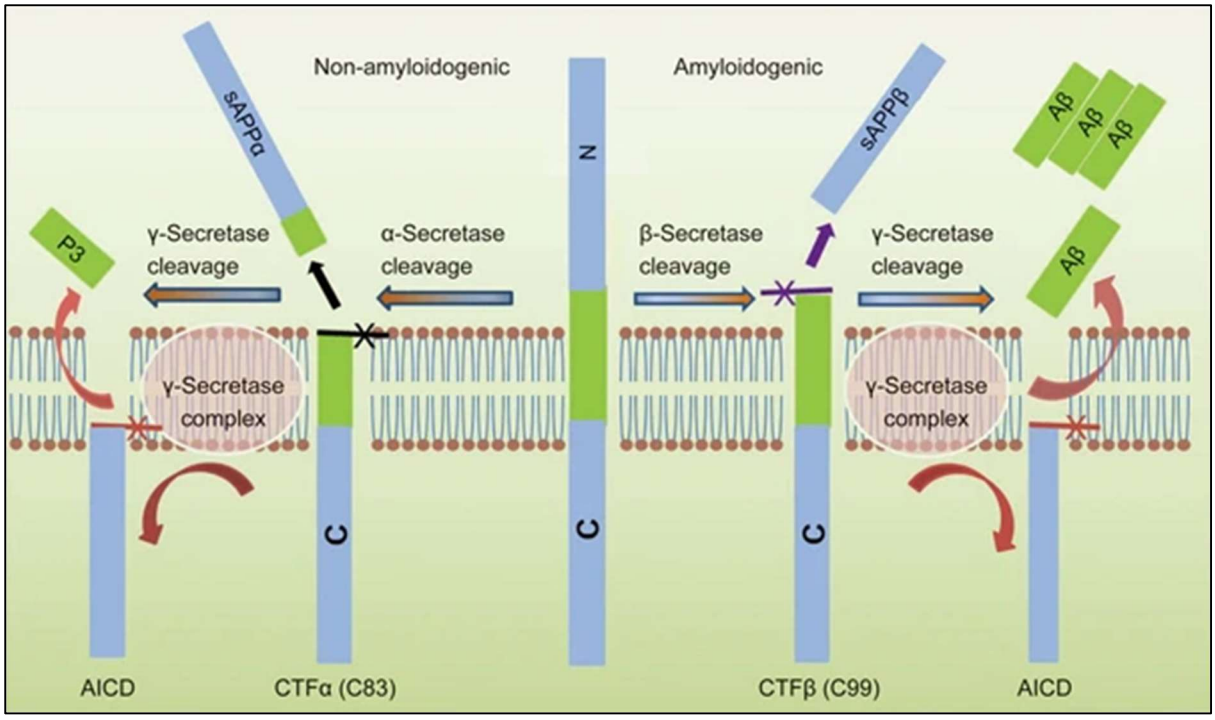

Figure 5.1 Amyloidogenic and non-amyloidogenic pathways of APP.
This diagram shows the two main processing pathways of APP. The amyloidogenic pathway (right) leads to the formation of soluble APPβ fragments (sAPPβ), Aβ peptides and the APP intracellular domain (AICD). As shown above, Aβ peptides tend to oligomerise, eventually forming fibrils and contributing to plaque formation. The non-amyloidogenic pathway (left) leads to the formation of soluble APPα fragments (sAPPα), P3 peptides and the AICD (Chen et al., 2017).

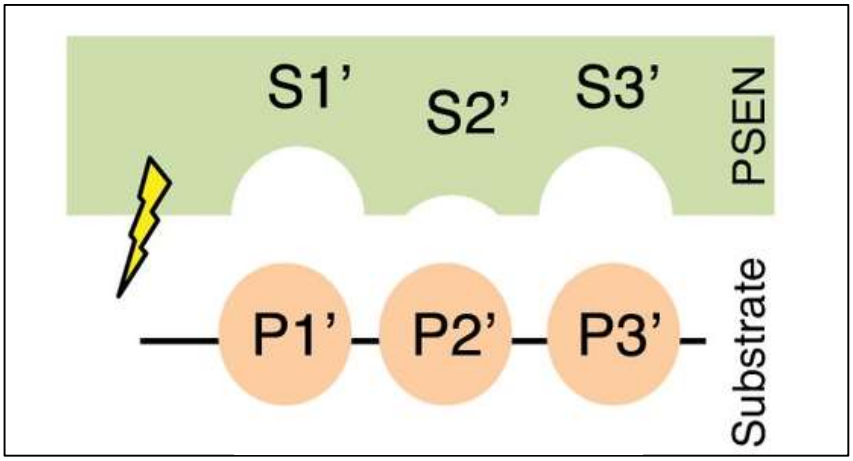

Figure 5.2 Putative S' pockets of presenilin, a critical component of the γ-secretase complex.
This diagram suggests there are three putative S-pockets in the presenilin active site, which provide a mechanism for processing the Aβ49 or Aβ48 in a stepwise tripeptide way. Interestingly, the S2' pocket fit a smaller size amino acid compared to S1' and S3' – this can serve as a regulatory mechanism of the γ-secretase complex (Bolduc et al., 2016).

The Aβ42/Aβ40 ratio has been linked to AD pathogenesis and has even been used in AD diagnosis and monitoring (Tang & Kepp, 2018; Amft et al., 2022). In fact, several early onset familial AD (EOFAD) mutations have been shown to increase this ratio. For instance, the T714I variant (EOFAD) produced a 10.8-fold increase in the Aβ42/Aβ40 ratio *in vitro* compared to the WT (Kumar-Singh et al., 2000). It is well known that mutations between positions 714 and 717 of APP770, can detrimentally increase this ratio as they interfere with γ-secretase cleavage site downstream of Aβ42 (Conidi et al., 2015; De Jonghe et al., 2001). This higher ratio is pathogenic because Aβ42 is more prone to aggregation and toxicity than Aβ40, and even a minor increase in the Aβ42/Aβ40 ratio can stabilise toxic oligomeric intermediates, which initially impair synaptic function and eventually lead to neuronal cell death (Kuperstein et al., 2010). Conversely, mutations like A673T (benign) can lower this ratio, suggesting a protective effect against AD (Jonsson et al., 2012).

Using this knowledge and focusing on APP and γ-secretase relationship, the molecular interactions and mechanisms between PSEN1 and APP will be explored in this chapter.

5.1.2 Aims

This study aims to investigate the impact of APP variants on the interaction between APP and γ-secretase (PSEN1 specifically) within the context of EOFAD. By applying protein modelling and structural bioinformatics approaches, this work seeks to elucidate how missense mutations may disrupt critical binding sites and contribute to the molecular mechanisms underlying AD pathogenesis and progression.

The experimentally resolved crystal structure of the APP–γ-secretase complex (PDB: 6IYC; Zhou et al., 2019) will serve as the structural template for comparative analyses. Quantitative measures of superimposition quality and evaluation of key binding residues will be used to identify pathogenic trends and structural deviations that may impair γ-secretase recognition or cleavage efficiency.

5.2 Specific methods

5.2.1 APP-PSEN1 model preparation and assessment

The cryo-EM structure of the γ-secretase complex bound to an APP C83 fragment (PDB ID: 6IYC; Zhou et al., 2019) was obtained from the Protein Data Bank and used as a structural template to investigate the effects of APP variants on γ-secretase binding. The structure was visualised and analysed in UCSF Chimera (v1.17.1).

ColabFold-predicted APP variant models (see **Table 2.1**) were imported into Chimera in .pdb format and superimposed onto the APP fragment of the ‘6IYC’ structure using the

‘Matchmaker’ function. The superimposition was performed for the APP WT and all APP variants across the three variant categories: EOFAD, CAA and benign. The superimposed region corresponded to residues 699–726, encompassing the TMD of APP. This fragment length was chosen to exclude minor IDRs within the APP fragment of the ‘6IYC’ structure, which could otherwise reduce alignment accuracy. The outputted ‘sequence alignment score’ – which accounts for residue similarities, secondary structure correspondence, and gap penalties – was recorded for each superimposed structure. Following superimposition, the original APP peptide chain from the 6IYC structure was removed to allow direct comparisons between the variant models and the γ-secretase (**Figure 5.3**).

To evaluate potential alterations in the APP–γ-secretase interface, the ‘Find Clashes/Contacts’ tool in Chimera was used to quantify interatomic overlapping interactions. The function identifies polar and non-polar interactions between selected residues based on van der Waals radii and overlap criteria (Pettersen et al., 2004). Analyses were performed using the default contact detection threshold (overlap > –0.4 Å) and clash threshold (overlap > 0.6 Å). For each variant model, the total number of favourable contacts (–0.4 Å ≤ overlap ≤ 0.6 Å), unfavourable clashes (>0.6 Å) and more severe clashes (>2.0Å) – between APP (residues 699–726) and PSEN1 – were recorded from the clashes/contacts list. Additionally, the worst atomic interaction was defined as the maximum overlap distance detected between a pair of atoms and was used to pinpoint the most destabilising contact site within each APP–PSEN1 model. The corresponding APP and PSEN1 residues involved were recorded to facilitate cross-model comparison. Conversely, the best interaction represented the atom pair with an overlap value closest to zero, indicating optimal spatial compatibility.

Hydrogen bonds (HBs) were assessed using Chimera’s ‘FindHBond’ tool under default geometrical and distance constraints, using the same ‘superimposition followed by deletion’ process depicted in **Figure 5.4**. The number and nature of HBs between APP and PSEN1 were recorded for both the experimental structure and the superimposed variant models. Collectively, these analyses enabled structural quantification of the potential disruptive effects of EOFAD, CAA, and benign APP variants on γ-secretase binding and substrate recognition.

5.2.2 Statistical analysis

Statistical analysis was applied to compare structural interaction metrics derived from the APP–PSEN1 models across APP variant groups (i.e. EOFAD, CAA and benign) (see **Table 2.1**). The statistical framework described in **2.7** was followed.

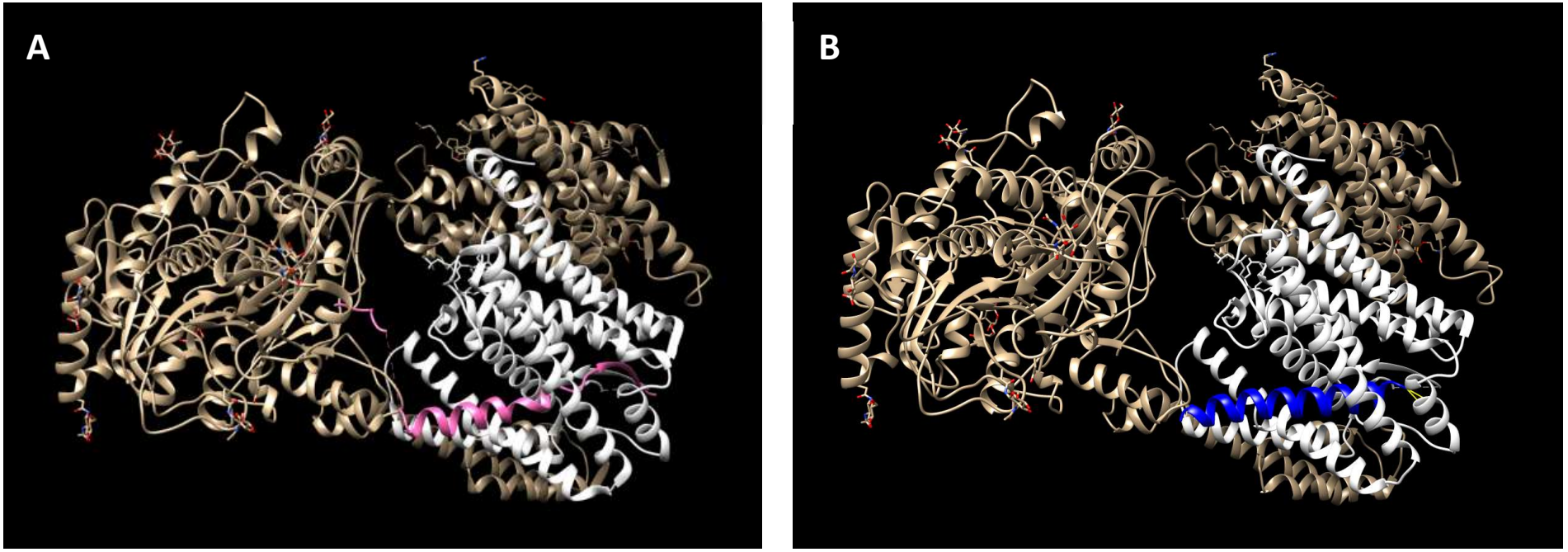

Figure 5.3 3D structures of γ-secretase complex linked to an APP fragment.

A) Figure showing the experimental '6IYC' crystal 3D structure of the γ-secretase complex (light brown) linked to an APP fragment C83 (pink) (Zhou et al., 2019) – the PSEN1 subunit (white) specifically interacts with the C83 fragment. **B)** Same '6IYC' 3D structure with a superimposed APP fragment (blue) – corresponding to the A673T variant, substituting the previous C83 segment (pink). This segment was used as a template for all APP models (WT and variants). After superimposition, the original C83 fragment (pink) was deleted, leaving in its place an APP model. Physical contact metrics were calculated to assess the structural deviation of the APP models with the γ-secretase complex.

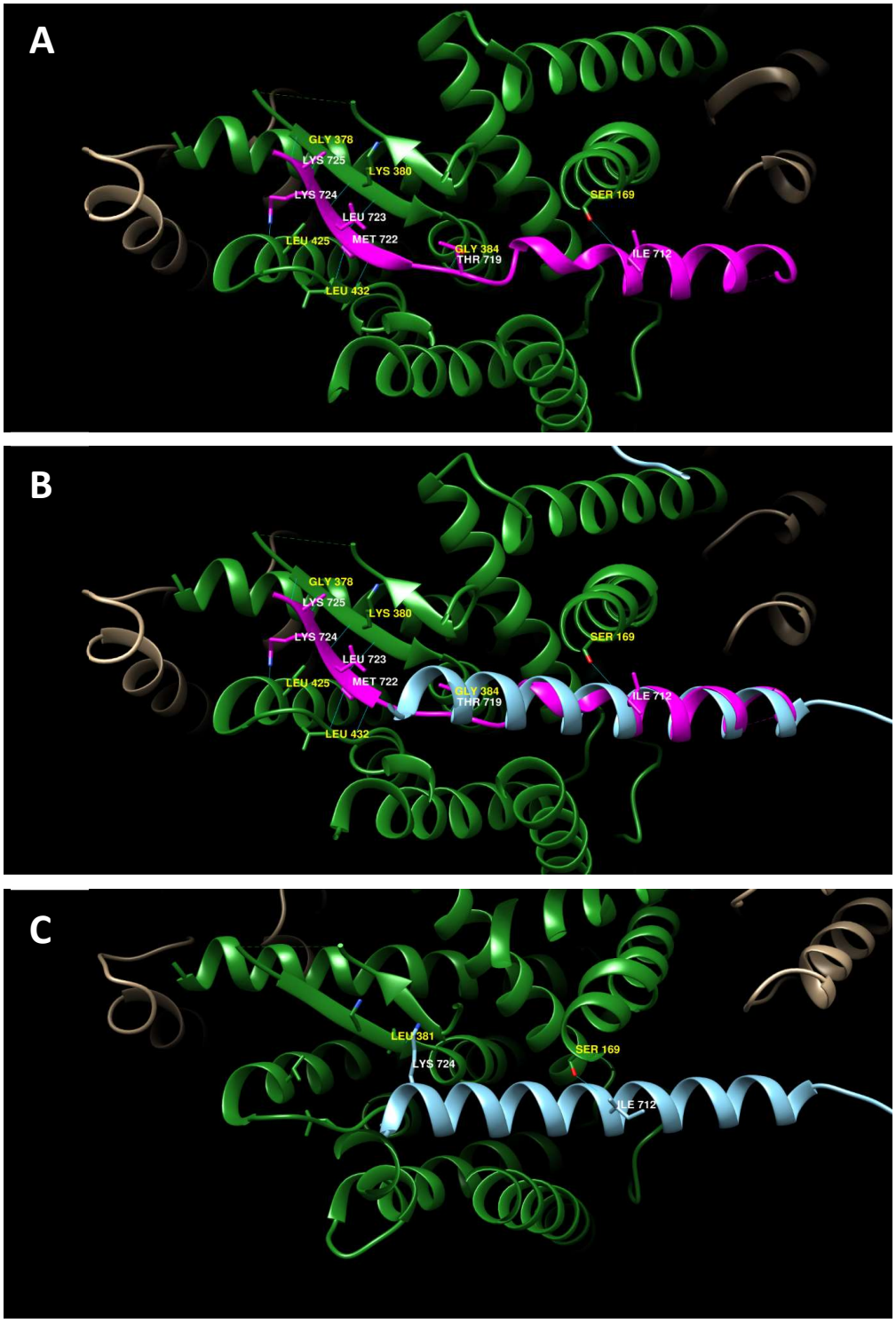

Figure 5.4 APP segment in complex with PSEN1 (γ-secretase).
Three-dimensional structures of the APP segment, from amino acid 699 to 725, bound to PSEN1 – with highlighted HBs (blue lines) and involved amino acids. Amino acids in white belong to the APP segment and those in yellow belong to the PSEN1 subunit. **A)** Crystal structure of APP (pink) bound to PSEN1 (green) (PDB ID: 6IYC). **B)** Same '6IYC' structure with a superimposed APP WT model (light blue). **C)** Same '6IYC' structure with a superimposed APP WT model (light blue), but with original APP segment (pink) removed.

5.3 Results

5.3.1 Superimposed APP segments on Aβ-γ-secretase complex

Superimposition metrics are summarised in **Table 5.1**. Statistically significant differences between the APP variant groups under the 'Sequence Alignment Score' column were found (Kruskal Wallis, p=0.004). Pairwise comparisons with Bonferroni correction (α = 0.017) showed that the benign and EOFAD groups were significantly different (p = 0.001), with the benign group having a higher median sequence alignment score (M = 90.95, IQR = 3.0) than the EOFAD group (M = 86.90, IQR = 2.8). The effect size for the magnitude of the differences between these groups was large (η^2 = 0.52). Under no other columns, the APP variant groups showed to get close to statical significance; however, outliers were present on the data on all the columns except the 'Sequence Alignment Score' and 'Clashes >2.0Å' (Tukey's fences, k=1.5). A variant from the EOAFAD group, V715M, was an outlier across three columns: 'All Contacts > -0.4Å', 'Contacts -0.4Å<x<0.6Å' and 'Clashes >0.6 Å'. The benign group had five outliers from four different variants, two outliers were under the 'Clashes >0.6 Å' column, two under the 'Max Overlap' column and one under the 'Min Distance' column.

5.3.2 Identification of frequent clashes in APP-PSEN1 interactions

The amino acids involved in clashes (>0.6 Å) in the APP-PSEN1 complex were identified from the clashes/contacts list from each of the APP models superimposed (WT and variants) (see **5.2.1**). These lists contained interatomic clashes (>0.6 Å) and the atoms involved from both APP and PSEN1 protein chains (data not shown).

Table 5.2 presents the amino acids involved in these interatomic interactions and the number of times they produced clashes. Across all 22 APP models (1 WT and 21 variants) fitted into the '6IYC' structure of the γ-secretase-APP complex, the top three APP amino acids most frequently involved in chases were marked in bold (**Table 5.2**). Across APP models, these top three amino acids were almost consistently lysine 726 (K726), lysine 724 (K724) and leucine 720 (L720). However, some APP models belonging to the EOFAD group did not follow this trend (highlighted yellow in **Table 5.2**) – these included T714I, V715M and L723P. For both T714I and V715M, the amino acids that caused the most overlaps were Lysine 726 (K726), Methionine 722 (M722) and Lysine 725 (K725) (descending number of clashes). Finally, for L723P, the amino acids that caused the most overlaps were Lysine 726 (K726), Lysine 725 (K725) and Leucine 720 (L720) (descending number of clashes).

							Worst interaction (Max overlap)		Best interaction (Overlap ≈ 0Å)
Type	Structure Name	Sequence Alignment Score	Contacts & Clashes (> -0.4Å)	Contacts (-0.4Å<x<0.6Å)	Clashes >0.6Å	Clashes >2.0Å	Overlap value (Å)	AA pairs (APP-PSEN1)	AA pairs (APP-PSEN1)
WT	WT APP	89	501	324	177	31	3.447	K724-I287	K726-L271
B	A201V	89.9	491	298	193	24	3.158	K726-L271	L723-L271
B	A235V	92	465	297	168	23	3.163	L720-L286	T719-W165
B	A479S	92	497	313	184	27	3.246	K724-I287	V717-I387
B	V562I	89	464	283	181	27	3.080	K724-I287	K726-R269
B	E599K	89	518	337	181	16	2.825	K724-I287	L720-L286
B	A673T	92.9	467	288	179	19	3.566	K724-I287	I716-W165
CAA	E693K	89	472	291	181	34	3.490	K726-L271	L723-F283
CAA	E693Q	89	465	296	169	22	2.822	L720-L286	M706-I180
CAA	D694N	89	471	295	176	26	2.996	K726-L271	K725-L268
CAA	L705V	89.9	502	327	175	14	3.210	L720-L286	K726-V272
EOFAD	K670N/M671L	89	473	299	174	28	3.371	K724-I287	L723-F283
EOFAD	T714A	85.5	456	289	167	17	3.347	L720-L286	K726-V272
EOFAD	T714I	87.8	525	335	190	17	2.913	K724-I287	M722-T256
EOFAD	V715M	86.9	570	372	198	20	3.096	K724-I287	K726-L271
EOFAD	I716V	88.3	517	338	179	26	2.856	K724-I287	M722-L268
EOFAD	V717F	85.5	484	309	175	26	2.950	L720-L286	K726-V722
EOFAD	V717G	84.1	472	294	178	30	3.327	K724-I287	K724-L286
EOFAD	V717I	88.3	469	297	172	23	2.957	L720-L286	K726-V272
EOFAD	V717L	86.9	466	286	180	25	2.954	L720-L286	K726-V272
EOFAD	L723P	90.7	456	295	161	17	2.973	L720-L286	K725-R269
EOFAD	K724N	85.5	427	271	156	19	3.192	L720-L286	K725-D257

Table 5.1 Superimposition and clashes/contacts metrics for γ-secretase bound to APP models (WT and variants).
Table containing information about the superimposition and interatomic overlap distances between APP and PSEN1. The output data includes the 'sequence alignment score', the number of contacts/clashes above or in between certain thresholds, the overlap value and amino acids involved in the worst interatomic interaction, and the amino acids involved in the best interatomic interaction – all of these across WT and EOFAD, CAA and benign variant groups. For the 'sequence alignment score', the three variant groups were statistically different (Kruskal Wallis, p=0.004). Pairwise comparisons showed that the benign and EOFAD groups were significantly different (Kruskal Wallis, Bonferroni's corrected α=0.017, p=0.001). Additionally, some outliers were identified (orange) (Tukey's fences, k=1.5). Legend: WT – wild type (grey); B – benign (blue); CAA – cerebral amyloid angiopathy (yellow); EOFAD – early onset familial AD (green).

WT		A201V		A235V		A479S		V562I		E599K	
AA	# Clashes	AA	# Clashes	AA	# Clashes	AA	# Clashes	AA	# Clashes	AA	# Clashes
LYS 726	**49**	**LYS 726**	**45**	**LYS 726**	**58**	**LYS 726**	**53**	**LYS 726**	**48**	**LYS 726**	**55**
LYS 724	**30**	**LYS 724**	**39**	**LYS 724**	**21**	**LYS 724**	**28**	**LYS 724**	**31**	**LYS 724**	**21**
LEU 720	**26**	**LEU 720**	**28**	**LEU 720**	**20**	**LEU 720**	**23**	**LEU 720**	**24**	**LEU 720**	**21**
LEU 723	15	LEU 723	20	MET 722	18	MET 722	21	MET 722	17	MET 722	20
MET 722	15	ILE 716	12	ILE 716	10	LEU 723	16	LEU 723	16	LYS 725	17
VAL 715	11	THR 719	12	ILE 718	9	VAL 715	11	VAL 715	11	LEU 723	12
THR 719	10	MET 722	11	LYS 725	8	THR 719	9	LYS 725	10	VAL 715	11
ILE 716	8	VAL 715	9	VAL 715	7	ILE 716	8	ILE 716	8	ILE 718	9
LYS 725	7	ILE 718	6	LEU 723	7	LYS 725	8	THR 719	8	THR 719	7
ILE 718	5	LYS 725	6	THR 719	7	ILE 718	6	ILE 718	7	ILE 716	6
VAL 707	1	MET 706	2	MET 706	2	MET 706	1	MET 706	1	VAL 721	1
		VAL 707	2	VAL 717	1					MET 706	1
		VAL 721	1								

K670N+M671L		A673T		E693K		E693Q		D694N		L705V	
AA	# Clashes	AA	# Clashes	AA	# Clashes	AA	# Clashes	AA	# Clashes	Atom	# Clashes
LYS 726	**45**	**LYS 726**	**38**	**LYS 726**	**46**	**LYS 726**	**48**	**LYS 726**	**53**	**LYS 726**	**42**
LYS 724	**31**	**LYS 724**	**35**	**LYS 724**	**35**	**LYS 724**	**28**	**LYS 724**	**28**	**LYS 724**	**23**
LEU 720	**27**	**LEU 720**	**29**	**LEU 720**	**29**	**LEU 720**	**23**	**LEU 720**	**25**	**LEU 720**	**20**
LEU 723	17	MET 722	15	LEU 723	20	MET 722	15	MET 722	16	MET 722	19
MET 722	14	THR 719	13	MET 722	13	LEU 723	13	LEU 723	12	LYS 725	17
LYS 725	10	ILE 716	11	VAL 715	10	VAL 715	11	VAL 715	11	LEU 723	12
VAL 715	9	LEU 723	11	THR 719	9	LYS 725	11	LYS 725	11	THR 719	12
ILE 716	8	VAL 715	8	ILE 716	8	THR 719	7	ILE 716	7	ILE 716	10
THR 719	8	ILE 718	8	LYS 725	6	ILE 716	6	THR 719	7	VAL 715	9
ILE 718	5	LYS 725	6	ILE 718	5	ILE 718	6	ILE 718	6	ILE 718	8
		MET 706	3			VAL 721	1			MET 706	2
		GLY 700	1							GLY 700	1
		VAL 707	1								

T714A		**T714I**		**V715M**		I716V		V717F		V717G	
AA	# Clashes	AA	# Clashes	AA	# Clashes	AA	# Clashes	AA	# Clashes	AA	# Clashes
LYS 726	**35**	**LYS 726**	**55**	**LYS 726**	**52**	**LYS 726**	**50**	**LYS 726**	**46**	**LYS 726**	**41**
LYS 724	**35**	**MET 722**	**23**	**MET 722**	**23**	**LYS 724**	**23**	**LYS 724**	**29**	**LYS 724**	**35**
LEU 720	**27**	**LYS 725**	**22**	**LYS 725**	**21**	**LEU 720**	**21**	**LEU 720**	**23**	**LEU 720**	**28**
LEU 723	17	LEU 720	21	LYS 724	20	LYS 725	20	MET 722	16	LEU 723	16
ILE 716	10	LYS 724	18	LEU 720	19	MET 722	19	LEU 723	12	MET 722	16
MET 722	9	LEU 723	13	MET 715	14	LEU 723	13	VAL 715	11	VAL 715	11
VAL 715	9	VAL 715	11	THR 719	13	VAL 715	11	LYS 725	9	THR 719	9
THR 719	9	ILE 718	10	LEU 723	13	ILE 718	9	ILE 716	8	ILE 716	8
ILE 718	7	ILE 716	7	ILE 716	10	THR 719	7	ILE 718	8	LYS 725	8
MET 706	3	THR 719	7	ILE 718	8	VAL 716	4	THR 719	7	ILE 718	5
LYS 725	2	MET 706	2	MET 706	3	VAL 721	1	PHE 717	6	VAL 707	1
VAL 721	2	VAL 721	1	VAL 721	1	MET 706	1				
VAL 717	1			VAL 707	1						
VAL 707	1										

V717I		V717L		**L723P**		K724N	
AA	# Clashes	AA	# Clashes	AA	# Clashes	AA	# Clashes
LYS 726	**45**	**LYS 726**	**48**	**LYS 726**	**54**	**LYS 726**	**44**
LYS 724	**28**	**LYS 724**	**31**	**LYS 725**	**29**	**LEU 720**	**24**
LEU 720	**23**	**LEU 720**	**22**	**LEU 720**	**26**	**ASN 724**	**19**
MET 722	16	MET 722	19	MET 722	13	MET 722	16
LEU 723	14	LEU 723	15	VAL 715	11	LEU 723	15
VAL 715	11	VAL 715	11	ILE 716	7	VAL 715	11
LYS 725	9	ILE 716	8	ILE 718	6	ILE 716	8
ILE 716	8	LYS 725	8	THR 719	5	THR 719	8
ILE 718	7	THR 719	8	PRO 723	4	ILE 718	6
THR 719	6	ILE 718	7	VAL 721	4	LYS 725	5
ILE 717	3	LEU 717	3	LYS 724	2		
MET 706	1						
VAL 721	1						

Table 5.2 Amino acids frequently involved in APP-PSEN1 clashes (>0.6 Å).

Table showing a list of the amino acids (from APP chain only) involved in clashes between PSEN1-APP peptide complex (PDB: 6IYC). For each of the APP models superimposed (WT and variants), the number of clashes (>0.6 Å) was recorded. Most models have the same top three amino acids causing the most clashes (green). However, some models have different amino acids in their top three (yellow). Legend: AA = amino acid

5.3.3 Hydrogen bond detection

Using the crystal '6IYC' structure, HBs between APP and PSEN1 were detected and assessed (**Table 5.3**) (Zhou et al., 2019). This process was repeated for each of the superimposed APP models (WT and variants) (**Figure 5.4**) (see **5.2.1**).

The detected HBs across all superimposed models, specifically the amino acids involved in these interactions, were annotated in **Table 5.3**. The original APP segment (pink in **Figure 5.4**) had the most HBs with PSEN1 (green in **Figure 5.4**), with a total of 9 – all of these highlighted in bold. The APP WT model had 2 HBs only. However, one of these bonds (I712-S169) was the same one as in the original '6IYC' structure. Particular attention was given to this HB across the other superimposed models in **Table 5.3.** In the benign group, 50% of variants kept this specific HB and the variants on this group had between 1-3 HBs each. For the CAA group, none of the variants kept the 'I712-S169 HB' and the variants had between 1-2 HBs each. Finally, within the EOFAD group, 64% of the variants had the 'I712-S169 HB' and they had between 2-4 HBs each (**Table 5.3**).

5.4 Discussion

5.4.1 Assessing number of favourable contacts and unfavourable clashes

The '6IYC' structure (Zhou et al., 2019) clearly displayed the interaction between the γ-secretase and the C83 segment of APP at the molecular level. **Figure 5.1** showed that the origin of the C83 APP segment is the non-amyloidogenic pathway – which starts by the initial cleavage by α-secretase at position 688-689 of APP770 (Chen et al., 2017; (APP|ALZFORUM, n.d.). Regardless of C83 coming from the non-amyloidogenic pathway, key interactions between APP and PSEN1 (γ-secretase) occur within the transmembrane region even for the C99 APP segment (from the amyloidogenic pathway). Hence, structural disruptive mechanisms can be explored using this experimental structure and the superimposition process followed in this chapter.

The data collated in **Table 5.1** showed the first difference between the variant groups (i.e. EOFAD, CAA and benign) under the 'sequence alignment score' column (Kruskal Wallis, $p=0.004$), specifically between the benign and EOFAD groups (Kruskal Wallis, Bonferroni's corrected $\alpha=0.017$, $p=0.001$) – with the benign group having a higher score on average compared to the EOFAD group (90.8 and 87.1 respectively). Since the effect size of this difference was large ($\eta^2 = 0.52$), it is plausible to think that these measurements are biologically relevant. The idea that benign variants should align better with the original APP structure than EOFAD variants is supported by this evidence. However, disruptions in alignment of EOFAD models were expected as many of the mutations in these variants take place within the transmembrane region of APP (amino acids range 699-725). Nonetheless,

Type	Structure Name	Number of HB	Amino acids involved (APP-PSEN1)
Original WT	Chain E	9	**K725-G378** (x2) **K724-L425** **L723-K380** (x2) **M722-L432** (x2) **T719-G384** **I712-S169**
Model WT	WT APP	2	K724-L381 **I712-S169**
B	A201V	2	K725-D257 **I712-S169**
B	A235V	1	K724-L381
B	A479S	2	K725-D257 K724-L381
B	V562I	2	K724-L381 **I712-S169**
B	E599K	2	K725-D257 K724-L381
B	A673T	3	K725-D257 K724-L381 **I712-S169**
CAA	E693K	1	K724-L381
CAA	E693Q	2	K725-D257 K724-L381
CAA	D694N	2	K725-D257 K724-L381
CAA	L705V	1	K724-L381
EOFAD	K670N+M671L	2	K724-L381 **I712-S169**
EOFAD	T714A	4	K726-P267 K726-G266 K725-D257 **I712-S169**
EOFAD	T714I	2	K725-D257 K724-L381
EOFAD	V715M	2	K725-D257 K724-L381
EOFAD	I716V	2	K725-D257 K724-L381
EOFAD	V717F	2	K725-D257 K724-L381
EOFAD	V717G	3	K725-D257 K724-L381 **I712-S169**
EOFAD	V717I	3	K725-D257 K724-L381 **I712-S169**
EOFAD	V717L	3	K725-D257 K724-L381 **I712-S169**
EOFAD	L723P	3	K726-G266 K724-L381 **I712-S169**
EOFAD	K724N	2	K725-D257 **I712-S169**

Table 5.3 List of hydrogen bonds between APP-PSEN1 structures.
Annotated HBs across different APP-PSEN1 models including the amino acids involved from each peptide. Information was collated for each of the superimposed models of APP (WT and variants) and for the original APP segment of the '6IYC' structure (Zhou et al., 2019). The original model (pink) had the highest number of HBs, totalling 9 – all of these are highlighted in bold. The APP WT (grey) has a total of 2 HBs – one of them being the same one as the original and highlighted in bold (i.e. I712-S169). The rest of the model variants, across all groups, followed a similar trend conserving the 'I712-S169' HB – to different degrees of consistency. Legend: HB = hydrogen bonds, WT = wild type (grey), B = benign (blue), CAA = cerebral amyloid angiopathy (yellow), EOFAD = early onset familial AD (green).

this result supports the 'sequence alignment score' as a valid metric for mutated superimposed structures.

Table 5.1 also highlighted some outliers (Tukey's fences, k=1.5), the most noticeable being V715M. This EOFAD variant stood out as an outlier in three different columns. These included the combined number of clashes and contacts (> -0.4Å), the number of favourable contacts (between -0.4Å and 0.6Å) and the number of unfavourable 'clashes >0.6Å'. Even when compared to the WT model, V715M had a higher number of total contacts and clashes, highlighting structural deviations from the template. Additionally, there were four more outliers within the benign group in two different columns. The first one was the 'clashes >0.6Å' column, where A201V and A235V stood out for having too many and too few clashes respectively – even compared to the WT. This is quite surprising as both benign mutations have an alanine to valine substitution within essentially the same region. According to the previous secondary structure prediction analysis (see **4.2.1** and **Figure 4.1**), the region encompassing amino acid 192 to 300 of APP was predicted to be intrinsically disordered. Hence, due to valine being a bulkier and more hydrophobic amino acid than alanine, these mutations could alter the flexibility of the intrinsic disordered region (IDR). This could lead to the overall structure having a slightly different orientation which would generate either more or less clashes compared to the groups' average or the WT. The final two outliers are under the 'overlap value' sub-column belonging to the 'worst interaction' column. Here, E599K and A673T stood out for having a low and a high overlap value respectively. Since the amino acid pair associated with their worst interaction is the same one (APP-PSEN1: K724-I287), it is possible that this is a key clash, and that the variation of the overlap value is due to the missense mutations being within IDRs.

Finally, it is worth mentioning the trends within the amino acid pairs that form the worst and best interactions. On the worst interaction column, where the amino acid pair with the highest overlap value are noted, the same 3 pairs of amino acids are identified: L720-L286, K724-I287 and K726-L721 (APP-PSEN1). This suggests that interactions at these amino acids are potentially key for correct processing of the APP segment, as superimposed APP models (WT and variants) do not undergo conformational changes into a β-strand structure and remain as an α-helix (**Figure 5.4B**). By contrast, the best interaction column contains 16 different amino acid pairs, revealing no clear pattern except the K726-V722 pair being the best favourable interaction in 4 EOFAD models and 1 CAA model.

5.4.2 Common overlapping amino acids in APP models

Table 5.2 presented the most common amino acids in the APP segment to have an overlap >0.6Å (i.e. clash) with PSEN1. The frequency of these clashes linked to specific common amino acids, highlighted their potentially relevant role in APP's normal processing. In 19 out of 22 different APP variants, including the WT, the top three most clashing amino acids and their relative order were K726 (highest number of clashes), K724 (2nd highest) and L720 (3rd

highest). Moreover, these amino acids were also part of a trend described above – they were included in the pairs causing the worst interactions in **Table 5.1**.

As seen in **Figure 5.4**, the superimposed APP models, including the APP WT and variants, do not have the capability of extending their chain and changing it from an α-helix to a β-strand. For this reason, the most clashing amino acids represent a basal level of clashes, a level where APP models can locally superimpose and orient themselves in space using the non-pathogenic C83 peptide as a template. However, there are three exceptions to this trend – these are the variant models T714I, V715M and L723P. These missense mutations are well-known EOFAD mutations, used by scientists to test different hypotheses under AD conditions (Olsson et al., 2014; Kakuda et al., 2006; Liu et al., 2022). In this context, these mutations deviate from the trend suggesting a distinct PSEN1 processing, based on the structural deviations involving different amino acids that the other variants. This is further supported by the fact that during superimpositions of multiple APP regions, some of these APP variants were classified as outliers multiple times within the EOFAD variant group (see **4.3.1** to **4.3.6**). For instance, the V715M APP variant was a constant outlier, standing out in 4 out 8 regional comparison tables. The L723P variant stood out in 1 out 8 regional comparison tables. Finally, although the T714I did not stand out in any of the mentioned tables, the T714A variant (which affects the same amino acid position) stood out in 4 out of 8 tables. Hence, this suggests that there might be significant differences in these variants' intrinsic structure, possibly affecting their normal processing at the γ-secretase stage.

5.4.3 Hydrogen bond disruption assessment

The HB analysis provided an understanding of the crucial HBs present in the APP-PSEN1 crystal structure (**Figure 5.4A**, **Table 5.3**). As expected, **Table 5.3** showed the original APP peptide (C83) had the highest number of HBs – a total of 9. After measuring the HBs from all the APP variants, including the APP WT model, the I712-S169 (APP-PSEN1) HB was seen to be generally conserved throughout the modelled variants (10/22) indicating a possible role in maintaining the structure and stability of the complex. Following this observation, it was noted that the CAA variants did not have that conserved I712-S169 HB. One possible cause for this could be the location of the CAA mutation zone (693-705) which would include a motif that inhibits γ-secretase according to van der Kant & Goldstein (2015) – this is the LVFFAED motif and extends from amino acid 688 to 694.

Furthermore, two more additional HBs can be found in the original APP-PSEN1 '6IYC' structure, specifically at positions 689 and 691 of APP (data not shown) – which locate them near the CAA mutation zone. The reason why these HBs were not part of the annotated HBs in **Table 5.3** is because the original '6IYC' structure is missing a few amino acids. These missing amino acids are within in a coil region that extends from position 689 to 698. This truncated coil region was considered not to be appropriate for template-based superimpositions, which is why the APP segment superimposed includes amino acid 699 to 726 only. However, in the case of CAA variants it could be possible that early disruptions of

HBs at position 689 and 691 could lead to a lack conformational changes that disrupts the I712-S169 HB.

Another interesting observation points at the original 2 HBs between L723 (APP) and K380 (PSEN1) – present in the '6IYC' complex. These bonds were not conserved on any of the APP variants, however the variants compensated this by having a HB between K724 (APP) and L381 (PSEN1) instead (**Figure 5.4**). The K724-L381 (APP-PSEN1) HB was present in 19 out 22 models (**Table 5.3**). This could suggest that the leucine-lysine interaction plays an important role in the elongation process of the APP C83 segment.

Finally, since K726 was the most clashing amino acid amongst the APP models (**Table 5.2**), it would be plausible to think that HBs at this position could also be unfavourable. Only two APP models have HBs at K726, these are T714A and L723P – two variants that have been flagged up before due to their abnormal patterns. Both EOFAD variants have an HB between K726 (APP) and G266 (PSEN1). However, this HB could be acting like the K724-L381 HB, as the original APP-PSEN1 structure has a HB at K725-G378 which involves the same amino acids (lysine and glycine). Nonetheless, T714A has an additional HB between K726 and P267 which is unique amongst the APP variants. Seeing that T714A has the facility to form HBs involving K726 could be problematic, considering it is the only model in doing so and both glycine and proline are known for affecting peptide shape.

5.4.4 Limitations and future steps

As previously mentioned, the superimposed APP models did not have the elongated β-strand shape that the APP peptide had in its crystal '6IYC' structure (**Figure 5.4**; Zhou et al., 2019), therefore superimposition metrics such as RMSD or atom pairs aligned could not be used. However, the value of using this experimental structure comes from gaining a structural insight into a very important processing step of APP. The fact that the APP-peptide came from C99 meant that it was from a non-amyloidogenic pathway. Therefore, any structural outliers or trends (especially those coming from the EOFAD group) could be investigated for potentially disrupting a normal processing scenario – as any structural changes could affect the normal functioning of the mechanism.

Additionally, like in Chapter 3 the statistical tests used did not have a high powerl due to low sampling. A potential solution could be to unify the EOFAD and CAA groups to create a 'pathological group', in addition to also increase the samples of the benign group. That way there could be two groups with at least 15 samples in each. This would make the tests more robust and allow more reliable statistical insights. On the downside, grouping EOFAD and CAA would mean that when exploring a trend within the pathological group there could be problems trailing it back to specific pathological events or mechanisms, since after all they are a different pathology.

Future steps for this research could focus on using molecular dynamics simulations to explore the time-dependent conformational changes in the APP segment and its interactions

with PSEN1 under various conditions, including the presence of different missense mutations. Furthermore, investigating how these structural deviations impact downstream APP processing, particularly at the γ-secretase cleavage site, could provide key insights into the mechanisms underlying the development of early onset familial AD. Additional studies could also incorporate high-throughput techniques such as cryo-electron microscopy (cryo-EM) to obtain more accurate models of the entire γ-secretase complex interacting with pathogenic and benign APP variants. This would allow further clarification of the clashing residue patterns identified, helping to better understand the molecular drivers of AD.

6 Acetylcholinesterase – APP interaction

6.1 Introduction

6.1.1 Overview of acetylcholinesterase

AChE is a key enzyme in the cholinergic system, primarily responsible for terminating synaptic transmission by hydrolysing acetylcholine into choline and acetic acid. This hydrolysis occurs rapidly at cholinergic synapses, especially at neuromuscular junctions, and prevents the overstimulation of acetylcholine receptors, allowing neurons and muscles to reset for subsequent signals (Trang & Khandhar, 2023). AChE, belonging to the serine hydrolase family, functions through a catalytic triad composed of serine, glutamate and histidine at positions 203, 334 and 447 respectively and which act in tandem to deacetylate acetylcholine (Zhou et al., 2010). This process restores AChE to its active form, ensuring efficient signal termination. Structurally, AChE is a versatile enzyme that can exist as a monomer (G1), dimer, or tetramer (G4), depending on its physiological location and function. Tetramers are often anchored to collagen-like tails via disulfide bonds, providing structural integrity in various tissues (Trang & Khandhar, 2023).

AChE plays an integral role in both the central and peripheral nervous systems, particularly in regions such as the brainstem, cerebellum, and autonomic nervous system. Moreover, it is found in skeletal muscle and even in red blood cells, which points to a broader distribution and functionality beyond neuronal synapses (Trang & Khandhar, 2023). Embryologically, AChE is involved in neural development, particularly during axonal growth, a time when its enzymatic role appears less pronounced, suggesting non-catalytic contributions to morphogenesis.

A particularly critical aspect of AChE's function and regulation is glycosylation. Glycosylation, the attachment of carbohydrate moieties to the enzyme, is essential for its stability, biosynthesis, and secretion. Human AChE (hACHE) is glycosylated at three conserved sites: aspargine-265, aspargine-350, and aspargine-464. These modifications are crucial for the enzyme's structural integrity and thermostability, as evidenced by site-directed mutagenesis studies that show significantly reduced secretion and heat stability when glycosylation sites are mutated (Velan et al., 1993; Xu et al., 2015). Notably, glycosylation does not seem to affect the enzyme's catalytic activity but does influence its conformational stability and susceptibility to heat inactivation (Sáez-Valero et al., 2001).

In the context of AD, AChE has drawn attention due to its altered expression and isoform distribution in the brains of AD patients. The cholinergic hypothesis of AD posits that a deficit in acetylcholine contributes to the cognitive decline observed in patients, and AChE's role in this context becomes pivotal. In AD, a shift from the tetrameric G4 form of AChE to the monomeric G1 form is observed, correlating with disease progression and the breakdown of cholinergic signalling (Trang & Khandhar, 2023). This shift is thought to

exacerbate cholinergic deficits by reducing the enzyme's efficiency at clearing acetylcholine from synaptic clefts, further impairing neuronal communication. Moreover, abnormal glycosylation patterns of the enzyme have been linked to the pathology of the disease (Sáez-Valero et al., 2001).

One of the primary treatment strategies for AD patients involves the use of AChEIs. These inhibitors mitigate AD symptoms by preventing acetylcholine turnover, thereby maintaining higher levels of acetylcholine at the synaptic junction. This prolonged presence of acetylcholine helps recalibrate neurotransmitter levels and potentiates cholinergic signalling. Patients treated with AChEIs often experience a deceleration in the symptomatic progression of AD, with improvements in attention span and other cognitive functions, though significant enhancement in short-term memory remains limited (Trang & Khandhar, 2023).

Despite their benefits, AChEIs do not halt the neurodegenerative processes of AD but rather provide symptomatic relief. Furthermore, the prolonged use of AChEIs may lead to adverse effects such as gastrointestinal disturbances, bradycardia, and muscle cramps. While AChEIs can improve some aspects of cognitive function, their effects are often temporary, and patients may develop tolerance over time, diminishing their therapeutic efficacy. Therefore, while AChEIs remain a key component of AD management, their role is limited to mitigating symptoms rather than addressing the underlying pathology of the disease.

6.1.2 AChE and APP interaction in AD

This chapter explored the AChE-APP interaction as it was highlighted by STRING to be a high-confidence interaction (see **Figure 3.4**, **Figure 3.6**). Additionally, significant work in the literature surrounding these proteins and their role in AD suggests that they could significantly contribute to AD's pathogenesis and progression.

As previously mentioned, AChE is primarily responsible for hydrolysing the neurotransmitter acetylcholine, helping regulate cholinergic signalling in the nervous system. However, as demonstrated by multiple studies, AChE has shown to facilitate the aggregation of amyloid-beta (Aβ) peptides, increasing the formation of amyloid plaques, and even formation of toxic AChE-Aβ fibrils (Carvajal & Inestrosa, 2011; Alvarez et al., 1998). Alvarez et al. (1997) showed that AChE accelerated the formation of aggregates of different truncated Aβ peptides and some of them, e.g. Aβ12-28, showed to form strong complexes with AChE. By using docking simulations Inestrosa et al. (2005) claimed that the Aβ key binding sites might be between position 12-16.

Studies in transgenic mice expressing both human APP and AChE genes showed increased amyloid deposition and earlier onset of plaque formation compared to mice expressing only APP (Rees et al., 2003). Moreover, Rees et al., (2005) demonstrated that amyloid burden in double transgenic mice was correlated with working memory impairment (i.e. total errors in the radial arm water maze test). Further support comes from Carvajal & Inestrosa (2011), who demonstrated that AChE-Aβ complexes significantly disrupt neuronal networks and

elevate intracellular calcium, leading to increased mitochondrial dysfunction and neurodegeneration. Additionally, Inestrosa et al. (2005) identified AChE had a higher affinity to bind to Aβ fibrils than soluble Aβ peptides which would indicate that AChE could exacerbate AD pathogenesis. When considering the findings by Nordberg et al. (2009) which describe that AChEIs such as donepezil and galantamine have been associated with increased levels of AChE in the cerebrospinal fluid (CSF), the pathogenic synergy even involving treatment becomes problematic.

The exact mechanisms through which AChE enhances Aβ fibril formation and toxicity are still under investigation. One possible explanation lies in the structural homology between AChE and Aβ itself. Cottingham et al. (2002) discovered that a peptide sequence in the C-terminal region of AChE can form amyloid fibrils, which may mimic the behaviour of Aβ fibrils and facilitate their aggregation. Jean et al. (2007) proposed that proteolytic fragments of AChE, particularly the T40 fragment, exhibit amyloidogenic properties, enhancing Aβ fibrillisation via heterologous seeding mechanisms. These fragments, formed through proteolytic cleavage, may accelerate amyloid nucleation and elongation, thereby exacerbating amyloid plaque formation (**Figure 6.1**).

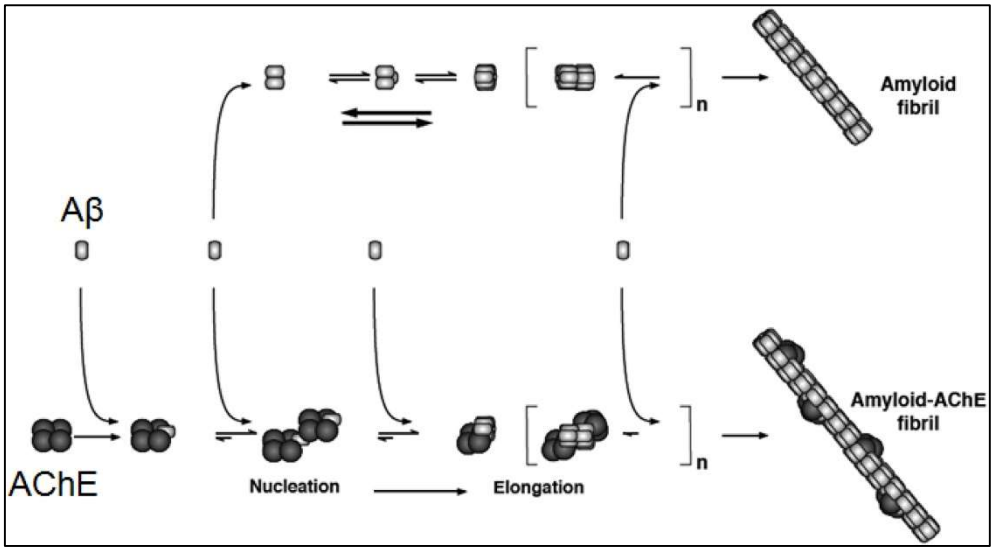

Figure 6.1 AChE involvement in nucleation and elongation of amyloid fibrils.
Figure showing AChE active role in reducing the lag phase of amyloid aggregates and promoting nucleation followed by elongation. Jean et al. (2007) specifies that it is a region within $AChE_{575-614}$ named T40 that can mimic the behaviour of amyloids promoting aggregation. Legend: AChE – acetylcholinesterase enzyme, Aβ – amyloid beta. Image taken from Carvajal & Inestrosa (2011).

Lastly, the interaction between AChE and Aβ may also affect APP regulation. Nalivaeva & Turner (2016) highlighted a reciprocal relationship where APP overexpression can downregulate AChE activity, while knockdown of APP can increase AChE levels. This interplay points to a complex regulatory mechanism in which both proteins influence each other, potentially creating a feedback loop that accelerates AD pathology. As both APP and AChE are implicated in amyloidogenesis, this regulatory relationship could serve as an important target for novel therapeutic interventions aimed at breaking the cycle of neurodegeneration.

6.1.3 Aims

There is sufficient supporting evidence to suggest that the interaction between acetylcholinesterase (AChE) and the amyloid precursor protein (APP) may play an important role in Alzheimer's disease (AD) pathology. AChE's capacity to promote amyloid-β (Aβ) aggregation and increase its toxicity, together with its altered enzymatic activity once associated with amyloid plaques, positions this enzyme as a potential contributor to AD progression.

This chapter aims to predict and characterise potential interaction interfaces between AChE and APP, including Aβ-derived peptides, using AlphaFold3-based structural modelling. The objective is to generate and evaluate structural complexes by assessing model confidence scores and interprotein contact features, thereby identifying plausible binding regions that may underpin the molecular relationship between AChE and APP in the context of AD pathophysiology.

6.2 Specific Methods

6.2.1 AChE–APP model preparation and assessment

The prediction of putative AChE–APP complexes was carried out using the AlphaFold Server (see **2.4.2**), powered by the AlphaFold3 architecture (Abramson et al., 2024). Canonical sequences for human acetylcholinesterase (AChE; UniProt ID: P22303) and amyloid precursor protein (APP; UniProt ID: P05067) were retrieved in FASTA format from UniProt (see **2.2.1**) (Bateman et al., 2022) and used as inputs for multimeric complex prediction. Five ranked models were generated for each complex, with associated confidence metrics including the per-residue pLDDT, global pTM, and interfacial ipTM scores. A model confidence score was calculated using the weighted formula described by Evans et al. (2021):

$$\textbf{Model confidence} = 0.8 \times \textbf{ipTM} + 0.2 \times \textbf{pTM}$$

Models with a composite model confidence ≥ 0.74 were retained for downstream structural interpretation, corresponding to “confident” interface predictions (ipTM ≥ 0.8) and “likely accurate” overall folds (pTM ≥ 0.5).

To contextualise and validate the predicted AChE–APP complexes, experimentally resolved AChE oligomeric structures were obtained from the Protein Data Bank (see **2.2.2**) (Berman, 2000). The AChE dimer (PDB ID: 4PQE; Dym et al., 2015) and tetramer (PDB ID: 1VZJ; Dvir et al., 2004) served as structural references for assessing AlphaFold3-predicted quaternary arrangements, particularly regarding active site accessibility and subunit orientation.

All models were visualised and analysed in UCSF Chimera (see **2.5.1**) (Pettersen et al., 2004). Predicted AChE–APP complexes were examined for potential binding interfaces, focusing on interactions involving the AChE active domain (residues 32–614) and APP regions corresponding to secretase cleavage sites. Chimera’s Find Clashes/Contacts function was employed under default settings (favourable contacts: overlap > –0.4 Å and < 0.6 Å) to identify interatomic interactions across the AChE–APP interface. The total number of contacts, unfavourable clashes (> 0.6 Å), and severe clashes (> 2.0 Å) were recorded. The worst atomic interaction was defined as the maximum overlap distance between any atom pair, while the best interaction corresponded to the overlap value closest to zero, representing optimal spatial compatibility.

These combined computational and structural analyses enabled the evaluation of high-confidence AChE–APP complexes, providing insight into possible interaction sites that may underpin the structural relationship between AChE and APP in AD pathology.

6.3 Results

6.3.1 Truncated Aβ peptides

The truncated Aβ peptides used by Alvarez et al. (1997) were modelled to see their interaction results could be recapitulated *in silico.* They used binding assays and found that both Aβ(1-16) and Aβ(12-28) formed complexes with AChE – the latter peptide forming particular strong ones. The other Aβ lengths included 9-21 and 25-35 (Alvarez et al., 1997) (**Table 6.1**). Furthermore, an additional Aβ peptide (Aβ12-16), from the study by Inestrosa et al. (2005), was incorporated to study key binding residues which were reported to be within that Aβ12-16 region.

The best scoring complex was AChE-Aβ(12-16) which had the highest ipTM (0.62) and pTM (0.93) scores, as well as the highest model confidence (0.68). The ipTM score is within the range of plausibility (0.6-0.8) where a complex could exist in real life conditions. None of the models had a confidence score above the ‘high confidence’ threshold (0.74).

The 3D binding interface of Aβ(12-16) with AChE was explored and found to be predicted within the AChE active site. The active site forms a cleft with 4 important regions: the

peripheral or P-site (located at the top of the cleft), the catalytic triad (at the bottom of the cleft, in the acylation or A-site), the acyl-binding pocket (on the A-site) and the choline-binding pocket (also on the A-site) (Rosenberry et al., 2017). The atoms of the Aβ(12-16) peptide, 46 in total, were investigated to find favourable contacts (overlap > -0.4 Å) with AChE – 119 favourable contacts were found. These contacts show favourable interactions between the Aβ(12-16) peptide and 3 out of 4 key regions of the catalytic cleft. Specifically, this peptide interacts with all the key amino acids that form the P-site (i.e. Y72, Y124, W286, Y341) and the choline binding pocket (i.e. W86, T337), and with 2 out of the 3 key amino acids that form the acyl binding pocket (i.e. F295, F297) (Rosenberry et al., 2017). The Aβ(12-16) peptide does not extend to being able to interact with the catalytic triad (**Figure 6.2**).

	Model Scores		Model confidence
Model Name	**ipTM**	**pTM**	
AChE-Aβ(1-16)	0.26	0.87	0.38
AChE-Aβ(9-21)	0.40	0.91	0.50
AChE-Aβ(12-28)	0.39	0.87	0.49
AChE-Aβ(25-35)	0.51	0.89	0.59
AChE-Aβ(12-16)	0.62	0.93	0.68

Table 6.1 Protein complex model scores of AChE and truncated Aβ peptides.
Table showing the model scores of predicted complexes formed and scored by AlphaFold Server (Abramson et al., 2024). The lengths of the Aβ peptides were based on experimental data by Alvarez et al. (1997) and computational insights by Inestrosa et al. (2005). The model confidence score follows the algorithm described by Evans et al. (2021). Legend: ipTM = interface predicted template modelling; pTM = predicted template modelling

6.3.2 Aβ40, Aβ42 and their processing residues

The complexes between AChE and Aβ40, Aβ42 and the residual amino acids from the amyloidogenic pathway were investigated. The reasoning behind involved the mentioned connection between AChE and Aβ, and the evidence-supported connection between PSEN1 and AChE. AChE can regulate PSEN1 levels and reduce γ-secretase activity, potentially contributing to the to a feedback loop with Aβ accumulation (García-Ayllón et al., 2014; Silveyra et al., 2012; Silveyra et al., 2008; Campanari et al., 2014). For this reason, these amyloidogenic products might play an influential role in ACHE-APP-PSEN1 relationship.

In addition to Aβ40 and Aβ42, the residual tripeptides of the γ-secretase processing of APP-C99 (see **6.1.1**) were modelled and investigated. However, the AlphaFold Server did not allow the predictive modelling of peptides with smaller length than 4 amino acids. Thus, the combination of two different tripeptide residuals were explored, e.g. peptides from Aβ48→Aβ42 or Aβ49→ Aβ40 pathway (**Table 6.2**).

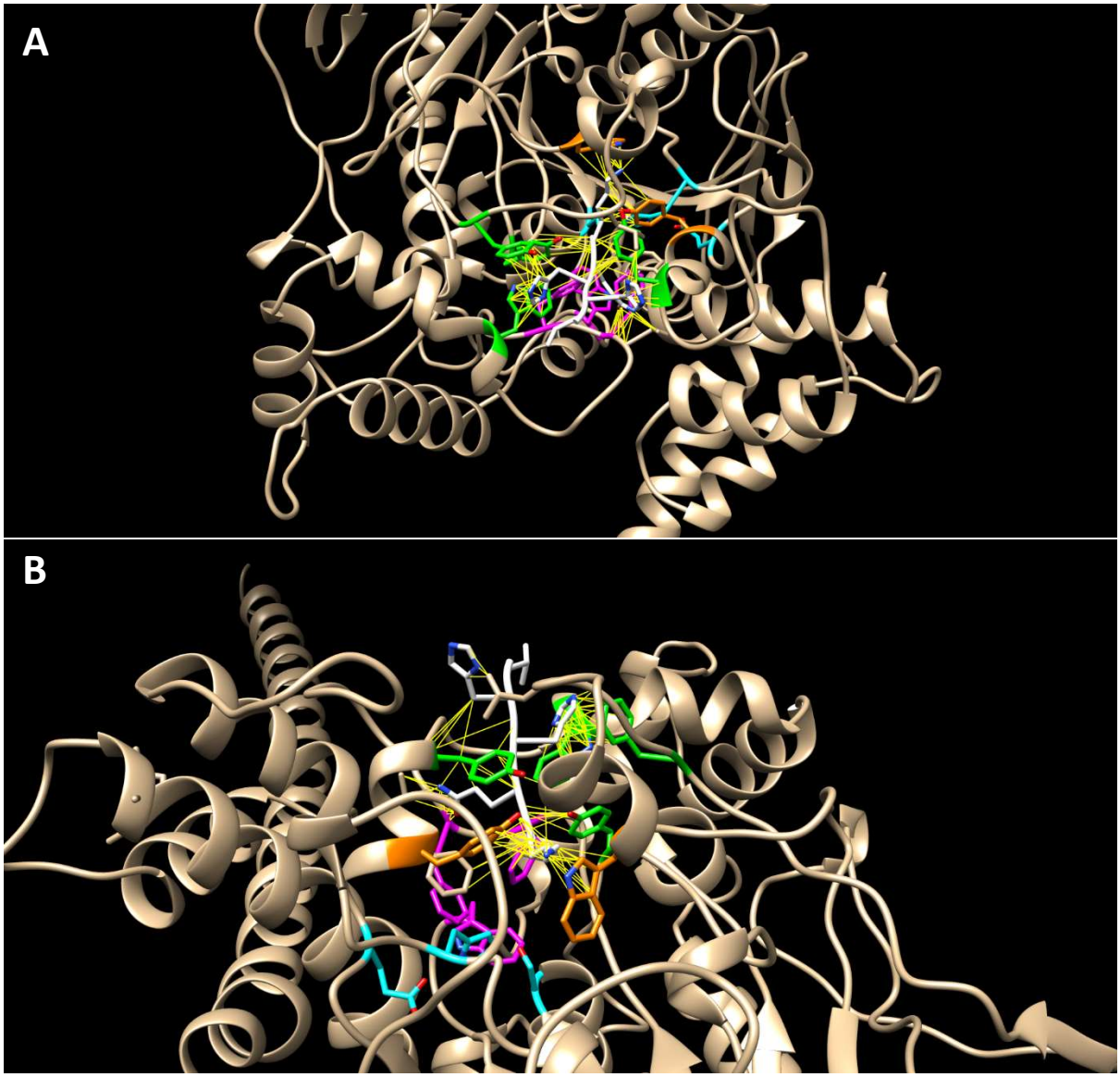

Figure 6.2 AChE-Aβ(12-16) protein complex.
Diagram showing the 3D protein complex between Aβ(12-16) (white) and AChE (light brown), alongside the favourable contacts between them (yellow lines). Key protein regions are coloured, and their atomic structures are shown: P-site (green), catalytic triad (cyan), acyl-binding pocket (magenta) and choline-binding pocket (orange) (Rosenberry et al., 2017). The Aβ(12-16) is formed by 46 atoms, these generated 119 favourable contacts. The contacts linked the Aβ(12-16) to almost all key amino acids forming the P-side, acyl-binding pocket and choline-binding pocket. It did not extend to being able to interact with the catalytic triad. Both figures show the same complex but from different distances: **A)** far view, **B)** close view.

The best ipTM score (0.56) and model confidence score (0.63) corresponds to the AChE-Aβ(40-46) complex. AChE-Aβ(42-48) had the highest pTM score (0.93). None of the models had a model confidence score above the 'high confidence' threshold (0.74).

The 3D binding interface of Aβ(40-46) with AChE and found that the Aβ peptide was modelled and located within ACHE's active site. Furthermore, the 43 atoms of the Aβ(40-46) were selected to find favourable contacts with AChE – 106 favourable contacts were found. These contacts show favourable interactions between the Aβ(40-46) peptide and all 4 of the regions that form the catalytic cleft of ACHE. Specifically, this peptide interacts with all the key amino acids that form the P-site (i.e. Y72, Y124, W286, Y341), 2 out of the 3 key amino acids that form the acyl binding site (i.e.F295, F297) and the catalytic triad (i.e. S203, H447), and 1 out of 2 amino acids that form the choline binding (i.e. Y337) (Rosenberry et al., 2017) (**Figure 6.3**).

	Model Scores		Model confidence
Model Name	ipTM	pTM	
AChE-Aβ42	0.20	0.88	0.34
AChE-Aβ40	0.22	0.88	0.35
AChE-Aβ(42-48)	0.52	0.93	0.60
AChE-Aβ(40-49)	0.53	0.92	0.61
AChE-Aβ(43-49)	0.55	0.92	0.62
AChE-Aβ(40-46)	0.56	0.92	0.63

Table 6.2 Protein complex model scores of AChE and amyloidogenic Aβ peptides.
Table showing the model scores of predicted complexes formed and scored by AlphaFold Server (Abramson et al., 2024). These specific Aβ peptides were chosen as they are products (or aggregates of tripeptide products) of the amyloidogenic processing of APP-C99 by PSEN1 (Bolduc et al., 2016). The model confidence score follows the algorithm described by Evans et al. (2021). Legend: ipTM = interface predicted template modelling; pTM = predicted template modelling

6.3.3 Glycosylated AChE structures

Noting the importance of glycosylation in AChE expressed in the literature, the effects of glycosylation on AChE were explored. Knowing that the glycosylation sites are at N265, N350 and N464, multiple combinations of these glycosylated amino acids were modelled (Xu et al., 2015; Velan et al., 1993) (**Table 6.3**). Considering the findings by Luk et al. (2012) and Xu et al. (2015), the following linear high-mannose glycan chain was added at the sites of glycosylation: NAG(NAG(MAN(MAN(MAN)))) (**Figure S9.2**).

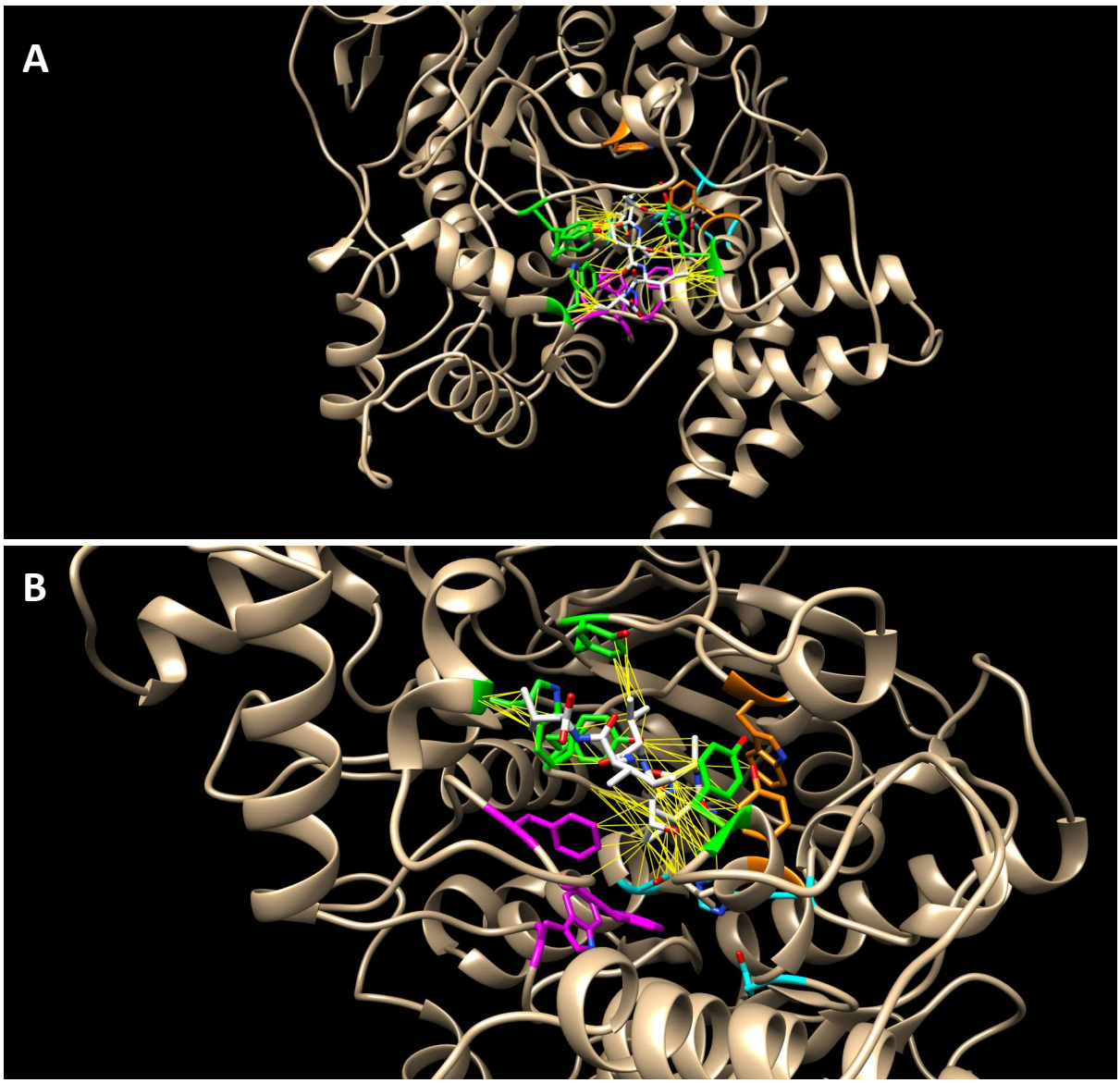

Figure 6.3 AChE- Aβ(40-46) protein complex.
These figures show the 3D complex between Aβ(40-46) (white) and AChE (light brown), alongside the favourable contacts between them (yellow lines). Key protein regions are coloured, and their atomic structures are shown: P-site (green), catalytic triad (cyan), acyl-binding pocket (magenta) and choline-binding pocket (orange) (Rosenberry et al., 2017). The Aβ(40-46) is formed by 43 atoms, these generated 106 favourable contacts. The contacts linked the Aβ peptide all 4 key regions of AChE's catalytic site. Both figures show the same complex but from different distances: **A)** far view, **B)** close view.

Generally, all glycan chains had elevated model scores when forming complexes with AChE. However, it was clear that the most successful one was ACHE_350gly – this is the AChE protein with a glycan chain (high in mannose) at N350 – which is also confirmed by the experiments of Xu et al. (2015). It had the highest ipTM (0.94) and shared the second highest pTM (0.92) alongside AChE_265_350gly (glycan chains at N265 and N350), only after the AChE model on its own (pTM = 0.94). Furthermore, with a model confidence score of 0.94, AChE_350gly was again the highest scoring model, indicating a high chance of this predicted structure existing *in vivo*. All the model confidence scores were above the 'high confidence' threshold (>0.74).

	Model Scores		Model confidence
Model Name	**ipTM**	**pTM**	
AChE	na	0.94	na
AChE_265gly	0.88	0.91	0.89
AChE_350gly	0.94	0.92	0.94
AChE_464gly	0.78	0.90	0.80
AChE_265_350gly	0.87	0.92	0.88
AChE_265_464gly	0.76	0.89	0.79
AChE_350_464gly	0.82	0.90	0.84
AChE_3xgly	0.82	0.90	0.84

Table 6.3 Protein complex model scores of AChE and high-mannose glycan chain.
The impact of glycosylation at specific positions in AChE was assessed. The type of glycan chain (high-mannose chain) and the glycosylation sites of AChE were taken from experimental data by Xu et al. (2015). The predicted complexes were formed and scored by AlphaFold Server (Abramson et al., 2024). The AChE model only has pTM score as it is not forming a complex with another biomolecule. The model confidence score follows the algorithm described by Evans et al. (2021). Legend: ipTM = interface predicted template modelling; pTM = predicted template modelling

Based on multiple claims about the importance of glycosylation in enzyme activity and conformation (Xu et al., 2015; Velan et al., 1993), previously high scored models (i.e. AChE-Aβ(12-16), AChE-Aβ(40-46)) were remodelled with glycosylated versions of AChE – some low score complex models were also remodelled (i.e. AChE-Aβ40, AChE-Aβ42). The impact glycosylation at position N350 of AChE was of particular interest – the model scores of these models can be seen in **Table 6.4**.

All models' scores had an improvement in their ipTM, pTM and thus also in the model confidence score. The ipTM scores of the complexes involving the two long Aβ chains (Aβ40 and Aβ42) were still below the 0.8 threshold to be considered accurate, but they significantly increased these scores to be in the 'potentially accurate' region, between 0.6-0.8. In general, the pTM scores remained the same or slightly increase compared to their

non-glycosylated complex equivalents. All the model confidence scores were above the 'high confidence' threshold (>0.74).

Model Name	Model Scores		Model confidence
	ipTM	pTM	
AChE_350gly-Aβ40	0.76	0.89	0.79
AChE_350gly-Aβ42	0.74	0.88	0.77
AChE_350gly-Aβ(12-16)	0.94	0.93	0.94
AChE_350gly-Aβ(40-46)	0.93	0.93	0.93

Table 6.4 Protein complex model scores of glycosylated AChE and different Aβ peptides. Remodelling of previously obtained complexes (between AChE and Aβ peptides) with a glycosylated AChE**.** The type of glycan chain (high-mannose chain) and the glycosylation sites (N350) of AChE were taken from experimental data by Xu et al. (2015). The predicted complexes were formed and scored by AlphaFold Server (Abramson et al., 2024). The model confidence score follows the algorithm described by Evans et al. (2021). Legend: ipTM = interface predicted template modelling; pTM = predicted template modelling

Comparisons between glycosylated AChE-Aβ complexes and their non-glycosylated counterparts were spatially assessed (**Figure 6.4**, **Figure 6.5**). The AChE-Aβ40 complex was chosen for this investigation (**Figure 6.4**) as it had higher model scores compared to Aβ42 (**Table 6.4**). The AChE-Aβ(40-46) complex (**Figure 6.5**) was also chosen, because even though it had lower model scores compared to the complexes with Ab(12-16), the AChE-Aβ(40-46) complex had contacts with 4/4 crucial sites of AChE's active site compared to 3/4 from the AChE-Aβ(12-16) (Rosenberry et al., 2017).

Both non-glycosylated and glycosylated models of AChE-Aβ40 had a very similar AChE chain when superimposed (**Figure 6.4A**). However, the shape of the Aβ40 chain within these complexes and the number of favourable contacts were different. The glycosylated complex had 322 contacts (**Figure 6.4B**) whereas the non-glycosylated one had 180 (**Figure 6.4C**). The number of conflictive clashes (overlap > 0.6 Å) for both glycosylated (41) and non-glycosylated (22) AChE-Aβ40 complexes were noted.

Similarly, the AChE chain on the glycosylated and non-glycosylated AChE-Aβ(40-46) complexes were highly similar when superimposed (**Figure 6.5A**). The orientation of the Aβ(40-46) peptide differed (**Figure 6.5B**), and so did the number of contacts and clashes between the glycosylated and non-glycosylated complexes. There were 106 contacts and 18 clashes for the non-glycosylated AChE-Aβ(40-46) complex, and 75 contacts and 4 clashes for the glycosylated one.

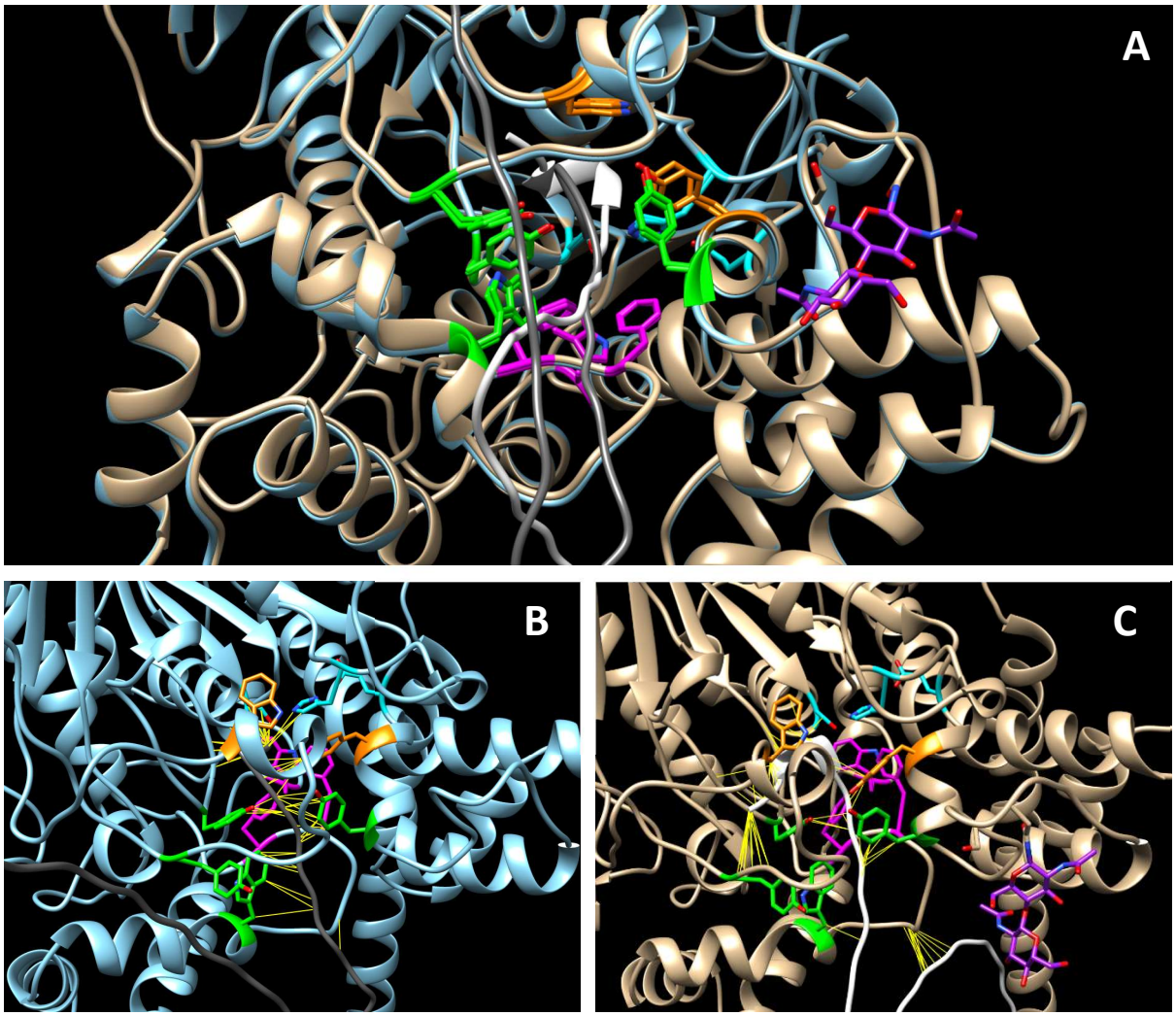

Figure 6.4 Non-glycosylated vs glycosylated AChE-Aβ40 protein complex.
A) Superimposed complexes showing the high similarity between the AChE chains. **B)** Non-glycosylated AChE-Aβ40 complex showing favourable contacts (yellow lines) between Aβ40 peptide and AChE chain. There were a total of 180 favourable contacts and 22 unfavourable clashes (not shown). **C)** Glycosylated AChE-Aβ40 complex showing favourable contacts (yellow lines) between Aβ40 peptide and AChE chain. There were a total of 322 favourable contacts and 41 unfavourable clashes (not shown). The high-mannose glycan chain was bound at position 350 of AChE. Colour scheme: non-glycosylated AChE chain (light blue), glycosylated AChE chain (light brown), Aβ40 chain from non-glycosylated complex (dim grey), Aβ40 chain from glycosylated complex (white), high-mannose glycan chain (purple), P-site (green), catalytic triad (cyan), acyl-binding pocket (magenta) and choline-binding pocket (orange).

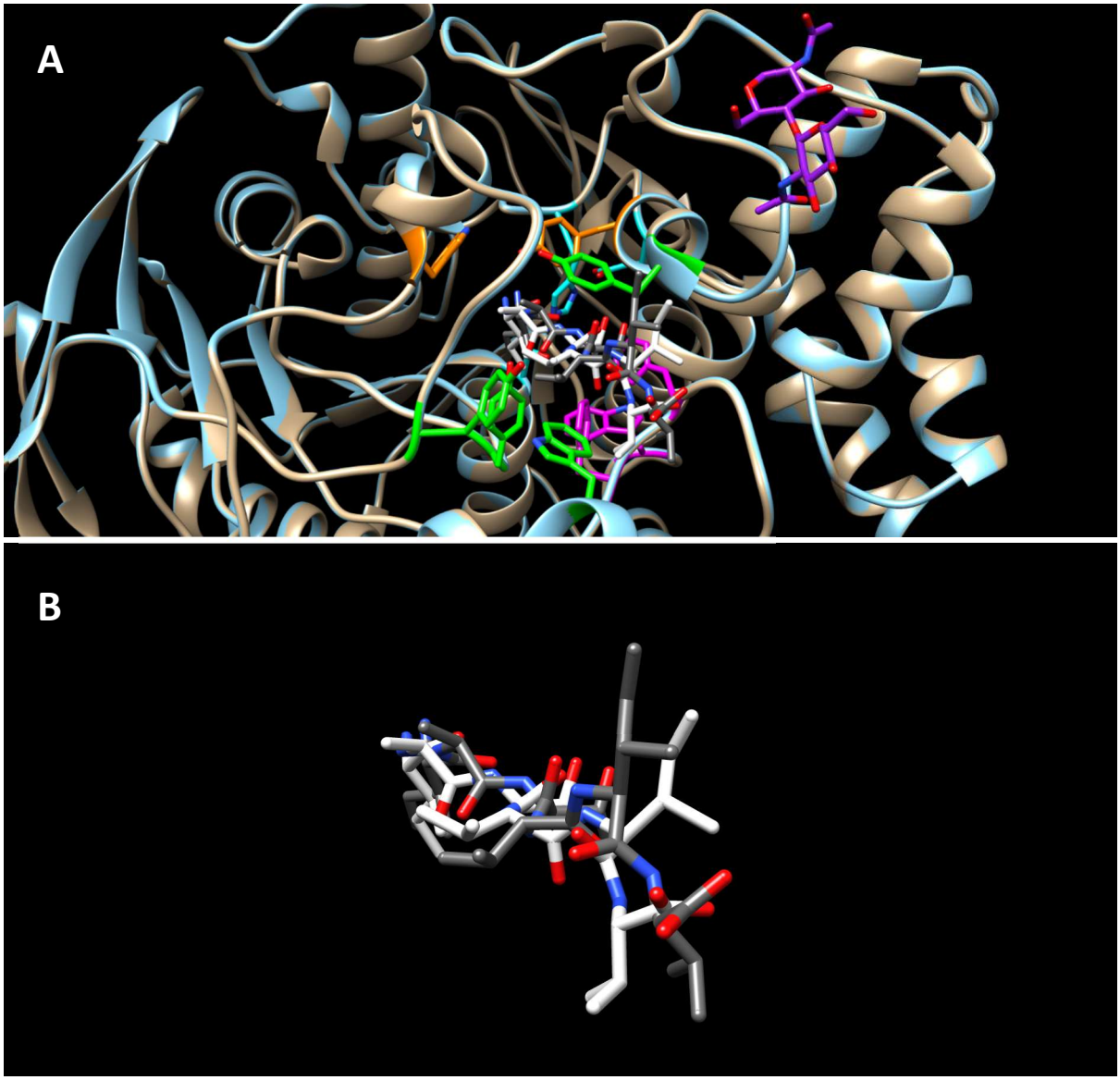

Figure 6.5 Non-glycosylated vs glycosylated AChE-Aβ(40-46) protein complex.
A) Superimposed complexes showing the high similarity between the AChE chains. **B)** Superimposed Aβ(40-46) peptides - these showed different orientation and number of clashes and contacts (not shown). There were 106 favourable contacts and 74 unfavourable clashes for the non-glycosylated complex, and 75 favourable contacts and 4 unfavourable clashes for the glycosylated complex. The high-mannose glycan chain was bound at position 350 of AChE. Colour scheme: non-glycosylated AChE chain (light blue), glycosylated AChE chain (light brown), Aβ(40-46) peptide from non-glycosylated complex (dim grey), Aβ(40-46) peptide from glycosylated complex (white), high-mannose glycan chain (purple), P-site (green), catalytic triad (cyan), acyl-binding pocket (magenta) and choline-binding pocket (orange).

6.3.4 APP transmembrane domain and AChE oligomers

As briefly mentioned before, previous studies discovered that patients with AD had a rise in monomeric (G1) and dimeric (G2) forms of AChE, and a decline of the tetrameric (G4) form (Fishman et al., 1986; García-Ayllón et al., 2010). As this study aimed to explore the relationship between APP and AChE, structural models were generated to identify potential binding interfaces that could act as inhibitors of AChE oligomerisation.

One dimer and one tetramer of the AChE protein were modelled, followed by the a dimer and a tetramer that included the transmembrane domain (TMD) of APP (from amino acid 700-724) (Barrett et al., 2012) (**Table 6.5**). The model scores of the sole AChE dimer were very high, obtaining an ipTM score of 0.85 – above the accuracy threshold at 0.8 – and a pTM score of 0.88, showing that the dimer structure could exist under physiological conditions. The addition of the TMD chain to the dimer generated a complex with lower model scores – an ipTM of 0.79 (falling below accuracy threshold) and a pTM of 0.85. The sole AChE tetramer had poor model scores, an ipTM of 0.4 and a pTM of 0.53. When coupled with a TMD chain, the model scores raised by a very small margin – ipTM = 0.41, pTM = 0.54. Both models containing the ACHE dimer had model confidence scores above the 'high' confidence threshold (>0.74).

	Model Scores		Model confidence
Model Name	ipTM	pTM	
AChEx2	0.85	0.88	0.86
AChEx4	0.4	0.53	0.43
AChEx2-APP(TMD)	0.79	0.85	0.80
AChEx4-APP(TMD)	0.41	0.54	0.44

Table 6.5 Protein complex scores of AChE oligomers coupled with the transmembrane domain of APP.
Modelling of AChE dimers (AChEx2) and tetramers (AChEx4) with and without a coupled APP segment corresponding to the TMD (from amino acid 700-724) (Barrett et al., 2012). The predicted complexes were formed and scored by AlphaFold Server (Abramson et al., 2024). The model confidence score follows the algorithm described by Evans et al. (2021). Legend: ipTM = interface predicted template modelling; pTM = predicted template modelling

The predicted models were compared to two crystal structures, one showing an almost complete AChE dimer (PDB: 4PQE; Dym et al., 2015) (**Figure 6.6B**) and one showing the protein regions involved in AChE tetramerisation (PDB: 1VZJ; Dvir et al., 2004) (**Figure 6.6D**). The 'Matchmaker' function was used to superimpose these crystal structures with the best generated models, i.e. AChE dimer (**Figure 6.6A**), and the AChE tetramer coupled to APP's TMD (**Figure 6.6C**), in order to obtain insights into their similarities. For the dimeric structures, the RMSD between 527 atom pairs (<2.0 Å) was 0.373 Å, and across all 528 pairs

it was 0.383 Å. For the tetrameric structures, the RMSD between 30 atom pairs (<2.0 Å) was 1.193 Å, and across all 34 pairs it was 1.783 Å.

The AChE dimer coupled with the TMD can be seen in **Figure S9.3A**. Unlike its tetrameric equivalent, the TMD in the dimeric structure was not located near the oligomerisation domain. The sole AChE tetramer can be seen in **Figure S9.3B**, its shape was not at all similar to the characteristic helical bundle presented by the crystal structure (**Figure 6.6D**).

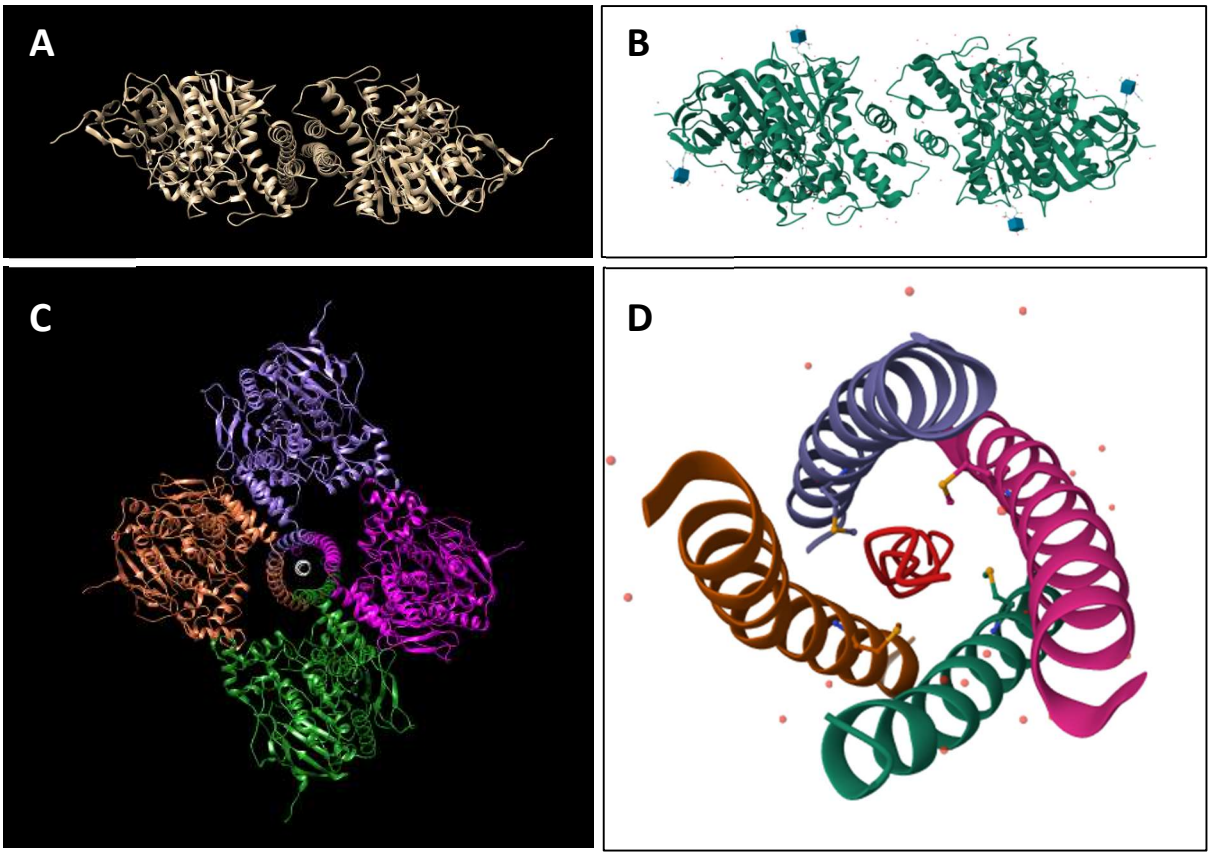

Figure 6.6 Protein structures of AChE oligomers.
A) Predicted AChE dimer. **B)** AChE dimer crystal structure (PDB: 4PQE; Dym et al., 2015). **C)** Predicted AChE tetramer complexed with APP's transmembrane domain (from amino acid 700 to 724). **D)** Crystal structure of the AChE oligomerisation domain forming a tetramer with a collagen tail (PDB: 1VZJ; Dvir et al., 2004).

6.4 Discussion

6.4.1 AChE-Aβ putative complexes

The initial aim of this study was to validate the experimental results obtained by Alvarez et al. (1997) and Inestrosa et al. (2005) by producing complexes that followed the trends described by them. It was expected for both the AChE-Aβ(12-28) complex and the AChE-Aβ(12-16) complex to have relatively high model complex score. However, as seen in **Table 6.1**, the AChE-Aβ(12-28) model had a poor ipTM score (< 0.6), thus becoming unlikely to exist in biological conditions. On the other hand, the AChE-Aβ(12-16) model had an ipTM between 0.6 and 0.8, also known as the 'grey zone', where predictions could be accurate but they could also be incorrect (Zhang & Skolnick, 2004). The pTM scores in **Table 6.1** are all high, well above the 0.5 threshold for an accurate folding of the complex. However, as seen in **Table 6.3**, the AChE individual model showed to have a very high pTM (0.94) and plDDT (predicted local distance difference test; >0.90; data not shown) which also measures how accurate a predicted structure would be compared to an experimental one (Magana & Kovalevskiy, 2024). Thus, it is likely that AChE's high pTM score could influence the pTM scores of AChE complexes and for that reason a higher emphasis should be placed on the ipTM scores, which measure the relative positions of the chains in the complex. The model confidence score also puts more weight on the ipTM score making it a useful measure to consider (see **6.2.1**). In fact, this measure indicated that none of the models in **Table 6.1** can be considered of 'high confidence' as they do not go above the 0.74 threshold.

In a pathological environment caused by AD, an overproduction of Aβ peptides (including residual peptides from amyloidogenic processing) could occur meaning that they could interact with other proteins (Chen et al., 2017). Considering the evidence suggesting a link between Aβ fibrils and AChE (Carvajal & Inestrosa, 2011; Alvarez et al., 1998), multiple models that included Aβ peptides and putative residual peptides from PSEN1 processing were generated. On **Table 6.2** none of the models had an ipTM score above 0.6, making their relative folding unlikely to exist under native conditions. All models on the table had a very high pTM score – potentially influenced by AChE's high confidence folding. None of the model confidence scores was particularly high and none went above the 'high confidence' threshold.

Regardless of the mediocre scoring, the best performing models of the tables mentioned above were explored. **Figure 6.2** showed the AChE-Aβ(12-16) protein complex was within the catalytic site of AChE and so was the AChE-Aβ(40-46) protein complex (**Figure 6.3**), creating 119 and 106 favourable contacts respectively. The fact that they were in the catalytic site of AChE creates questions regarding their ability to act as a competitor inhibitor of acetylcholine. Even though the AChE-Aβ(40-46) model had less contacts, the Aβ(40-46) peptide was able to interact with all 4 important regions of the catalytic site, whereas the Aβ(12-16) peptide interacted with 3 out of 4.

6.4.2 Glycosylation impact

In **Table 6.3**, different glycosylation sites were incorporated into some of the AChE models and it allowed for corroboration of the findings by Xu et al. (2015) – specifically about the importance of glycosylation at position 350. The model scores were all generally high, but the best ipTM score corresponded to the AChE_350gly model (glycosylated AChE at position 350; 0.94). This model also had a very high pTM score, second only to the AChE stand-alone model. All models in **Table 6.3** had a model confidence above the 'high confidence' threshold (0.74) indicating that these glycosylation sites are likely to exist in real physiological conditions, potentially having a relevant role in normal AChE functioning.

The performance of the glycosylated AChE variant at position 350 was subsequently examined within protein complexes. **Table 6.4** showed a significant increase in the ipTM scores, especially when compared with previous commonly low scores (**Table 6.1**, **Table 6.2**).

These improved scores raised an important question: do the improved ipTM scores reflect a better interaction between AChE and Aβ peptides, or are they mainly due to a stable and confident bond with the glycan chain? To address this, the AChE-Aβ40 complex and the AChE-Aβ(40-46) complex were invesitigated (**Figure 6.4**, **Figure 6.5**). As shown by **Figure 6.4A** and **Figure 6.5A**, the AChE chains are basically identical when superimposed meaning that no major conformational change occurs as a consequence of the added glycan chain. However, the Aβ peptides do undergo slightly changes in orientation (**Figure 6.5B**) or have their chains redirected / rearranged in space (**Figure 6.4B-C**). Additionally, the number of contacts and clashes increased on the glycosylated AChE-Aβ40 complex compared to the non-glycosylated one. Interestingly, the contacts and clashes decreased in number on the glycosylated AChE-Aβ(40-46) complex compared to the non-glycosylated equivalent. To investigate this further, all complexes listed in **Table 6.4** were analysed and compared with their non-glycosylated counterparts. The resulting data are presented in **Table 6.6**.

All glycosylated AChE–Aβ complexes displayed an increased number of contacts and clashes involving the Aβ peptides compared with their non-glycosylated counterparts (**Table 6.6**). The only exception was the Aβ(40-46) peptide, which produced less contacts and clashes being part of the glycosylated AChE-Aβ(40-46) complex compared to the non-glycosylated one. The fact that the number of unfavourable clashes decreased suggests that this peptide is able to better accommodate within the AChE active site of the glycosylated chain. This complex formation is further supported by a high model confidence (0.93), increasing its possibilities of existing under physiological conditions.

Finally, the increased glycosylation of AChE observed on AD, introduces a scenario in which this complex could be more easily formed (Sáez-Valero et al., 2001). However, considering the amyloidogenic mechanisms, it would be difficult to create this 6-amino-acid-long peptide (Aβ40-46) but perhaps increased production of amyloidogenic residual tripeptides could increase the chances of them interacting with the AChE active site.

Model	Atoms	Contacts (> -0.4 Å)	Clashes (> 0.6 Å)	Model confidence
AChE-Aβ40	306	180	22	0.35
AChE_350gly-Aβ40	306	322	41	0.79
AChE-Aβ42	319	148	12	0.34
AChE_350gly-Aβ42	319	218	26	0.77
AChE-Aβ(40-46)	43	106	18	0.63
AChE_350gly-Aβ(40-46)	43	75	4	0.93
AChE-Aβ(12-16)	46	119	18	0.68
AChE_350gly-Aβ(12-16)	46	151	28	0.94

Table 6.6 Contacts and clashes produced by Aβ peptides of glycosylated and non-glycosylated AChE-Aβ complexes.
Information about favourable contacts and unfavourable clashes on specific complexes and their glycosylated equivalents. The data showed that Aβ peptides belonging to glycosylated complexes produced more contacts and clashes compared to the ones part of non-glycosylated complexes. The only exemption came from the glycosylated AChE-Aβ(40-46) complex (yellow) whose Aβ(40-46) peptide produced less contacts and clashes than in the non-glycosylated complex. The 'Atoms' column refers to the number of atoms forming the Aβ peptide and the model confidence scores considers both ipTM and pTM scores.

6.4.3 Disruptive oligomerisation of AChE

The objective was to identify a region within APP capable of disrupting AChE oligomerisation, thereby linking the findings of Fishman et al. (1986) with those of Nalivaeva and Turner (2016). In order words, attribute the decrease in G4 forms of AChE and the increase in G1 ones to the imbalance of a putative AChE-APP regulatory system. A possible way in which this could happen would be if APP, or a region of APP, were to inhibit the formation of AChE oligomers. Hence the generation of predicted complexes between AChE dimers and tetramers and the TMD of APP.

In **Table 6.5**, AChE dimers seem to do better without the addition of TMD to the protein complex. On the other hand, the AChE tetramer bound to TMD seemed to have a slight positive effect on the complex scores, plus it radically changed the tetrameric shape, making it more similar to a real crystal structure of an AChE tetramer (**Figure 6.6C**, **Figure 6.6D**, **Figure S9.3**). After superimposing **Figure 6.6C** and **Figure 6.6D**, there was an RMSD of 1.193 Å between 30 atom pairs (<2.0 Å), and an RMSD of 1.783 Å across all 34 pairs. it was. By general consensus, superimposed structure with an RMSD below 2.0 Å are considered to be homologous. Hence, it can be inferred that APP's TMD chain has the potential to interfere with G4 tetramer formation by acting as a substitute for the collagen tail.

6.4.4 Limitations and future steps

This chapter aimed to generate AChE-Aβ models with potential to exist *in vivo*. Hence, in order to further investigate how the interaction between Aβ and AChE would work, docking studies could be performed. This would help understanding the potential binding interactions between the two peptides, providing initial insights into their possible binding modes. Furthermore, carrying out molecular dynamics simulations would allow to take the interaction predictions from docking studies and explore how these complexes behave dynamically over time in a physiologically relevant environment (e.g., solvent, temperature, ionic conditions).

Given the literature supporting the interactions between AChE and Aβ fibrils, it would have been interesting to try to model these interactions computationally, perhaps on a different platform that allows the upload of existing crystal structures or processed ones (e.g. AutoDock Vina, HADDOCK). A lot of information on the structure of Aβ fibrils has become available (Yang et al., 2022) so it would be a good time to further explore this hypothesis.

It is not possible to create a narrative of the AD pathology solely on computational work and appropriate experimental procedures need to be done in order to know more about certain findings. For instance, co-immunoprecipitations experiments could be performed to test direct physical interactions between AChE and Aβ peptides. Alternatively, surface plasmon resonance studies could be done to quantitatively measure binding affinities and kinetics between AChE and Aβ peptides.

7 Conclusions

In conclusion, this bioinformatics investigation into the amyloid precursor protein (APP) and its interactions with PSEN1 and AChE has provided critical insights into the molecular underpinnings of Alzheimer's disease (AD). The structural modelling of APP variants, particularly those involved in EOFAD, highlighted how specific mutations like T714A and V715M introduce significant structural disruptions in key domains, which could affect amyloidogenic cleavage and contribute to the toxic accumulation of amyloid-beta (Aβ) peptides. The superimposition and hydrogen bond analysis revealed critical deviations in the APP-PSEN1 interaction, particularly in EOFAD variants that showed aberrant interactions at the γ-secretase cleavage site. These findings underscore the importance of structural stability in APP processing, particularly in regions that are critical for the cleavage events leading to Aβ formation, a hallmark of AD pathology. The analysis of AChE's role, particularly in its interaction with Aβ peptides, shed light on the complex relationship between cholinergic and amyloidogenic systems in AD. While the predicted models for AChE-Aβ complexes were not as robust as anticipated, the results suggested that glycosylation plays a crucial role in modulating AChE's structural stability and its potential interactions with Aβ. This interplay between glycosylation and AChE function could represent a novel pathway for therapeutic intervention, particularly in mitigating the cholinergic deficits observed in AD patients. These results also suggest a broader interrelationship between cholinergic signalling and APP processing, offering a more integrated perspective on AD pathogenesis. However, the research would have benefitted from larger sample sizes and more sophisticated methods, such as molecular dynamics simulations, to better capture the dynamic nature of these protein interactions and to provide a more comprehensive understanding of their physiological relevance.

As a future direction, creating a centralised database containing pathogenicity-related structural and molecular information for AD mutations could greatly enhance the ability to predict the pathogenic potential of new mutations. This database could incorporate data from computational modelling, experimental findings, and clinical outcomes, thereby serving as a valuable resource for researchers and clinicians alike. By systematically cataloguing the structural deviations and molecular mechanisms underlying pathogenic mutations, this tool would allow for a more informed approach to designing targeted treatments for AD, ultimately advancing the field toward personalised medicine approaches. Such a database could also bridge the gap between bioinformatics and experimental research, promoting the validation of computational findings and the development of novel therapeutic strategies.

8 References

8.1 Chapter 1

Alzheimer's Society. (2023). *Local dementia statistics | Alzheimer's Society*. Www.alzheimers.org.uk. https://www.alzheimers.org.uk/about-us/policy-and-influencing/local-dementia-statistics

Areosa, S. A., Sherriff, F., & McShane, R. (2005). Memantine for dementia. *The Cochrane Database of Systematic Reviews*, *3*, CD003154. https://doi.org/10.1002/14651858.cd003154.pub4

Bartus, R., Dean, R., Beer, B., & Lippa, A. (1982). The Cholinergic Hypothesis of Geriatric Memory Dysfunction. *Science*, *217*(4558), 408–414. https://doi.org/10.1126/science.7046051

Bateman, A., Martin, M.-J., Orchard, S., Magrane, M., Ahmad, S., Alpi, E., Bowler-Barnett, E. H., Britto, R., Bye-A-Jee, H., Cukura, A., Denny, P., Dogan, T., Ebenezer, T., Fan, J., Garmiri, P., da Costa Gonzales, L. J., Hatton-Ellis, E., Hussein, A., Ignatchenko, A., & Insana, G. (2022). UniProt: the Universal Protein Knowledgebase in 2023. *Nucleic Acids Research*, *51*(D1). https://doi.org/10.1093/nar/gkac1052

Bekdash, R. A. (2021). The Cholinergic System, the Adrenergic System and the Neuropathology of Alzheimer's Disease. *International Journal of Molecular Sciences*, *22*(3), 1273. https://doi.org/10.3390/ijms22031273

Bekris, L. M., Yu, C.-E., Bird, T. D., & Tsuang, D. W. (2010). Review Article: Genetics of Alzheimer Disease. *Journal of Geriatric Psychiatry and Neurology*, *23*(4), 213–227. https://doi.org/10.1177/0891988710383571

Bellenguez, C., Küçükali, F., Jansen, I. E., Kleineidam, L., Moreno-Grau, S., Amin, N., Naj, A. C., Campos-Martin, R., Grenier-Boley, B., Andrade, V., Holmans, P. A., Boland, A., Damotte, V., van der Lee, S. J., Costa, M. R., Kuulasmaa, T., Yang, Q., de Rojas, I., Bis, J. C., & Yaqub, A. (2022). New insights into the genetic etiology of Alzheimer's disease and related dementias. *Nature Genetics*, *54*(4). https://doi.org/10.1038/s41588-022-01024-z

Bird, T. D. (2008). Genetic aspects of Alzheimer disease. *Genetics in Medicine*, *10*(4), 231–239. https://doi.org/10.1097/gim.0b013e31816b64dc

Bliss, T. V. P., & Cooke, S. F. (2011). Long-term potentiation and long-term depression: a clinical perspective. *Clinics*, *66*(1), 3–17. https://doi.org/10.1590/s1807-59322011001300002

Brown, B. M., Peiffer, J. J., Sohrabi, H. R., Mondal, A., Gupta, V. B., Rainey-Smith, S. R., Taddei, K., Burnham, S., Ellis, K. A., Szoeke, C., Masters, C. L., Ames, D., Rowe, C. C., & Martins, R. N. (2012). Intense physical activity is associated with cognitive performance in the elderly. *Translational Psychiatry*, *2*(11), e191–e191. https://doi.org/10.1038/tp.2012.118

Bubley, A., Erofeev, A., Gorelkin, P., Beloglazkina, E., Majouga, A., & Krasnovskaya, O. (2023). Tacrine-Based Hybrids: Past, Present, and Future. *International Journal of Molecular Sciences*, *24*(2), 1717. https://doi.org/10.3390/ijms24021717

Byun, J., Srivithya Vellampatti, Chatterjee, P., Sun Ha Hwang, Byoung Choul Kim, & Lee, J. (2023). Characterization of the role of Kunitz-type protease inhibitor domain in dimerization of amyloid precursor protein. *Journal of Computational Chemistry*, *44*(15), 1437–1445. https://doi.org/10.1002/jcc.27100

Chang, K. J., Hong, C. H., Lee, K. S., Kang, D. R., Lee, J. D., Choi, S. H., Kim, S. Y., Na, D. L., Seo, S. W., Kim, D.-K., Lee, Y., Chung, Y. K., Lim, K. Y., Noh, J. S., Park, J., & Son, S. J. (2017). Mortality Risk after

Diagnosis of Early-Onset Alzheimer's Disease versus Late-Onset Alzheimer's Disease: A Propensity Score Matching Analysis. *Journal of Alzheimer's Disease*, *56*(4), 1341–1348. https://doi.org/10.3233/jad-161181

Chen, G., Xu, T., Yan, Y., Zhou, Y., Jiang, Y., Melcher, K., & Xu, H. E. (2017). Amyloid beta: structure, biology and structure-based therapeutic development. *Acta Pharmacologica Sinica*, *38*(9), 1205–1235. https://doi.org/10.1038/aps.2017.28

Corder, E., Saunders, A., Strittmatter, W., Schmechel, D., Gaskell, P., Small, G., Roses, A., Haines, J., & Pericak-Vance, M. (1993). Gene dose of apolipoprotein E type 4 allele and the risk of Alzheimer's disease in late onset families. *Science*, *261*(5123), 921–923. https://doi.org/10.1126/science.8346443

Coronel, R., Bernabeu-Zornoza, A., Palmer, C., Muñiz-Moreno, M., Zambrano, A., Cano, E., & Liste, I. (2018). Role of Amyloid Precursor Protein (APP) and Its Derivatives in the Biology and Cell Fate Specification of Neural Stem Cells. *Molecular Neurobiology*, *55*(9), 7107–7117. https://doi.org/10.1007/s12035-018-0914-2

Crary, J. F., Trojanowski, J. Q., Schneider, J. A., Abisambra, J. F., Abner, E. L., Alafuzoff, I., Arnold, S. E., Attems, J., Beach, T. G., Bigio, E. H., Cairns, N. J., Dickson, D. W., Gearing, M., Grinberg, L. T., Hof, P. R., Hyman, B. T., Jellinger, K., Jicha, G. A., Kovacs, G. G., & Knopman, D. S. (2014). Primary age-related tauopathy (PART): a common pathology associated with human aging. *Acta Neuropathologica*, *128*(6), 755–766. https://doi.org/10.1007/s00401-014-1349-0

Cui, M. Y., Lin, Y., Sheng, J. Y., Zhang, X., & Cui, R. J. (2018). Exercise Intervention Associated with Cognitive Improvement in Alzheimer's Disease. *Neural Plasticity*, *2018*, 1–10. https://doi.org/10.1155/2018/9234105

Cummings, J. L., Morstorf, T., & Zhong, K. (2014). Alzheimer's disease drug-development pipeline: few candidates, frequent failures. *Alzheimer's Research & Therapy*, *6*(4), 37. https://doi.org/10.1186/alzrt269

Davies, P., & Maloney, A. J. (1976). Selective loss of central cholinergic neurons in Alzheimer's disease. *The Lancet*, *308*(8000), 1403. https://doi.org/10.1016/s0140-6736(76)91936-x

Duggan, M., Torkzaban, B., Mohseni Ahooyi, T., Khalili, K., & Gordon, J. (2020). Age Related Neurodegenerative Diseases. *Journal of Cellular Physiology*, *235*(4), 3131–3141. https://doi.org/10.1002/jcp.29248

Dyrks, T., Weidemann, A., Multhaup, G., Salbaum, J. M., Lemaire, H. G., Kang, J., Müller-Hill, B., Masters, C. L., & Beyreuther, K. (1988). Identification, transmembrane orientation and biogenesis of the amyloid A4 precursor of Alzheimer's disease. *The EMBO Journal*, *7*(4), 949–957. https://doi.org/10.1002/j.1460-2075.1988.tb02900.x

Ehrenberg, A. J., Nguy, A. K., Theofilas, P., Dunlop, S., Suemoto, C. K., Di Lorenzo Alho, A. T., Leite, R. P., Diehl Rodriguez, R., Mejia, M. B., Rüb, U., Farfel, J. M., de Lucena Ferretti-Rebustini, R. E., Nascimento, C. F., Nitrini, R., Pasquallucci, C. A., Jacob-Filho, W., Miller, B., Seeley, W. W., Heinsen, H., & Grinberg, L. T. (2017). Quantifying the accretion of hyperphosphorylated tau in the locus coeruleus and dorsal raphe nucleus: the pathological building blocks of early Alzheimer's disease. *Neuropathology and Applied Neurobiology*, *43*(5), 393–408. https://doi.org/10.1111/nan.12387

Epperly, T., Dunay, M. A., & Boice, J. L. (2017). Alzheimer Disease: Pharmacologic and Nonpharmacologic Therapies for Cognitive and Functional Symptoms. *American Family Physician*, *95*(12), 771–778. https://www.aafp.org/pubs/afp/issues/2017/0615/p771.html

Ferrari, C., & Sorbi, S. (2021). The complexity of Alzheimer's disease: an evolving puzzle. *Physiological Reviews*, *101*(3), 1047–1081. https://doi.org/10.1152/physrev.00015.2020

Frisoni, G. B., Altomare, D., Thal, D. R., Ribaldi, F., van der Kant, R., Ossenkoppele, R., Blennow, K., Cummings, J., van Duijn, C., Nilsson, P. M., Dietrich, P.-Y., Scheltens, P., & Dubois, B. (2022). The probabilistic model of Alzheimer disease: the amyloid hypothesis revised. *Nature Reviews Neuroscience*, *23*(1), 53–66. https://doi.org/10.1038/s41583-021-00533-w

Gasiorowska, A., Wydrych, M., Drapich, P., Zadrozny, M., Steczkowska, M., Niewiadomski, W., & Niewiadomska, G. (2021). The Biology and Pathobiology of Glutamatergic, Cholinergic, and Dopaminergic Signaling in the Aging Brain. *Frontiers in Aging Neuroscience*, *13*. https://doi.org/10.3389/fnagi.2021.654931

Glenner, G. G., & Wong, C. W. (1984). Alzheimer's disease: Initial Report of the Purification and Characterization of a Novel Cerebrovascular Amyloid Protein. *Biochemical and Biophysical Research Communications*, *120*(3), 885–890. https://doi.org/10.1016/s0006-291x(84)80190-4

Goedert, M., Spillantini, M. G., & Crowther, R. A. (1991). Tau Proteins and Neurofibrillary Degeneration. *Brain Pathology*, *1*(4), 279–286. https://doi.org/10.1111/j.1750-3639.1991.tb00671.x

Golde, T. E., & Levey, A. I. (2023). Immunotherapies for Alzheimer's disease. *Science*, *382*(6676), 1242–1244. https://doi.org/10.1126/science.adj9255

Gouilly, D., Rafiq, M., Nogueira, L., Salabert, A.-S., Payoux, P., Péran, P., & Pariente, J. (2023). Beyond the amyloid cascade: An update of Alzheimer's disease pathophysiology. *Revue Neurologique*. https://doi.org/10.1016/j.neurol.2022.12.006

Graff, M. J. L., Vernooij-Dassen, M. J. M., Thijssen, M., Dekker, J., Hoefnagels, W. H. L., & Rikkert, M. G. M. O. (2006). Community based occupational therapy for patients with dementia and their care givers: randomised controlled trial. *BMJ*, *333*(7580), 1196. https://doi.org/10.1136/bmj.39001.688843.be

Grüninger, F. (2015). Invited review: Drug development for tauopathies. *Neuropathology and Applied Neurobiology*, *41*(1), 81–96. https://doi.org/10.1111/nan.12192

Guerreiro, R. J., Gustafson, D. R., & Hardy, J. (2012). The genetic architecture of Alzheimer's disease: beyond APP, PSENs and APOE. *Neurobiology of Aging*, *33*(3), 437–456. https://doi.org/10.1016/j.neurobiolaging.2010.03.025

Haass, C., Kaether, C., Thinakaran, G., & Sisodia, S. (2012). Trafficking and Proteolytic Processing of APP. *Cold Spring Harbor Perspectives in Medicine*, *2*(5), a006270–a006270. https://doi.org/10.1101/cshperspect.a006270

Hameed, S., Fuh, J.-L., Senanarong, V., Ebenezer, E. G. M., Looi, I., Dominguez, J. C., Park, K. W., Karanam, A. K., & Simon, O. (2020). Role of Fluid Biomarkers and PET Imaging in Early Diagnosis and its Clinical Implication in the Management of Alzheimer's Disease. *Journal of Alzheimer's Disease Reports*, *4*(1), 21–37. https://doi.org/10.3233/adr-190143

Hampel, H., Hardy, J., Blennow, K., Chen, C., Perry, G., Kim, S. H., Villemagne, V. L., Aisen, P., Vendruscolo, M., Iwatsubo, T., Masters, C. L., Cho, M., Lannfelt, L., Cummings, J. L., & Vergallo, A. (2021). The Amyloid-β Pathway in Alzheimer's Disease. *Molecular Psychiatry*, *26*(10). https://doi.org/10.1038/s41380-021-01249-0

Hane, F. T., Robinson, M., Lee, B. Y., Bai, O., Leonenko, Z., & Albert, M. S. (2017). Recent Progress in Alzheimer's Disease Research, Part 3: Diagnosis and Treatment. *Journal of Alzheimer's Disease*, *57*(3), 645–665. https://doi.org/10.3233/jad-160907

Hardy, J., & Higgins, G. (1992). Alzheimer's disease: the amyloid cascade hypothesis. *Science*, *256*(5054), 184–185. https://doi.org/10.1126/science.1566067

Hascup, K. N., & Hascup, E. R. (2016). Soluble Amyloid-β42 Stimulates Glutamate Release through Activation of the α7 Nicotinic Acetylcholine Receptor. *Journal of Alzheimer's Disease*, *53*(1), 337–347. https://doi.org/10.3233/jad-160041

Howard, R., McShane, R., Lindesay, J., Ritchie, C., Baldwin, A., Barber, R., Burns, A., Dening, T., Findlay, D., Holmes, C., Hughes, A., Jacoby, R., Jones, R., Jones, R., McKeith, I., Macharouthu, A., O'Brien, J., Passmore, P., Sheehan, B., & Juszczak, E. (2012). Donepezil and Memantine for Moderate-to-Severe Alzheimer's Disease. *New England Journal of Medicine*, *366*(10), 893–903. https://doi.org/10.1056/nejmoa1106668

Hu, Y., Qu, Z., Cao, S., Li, Q., Ma, L., Krencik, R., Xu, M., & Liu, Y. (2016). Directed differentiation of basal forebrain cholinergic neurons from human pluripotent stem cells. *Journal of Neuroscience Methods*, *266*, 42–49. https://doi.org/10.1016/j.jneumeth.2016.03.017

Jin, M., Shepardson, N., Yang, T., Chen, G., Walsh, D., & Selkoe, D. J. (2011). Soluble amyloid -protein dimers isolated from Alzheimer cortex directly induce Tau hyperphosphorylation and neuritic degeneration. *Proceedings of the National Academy of Sciences*, *108*(14), 5819–5824. https://doi.org/10.1073/pnas.1017033108

Kang, J., Lemaire, H.-G., Unterbeck, A., Salbaum, J. M., Masters, C. L., Grzeschik, K.-H., Multhaup, G., Beyreuther, K., & Müller-Hill, B. (1987). The precursor of Alzheimer's disease amyloid A4 protein resembles a cell-surface receptor. *Nature*, *325*(6106), 733–736. https://doi.org/10.1038/325733a0

Karch, C. M., & Goate, A. M. (2015). Alzheimer's Disease Risk Genes and Mechanisms of Disease Pathogenesis. *Biological Psychiatry*, *77*(1), 43–51. https://doi.org/10.1016/j.biopsych.2014.05.006

Karikari, T. K., Pascoal, T. A., Ashton, N. J., Janelidze, S., Benedet, A. L., Rodriguez, J. L., Chamoun, M., Savard, M., Kang, M. S., Therriault, J., Schöll, M., Massarweh, G., Soucy, J.-P., Höglund, K., Brinkmalm, G., Mattsson, N., Palmqvist, S., Gauthier, S., Stomrud, E., & Zetterberg, H. (2020). Blood phosphorylated tau 181 as a biomarker for Alzheimer's disease: a diagnostic performance and prediction modelling study using data from four prospective cohorts. *The Lancet Neurology*, *19*(5), 422–433. https://doi.org/10.1016/s1474-4422(20)30071-5

Kemp, N., & Bashir, Z. I. (1999). Induction of LTD in the adult hippocampus by the synaptic activation of AMPA/kainate and metabotropic glutamate receptors. *Neuropharmacology*, *38*(4), 495–504. https://doi.org/10.1016/s0028-3908(98)00222-6

Kosik, K. S., Joachim, C. L., & Selkoe, D. J. (1986). Microtubule-associated protein tau (tau) is a major antigenic component of paired helical filaments in Alzheimer disease. *Proceedings of the National Academy of Sciences*, *83*(11), 4044–4048. https://doi.org/10.1073/pnas.83.11.4044

Kume, T., & Takada-Takatori, Y. (2018). *Nicotinic Acetylcholine Receptor Signaling: Roles in Neuroprotection* (A. Akaike, S. Shimohama, & Y. Misu, Eds.). PubMed; Springer. https://www.ncbi.nlm.nih.gov/books/NBK543546/

Kurth, V., Ogorek, I., Münch, C., Lopez-Rios, J., Solenne Ousson, Lehmann, S., Katja Nieweg, Anton J.M. Roebroek, Pietrzik, C. U., Beher, D., & Sascha Weggen. (2023). Pathogenic Aβ production by heterozygous PSEN1 mutations is intrinsic to the mutant protein and not mediated by conformational hindrance of wild-type PSEN1. *Journal of Biological Chemistry*, *299*(8), 104997–104997. https://doi.org/10.1016/j.jbc.2023.104997

Lacor, P. N., Buniel, M. C., Furlow, P. W., Sanz Clemente, A., Velasco, P. T., Wood, M., Viola, K. L., & Klein, W. L. (2007). A Oligomer-Induced Aberrations in Synapse Composition, Shape, and Density Provide a Molecular Basis for Loss of Connectivity in Alzheimer's Disease. *Journal of Neuroscience*, *27*(4), 796–807. https://doi.org/10.1523/jneurosci.3501-06.2007

Lai, F., & Williams, R. S. (1989). A Prospective Study of Alzheimer Disease in Down Syndrome. *Archives of Neurology*, *46*(8), 849–853. https://doi.org/10.1001/archneur.1989.00520440031017

Lambert, J.-C., Ramirez, A., Grenier-Boley, B., & Bellenguez, C. (2023). Step by step: towards a better understanding of the genetic architecture of Alzheimer's disease. *Molecular Psychiatry*, *28*, 2716–2727. https://doi.org/10.1038/s41380-023-02076-1

Lamptey, R., Chaulagain, B., Trivedi, R., Gothwal, A., Layek, B., & Singh, J. (2022). A Review of the Common Neurodegenerative Disorders: Current Therapeutic Approaches and the Potential Role of Nanotherapeutics. *ProQuest*, *23*(3), 1851. https://doi.org/10.3390/ijms23031851

Landrum, M. J., Lee, J. M., Riley, G. R., Jang, W., Rubinstein, W. S., Church, D. M., & Maglott, D. R. (2014). ClinVar: public archive of relationships among sequence variation and human phenotype. *Nucleic Acids Research*, *42*(Database issue), D980–D985. https://doi.org/10.1093/nar/gkt1113

Laver, K., Dyer, S., Whitehead, C., Clemson, L., & Crotty, M. (2016). Interventions to delay functional decline in people with dementia: a systematic review of systematic reviews. *BMJ Open*, *6*(4), e010767. https://doi.org/10.1136/bmjopen-2015-010767

Liu, C.-C., Kanekiyo, T., Xu, H., & Bu, G. (2013). Apolipoprotein E and Alzheimer disease: risk, Mechanisms and Therapy. *Nature Reviews Neurology*, *9*(2), 106–118. https://doi.org/10.1038/nrneurol.2012.263

Mandelkow, E., Starmer, K., Vogel, R., & Thies, E. (2003). Clogging of axons by tau, inhibition of axonal traffic and starvation of synapses. *Neurobiology of Aging*, *24*(8), 1079–1085. https://doi.org/10.1016/j.neurobiolaging.2003.04.007

Mapstone, M., Cheema, A. K., Fiandaca, M. S., Zhong, X., Mhyre, T. R., MacArthur, L. H., Hall, W. J., Fisher, S. G., Peterson, D. R., Haley, J. M., Nazar, M. D., Rich, S. A., Berlau, D. J., Peltz, C. B., Tan, M. T., Kawas, C. H., & Federoff, H. J. (2014). Plasma phospholipids identify antecedent memory impairment in older adults. *Nature Medicine*, *20*(4), 415–418. https://doi.org/10.1038/nm.3466

Mayer, M. L., & Westbrook, G. L. (1987). The physiology of excitatory amino acids in the vertebrate central nervous system. *Progress in Neurobiology*, *28*(3), 197–276. https://doi.org/10.1016/0301-0082(87)90011-6

Mendez, M. F. (2019). Early-onset alzheimer disease and its variants. *CONTINUUM: Lifelong Learning in Neurology*, *25*(1), 34–51. https://doi.org/10.1212/con.0000000000000687

Min, H., Kim, J., Kim, Y.-J., Yoon, M.-S., Pratley, R. E., & Lee, Y.-H. (2017). Measurement of altered APP isoform expression in adipose tissue of diet-induced obese mice by absolute quantitative real-time PCR. *Animal Cells and Systems*, *21*(2), 100–107. https://doi.org/10.1080/19768354.2017.1290679

Misrani, A., Tabassum, S., & Yang, L. (2021). Mitochondrial Dysfunction and Oxidative Stress in Alzheimer's Disease. *Frontiers in Aging Neuroscience*, *13*. https://doi.org/10.3389/fnagi.2021.617588

Nakamura, T., & Lipton, S. A. (2010). Preventing Ca2+-mediated nitrosative stress in neurodegenerative diseases: Possible pharmacological strategies. *Cell Calcium*, *47*(2), 190–197. https://doi.org/10.1016/j.ceca.2009.12.009

Neundörfer, G. (2003). The discovery of Alzheimer's disease. *Dialogues in Clinical Neuroscience*, *5*(1), 101. https://www.ncbi.nlm.nih.gov/pmc/articles/PMC3181715/

Nhan, H. S., Chiang, K., & Koo, E. H. (2014). The multifaceted nature of amyloid precursor protein and its proteolytic fragments: friends and foes. *Acta Neuropathologica*, *129*(1), 1–19. https://doi.org/10.1007/s00401-014-1347-2

Nurk, S., Koren, S., Rhie, A., Rautiainen, M., Bzikadze, A. V., Mikheenko, A., Vollger, M. R., Altemose, N., Uralsky, L., Gershman, A., Aganezov, S., Hoyt, S. J., Diekhans, M., Logsdon, G. A., Alonge, M., Antonarakis, S. E., Borchers, M., Bouffard, G. G., Brooks, S. Y., & Caldas, G. V. (2022). The complete sequence of a human genome. *Science*, *376*(6588), 44–53. https://doi.org/10.1126/science.abj6987

Office for National Statistics. (2023, April 11). *Death registration summary statistics, England and Wales - Office for National Statistics*. Www.ons.gov.uk. https://www.ons.gov.uk/peoplepopulationandcommunity/birthsdeathsandmarriages/deaths/articles/deathregistrationsummarystatisticsenglandandwales/2022

Olsson, F., Schmidt, S., Althoff, V., Munter, L., Jin, S., Rosqvist, S., Lendahl, U., Multhaup, G., & Lundkvist, J. (2014, January 17). *Characterization of Intermediate Steps in Amyloid Beta (Aβ) Production Under Near-Native Conditions*. The Journal of Biological Chemistry. https://pubmed.ncbi.nlm.nih.gov/24225948/

Opler, L. A., Medalia, A., Opler, M. G., & Stahl, S. M. (2013). Pharmacotherapy of cognitive deficits in schizophrenia. *CNS Spectrums*, *19*(2), 142–156. https://doi.org/10.1017/s1092852913000771

Perry, E. K., Gibson, P. H., Blessed, G., Perry, R. H., & Tomlinson, B. E. (1977). Neurotransmitter enzyme abnormalities in senile dementia. *Journal of the Neurological Sciences*, *34*(2), 247–265. https://doi.org/10.1016/0022-510x(77)90073-9

Pfundstein, G., Nikonenko, A. G., & Sytnyk, V. (2022). Amyloid precursor protein (APP) and amyloid β (Aβ) interact with cell adhesion molecules: Implications in Alzheimer's disease and normal physiology. *Frontiers in Cell and Developmental Biology*, *10*. https://doi.org/10.3389/fcell.2022.969547

Priller, C., Bauer, T., Mitteregger, G., Krebs, B., Kretzschmar, H. A., & Herms, J. (2006). Synapse Formation and Function Is Modulated by the Amyloid Precursor Protein. *Journal of Neuroscience*, *26*(27), 7212–7221. https://doi.org/10.1523/JNEUROSCI.1450-06.2006

Qing, H., Li, N.-M., Liu, K.-F., Qiu, Y.-J., Zhang, H.-H., & Nakanishi, H. (2019). Mutations of beta-amyloid precursor protein alter the consequence of Alzheimer's disease pathogenesis. *Neural Regeneration Research*, *14*(4), 658. https://doi.org/10.4103/1673-5374.247469

Ramirez-Bermudez, J. (2012). Alzheimer's Disease: Critical Notes on the History of a Medical Concept. *Archives of Medical Research*, *43*(8), 595–599. https://doi.org/10.1016/j.arcmed.2012.11.008

Rapoport, M., Dawson, H. N., Binder, L. I., Vitek, M. P., & Ferreira, A. (2002). Tau is essential to β-amyloid-induced neurotoxicity. *Proceedings of the National Academy of Sciences of the United States of America*, *99*(9), 6364–6369. https://doi.org/10.1073/pnas.092136199

Schneider, J. A. (2022). Neuropathology of Dementia Disorders. *CONTINUUM: Lifelong Learning in Neurology*, *28*(3), 834. https://doi.org/10.1212/CON.0000000000001137

Semwal, B. C., & Garabadu, D. (2020). Amyloid beta (1–42) downregulates adenosine-2b receptors in addition to mitochondrial impairment and cholinergic dysfunction in memory-sensitive mouse brain regions. *Journal of Receptors and Signal Transduction*, *40*(6), 531–540. https://doi.org/10.1080/10799893.2020.1767136

Sevigny, J., Chiao, P., Bussière, T., Weinreb, P. H., Williams, L., Maier, M., Dunstan, R., Salloway, S., Chen, T., Ling, Y., O'Gorman, J., Qian, F., Arastu, M., Li, M., Chollate, S., Brennan, M. S., Quintero-Monzon, O., Scannevin, R. H., Arnold, H. M., & Engber, T. (2016). The antibody aducanumab reduces Aβ plaques in Alzheimer's disease. *Nature*, *537*(7618), 50–56. https://doi.org/10.1038/nature19323

Shankar, G. M., Li, S., Mehta, T. H., Garcia-Munoz, A., Shepardson, N. E., Smith, I., Brett, F. M., Farrell, M. A., Rowan, M. J., Lemere, C. A., Regan, C. M., Walsh, D. M., Sabatini, B. L., & Selkoe, D. J. (2008). Amyloid-β protein dimers isolated directly from Alzheimer's brains impair synaptic plasticity and memory. *Nature Medicine*, *14*(8), 837–842. https://doi.org/10.1038/nm1782

Shi, M., Chu, F., Zhu, F., & Zhu, J. (2022). Impact of anti-amyloid-β Monoclonal Antibodies on the Pathology and Clinical Profile of Alzheimer's disease: a Focus on Aducanumab and Lecanemab. *Frontiers in Aging Neuroscience*, *14*(1). https://doi.org/10.3389/fnagi.2022.870517

Sims, J. R., Zimmer, J. A., Evans, C. D., Lu, M., Ardayfio, P., Sparks, J., Wessels, A. M., Shcherbinin, S., Wang, H., Monkul Nery, E. S., Collins, E. C., Solomon, P., Salloway, S., Apostolova, L. G., Hansson, O., Ritchie, C., Brooks, D. A., Mintun, M., Skovronsky, D. M., & TRAILBLAZER-ALZ 2 Investigators. (2023). Donanemab in Early Symptomatic Alzheimer Disease: The TRAILBLAZER-ALZ 2 Randomized Clinical Trial. *JAMA*, *330*(6). https://doi.org/10.1001/jama.2023.13239

Sinha, S., Anderson, J. P., Barbour, R., Basi, G. S., Caccavello, R., Davis, D., Doan, M., Dovey, H. F., Frigon, N., Hong, J., Jacobson-Croak, K., Jewett, N., Keim, P., Knops, J., Lieberburg, I., Power, M., Tan, H., Tatsuno, G., Tung, J., & Schenk, D. (1999). Purification and cloning of amyloid precursor protein beta-secretase from human brain. *Nature*, *402*(6761), 537–540. https://doi.org/10.1038/990114

Sofi, F., Valecchi, D., Bacci, D., Abbate, R., Gensini, G. F., Casini, A., & Macchi, C. (2010). Physical activity and risk of cognitive decline: a meta-analysis of prospective studies. *Journal of Internal Medicine*, *269*(1), 107–117. https://doi.org/10.1111/j.1365-2796.2010.02281.x

Soscia, S. J., Kirby, J. E., Washicosky, K. J., Tucker, S. M., Ingelsson, M., Hyman, B., Burton, M. A., Goldstein, L. E., Duong, S., Tanzi, R. E., & Moir, R. D. (2010). The Alzheimer's Disease-Associated Amyloid β-Protein Is an Antimicrobial Peptide. *PLoS ONE*, *5*(3), e9505. https://doi.org/10.1371/journal.pone.0009505

Sperling, R. A., Jack, C. R., Black, S. E., Frosch, M. P., Greenberg, S. M., Hyman, B. T., Scheltens, P., Carrillo, M. C., Thies, W., Bednar, M. M., Black, R. S., Brashear, H. R., Grundman, M., Siemers, E. R., Feldman, H. H., & Schindler, R. J. (2011). Amyloid-related imaging abnormalities in amyloid-modifying therapeutic trials: Recommendations from the Alzheimer's Association Research Roundtable Workgroup. *Alzheimer's & Dementia*, *7*(4), 367–385. https://doi.org/10.1016/j.jalz.2011.05.2351

St George-Hyslop, P., Tanzi, R., Polinsky, R., Haines, J., Nee, L., Watkins, P., Myers, R., Feldman, R., Pollen, D., Drachman, D., & al., e. (1987). The genetic defect causing familial Alzheimer's disease maps on chromosome 21. *Science*, *235*(4791), 885–890. https://doi.org/10.1126/science.2880399

Swanson, C. J., Zhang, Y., Dhadda, S., Wang, J., Kaplow, J., Lai, R. Y. K., Lannfelt, L., Bradley, H., Rabe, M., Koyama, A., Reyderman, L., Berry, D. A., Berry, S., Gordon, R., Kramer, L. D., & Cummings, J. L. (2021). A randomized, double-blind, phase 2b proof-of-concept clinical trial in early Alzheimer's disease with lecanemab, an anti-Aβ protofibril antibody. *Alzheimer's Research & Therapy*, *13*(1). https://doi.org/10.1186/s13195-021-00813-8

Tanzi, R. E. (2012). The Genetics of Alzheimer Disease. *Cold Spring Harbor Perspectives in Medicine*, *2*(10), a006296–a006296. https://doi.org/10.1101/cshperspect.a006296

TCW, J., & Goate, A. M. (2016). Genetics of β-Amyloid Precursor Protein in Alzheimer's Disease. *Cold Spring Harbor Perspectives in Medicine*, *7*(6), a024539. https://doi.org/10.1101/cshperspect.a024539

Theuns, J., Jurgen Del-Favero, Dermaut, B., Cornelia, Backhovens, H., Van, M., Serneels, S., Corsmit, E., Christine Van Broeckhoven, & Cruts, M. (2000). Genetic variability in the regulatory region of presenilin 1 associated with risk for Alzheimer's disease and variable expression. *Human Molecular Genetics*, *9*(3), 325–331. https://doi.org/10.1093/hmg/9.3.325

Troutwine, B. R., Hamid, L., Lysaker, C. R., Strope, T. A., & Wilkins, H. M. (2022). Apolipoprotein E and Alzheimer's disease. *Acta Pharmaceutica Sinica. B*, *12*(2), 496–510. https://doi.org/10.1016/j.apsb.2021.10.002

Turner, P. R., O'Connor, K., Tate, W. P., & Abraham, W. C. (2003). Roles of amyloid precursor protein and its fragments in regulating neural activity, plasticity and memory. *Progress in Neurobiology*, *70*(1), 1–32. https://doi.org/10.1016/s0301-0082(03)00089-3

van der Kant, R., Goldstein, L. S. B., & Ossenkoppele, R. (2019). Amyloid-β-independent regulators of tau pathology in Alzheimer disease. *Nature Reviews Neuroscience*, *21*(1), 21–35. https://doi.org/10.1038/s41583-019-0240-3

Verghese, P. B., Castellano, J. M., & Holtzman, D. M. (2011). Apolipoprotein E in Alzheimer's disease and other neurological disorders. *The Lancet Neurology*, *10*(3), 241–252. https://doi.org/10.1016/s1474-4422(10)70325-2

Vogt, A.-C. S., Jennings, G. T., Mohsen, M. O., Vogel, M., & Bachmann, M. F. (2023). Alzheimer's Disease: A Brief History of Immunotherapies Targeting Amyloid β. *International Journal of Molecular Sciences*, *24*(4), 3895. https://doi.org/10.3390/ijms24043895

Wang, G., Estrella, A., Hakim, O., Milazzo, P., Patel, S., Pintagro, C., Li, D., Zhao, R., Vance, D. E., & Li, W. (2022). Mini-Mental State Examination and Montreal Cognitive Assessment as Tools for Following Cognitive Changes in Alzheimer's Disease Neuroimaging Initiative Participants. *Journal of Alzheimer's Disease*, *90*(1), 263–270. https://doi.org/10.3233/jad-220397

Wang, H.-Y., Li, W., Benedetti, N. J., & Lee, D. H. S. (2003). Alpha 7 nicotinic acetylcholine receptors mediate beta-amyloid peptide-induced tau protein phosphorylation. *The Journal of Biological Chemistry*, *278*(34), 31547–31553. https://doi.org/10.1074/jbc.M212532200

Wang, Z., Wang, B., Yang, L., Guo, Q., Aithmitti, N., Songyang, Z., & Zheng, H. (2009). Presynaptic and Postsynaptic Interaction of the Amyloid Precursor Protein Promotes Peripheral and Central Synaptogenesis. *Journal of Neuroscience*, *29*(35), 10788–10801. https://doi.org/10.1523/jneurosci.2132-09.2009

Wattmo, C., & Wallin, Å. K. (2017). Early- versus late-onset Alzheimer's disease in clinical practice: cognitive and global outcomes over 3 years. *Alzheimer's Research & Therapy*, *9*(1), 70. https://doi.org/10.1186/s13195-017-0294-2

Whitehouse, P. J., Price, D. L., Struble, R. G., Clark, A. W., Coyle, J. T., & Delon, M. R. (1982). Alzheimer's disease and senile dementia: loss of neurons in the basal forebrain. *Science (New York, N.Y.)*, *215*(4537), 1237–1239. https://doi.org/10.1126/science.7058341

Wightman, D. P., Jansen, I. E., Savage, J. E., Shadrin, A. A., Bahrami, S., Holland, D., Rongve, A., Børte, S., Winsvold, B. S., Drange, O. K., Martinsen, A. E., Skogholt, A. H., Willer, C., Bråthen, G., Bosnes, I., Nielsen, J. B., Fritsche, L. G., Thomas, L. F., Pedersen, L. M., & Gabrielsen, M. E. (2021). A genome-wide association study with 1,126,563 individuals identifies new risk loci for Alzheimer's disease. *Nature Genetics*, *53*(9), 1276–1282. https://doi.org/10.1038/s41588-021-00921-z

Wisniewski, K. E., Dalton, A. J., McLachlan, D. R. C., Wen, G. Y., & Wisniewski, H. M. (1985). Alzheimer's disease in Down's syndrome: Clinicopathologic studies. *Neurology*, *35*(7), 957–957. https://doi.org/10.1212/wnl.35.7.957

Wood, J. G., Mirra, S. S., Pollock, N. J., & Binder, L. I. (1986). Neurofibrillary tangles of Alzheimer disease share antigenic determinants with the axonal microtubule-associated protein tau (tau). *Proceedings of the National Academy of Sciences*, *83*(11), 4040–4043. https://doi.org/10.1073/pnas.83.11.4040

Woods, B., Aguirre, E., Spector, A. E., & Orrell, M. (2012). Cognitive stimulation to improve cognitive functioning in people with dementia. *Cochrane Database of Systematic Reviews*, *2*(2). https://doi.org/10.1002/14651858.cd005562.pub2

World Health Organisation, & Alzheimer's Disease International. (2017, December 7). *Global Action Plan on the Public Health Response to Dementia 2017 - 2025*. Www.who.int. https://www.who.int/publications/i/item/global-action-plan-on-the-public-health-response-to-dementia-2017---2025

World Health Organization. (2021). *Global status report on the public health response to dementia*. World Health Organization.

Zhang, B., Maiti, A., Shively, S., Lakhani, F., McDonald-Jones, G., Bruce, J., Lee, E. B., Xie, S. X., Joyce, S., Li, C., Toleikis, P. M., Lee, V. M.-Y. ., & Trojanowski, J. Q. (2004). Microtubule-binding drugs offset tau sequestration by stabilizing microtubules and reversing fast axonal transport deficits in a tauopathy model. *Proceedings of the National Academy of Sciences*, *102*(1), 227–231. https://doi.org/10.1073/pnas.0406361102

Zhang, Y., Chen, H., Li, R., Sterling, K., & Song, W. (2023). Amyloid β-based therapy for Alzheimer's disease: challenges, successes and future. *Signal Transduction and Targeted Therapy*, *8*(1), 1–26. https://doi.org/10.1038/s41392-023-01484-7

Zhao, Y.-J., Han, H.-Z., Liang, Y., Shi, C.-Z., Zhu, Q.-C., & Yang, J. (2015). Alternative splicing ofVEGFA,APPandNUMBgenes in colorectal cancer. *World Journal of Gastroenterology*, *21*(21), 6550. https://doi.org/10.3748/wjg.v21.i21.6550

Zhu, X.-C., Tan, L., Wang, H.-F., Jiang, T., Cao, L., Wang, C., Wang, J., Tan, C.-C., Meng, X.-F., & Yu, J.-T. (2015). Rate of early onset Alzheimer's disease: a systematic review and meta-analysis. *Annals of Translational Medicine*, *3*(3). https://doi.org/10.3978/j.issn.2305-5839.2015.01.19

Živanović, M., Aracki Trenkić, A., Milošević, V., Stojanov, D., Mišić, M., Radovanović, M., & Radovanović, V. (2023). The role of magnetic resonance imaging in the diagnosis and prognosis of dementia. *Biomolecules & Biomedicine*, *23*(2), 209–224. https://doi.org/10.17305/bjbms.2022.8085

8.2 Chapter 2

Abramson, J., Adler, J., Dunger, J., Evans, R., Green, T., Pritzel, A., Ronneberger, O., Willmore, L., Ballard, A. J., Bambrick, J., Bodenstein, S. W., Evans, D. A., Hung, C.-C., O'Neill, M., Reiman, D., Tunyasuvunakool, K., Wu, Z., Žemgulytė, A., Arvaniti, E., & Beattie, C. (2024). Accurate structure prediction of biomolecular interactions with AlphaFold 3. *Nature*, *630*, 1–3. https://doi.org/10.1038/s41586-024-07487-w

Altschul, S., Madden, T., Schäffer, A., Zhang, J., Miller, W., & Lipman, D. (1997). Gapped BLAST and PSI-BLAST: a new generation of protein database search programs. *Nucleic Acids Research*, *25*(17), 3389–3402. https://doi.org/10.1093/nar/25.17.3389

Ancolio, K., Dumanchin, C., Barelli, H., Warter, J. M., Brice, A., Campion, D., Frebourg, T., & Checler, F. (1999). Unusual phenotypic alteration of amyloid precursor protein (APP) maturation by a new Val-715 -> Met APP-770 mutation responsible for probable early-onset Alzheimer's disease. *Proceedings of the National Academy of Sciences*, *96*(7), 4119–4124. https://doi.org/10.1073/pnas.96.7.4119

APP | ALZFORUM. (n.d.). Www.alzforum.org. Retrieved July 4, 2024, from https://www.alzforum.org/mutations/app

Bateman, A., Martin, M.-J., Orchard, S., Magrane, M., Ahmad, S., Alpi, E., Bowler-Barnett, E. H., Britto, R., Bye-A-Jee, H., Cukura, A., Denny, P., Dogan, T., Ebenezer, T., Fan, J., Garmiri, P., da Costa Gonzales, L. J., Hatton-Ellis, E., Hussein, A., Ignatchenko, A., & Insana, G. (2022). UniProt: the Universal Protein Knowledgebase in 2023. *Nucleic Acids Research*, *51*(D1). https://doi.org/10.1093/nar/gkac1052

Berman, H. M. (2000). The Protein Data Bank. *Nucleic Acids Research*, *28*(1), 235–242. https://doi.org/10.1093/nar/28.1.235

Bertram, L., & Tazi, R. E. (2005). The genetic epidemiology of neurodegenerative disease. *Journal of Clinical Investigation*, *115*(6), 1449–1457. https://doi.org/10.1172/jci24761

Bolduc, D. M., Montagna, D. R., Seghers, M. C., Wolfe, M. S., & Selkoe, D. J. (2016). The amyloid-beta forming tripeptide cleavage mechanism of γ-secretase. *ELife*, *5*. https://doi.org/10.7554/elife.17578

Buchan, D. W. A., Moffat, L., Lau, A., Kandathil, S., & Jones, D. (2024). Deep learning for the PSIPRED Protein Analysis Workbench. *Nucleic Acids Research*, *52*(W1). https://doi.org/10.1093/nar/gkae328

Bugiani, O., Giaccone, G., Rossi, G., Mangieri, M., Capobianco, R., Morbin, M., Mazzoleni, G., Cupidi, C., Marcon, G., Giovagnoli, A., Bizzi, A., Di Fede, G., Puoti, G., Carella, F., Salmaggi, A., Romorini, A., Patruno, G. M., Magoni, M., Padovani, A., & Tagliavini, F. (2010). Hereditary Cerebral Hemorrhage With Amyloidosis Associated With the E693K Mutation of APP. *Archives of Neurology*, *67*(8). https://doi.org/10.1001/archneurol.2010.178

Chartier-Harlin, M.-C., Crawford, F., Houlden, H., Warren, A., Hughes, D., Fidani, L., Goate, A., Rossor, M., Roques, P., Hardy, J., & Mullan, M. (1991). Early-onset Alzheimer's disease caused by mutations at codon 717 of the β-amyloid precursor protein gene. *Nature*, *353*(6347), 844–846. https://doi.org/10.1038/353844a0

Eckman, C. B., Mehta, N. D., Crook, R., Perez-tur, J., Prihar, G., Pfeiffer, E., Graff-Radford, N., Hinder, P., Yager, D., Zenk, B., Refolo, L. M., Mihail Prada, C., Younkin, S. G., Hutton, M., & Hardy, J. (1997). A New Pathogenic Mutation in the APP Gene (I716V) Increases the Relative Proportion of Aβ42(43). *Human Molecular Genetics*, *6*(12), 2087–2089. https://doi.org/10.1093/hmg/6.12.2087

Evans, R., O'Neill, M., Pritzel, A., Antropova, N., Senior, A., Green, T., Žídek, A., Bates, R., Blackwell, S., Yim, J., Ronneberger, O., Bodenstein, S., Zielinski, M., Bridgland, A., Potapenko, A., Cowie, A., Tunyasuvunakool, K., Jain, R., Clancy, E., & Kohli, P. (2021). Protein complex prediction with AlphaFold-Multimer. *BioRxiv*. https://doi.org/10.1101/2021.10.04.463034

Grabowski, T. J., Cho, H. S., Vonsattel, J. P. G., Rebeck, G. W., & Greenberg, S. M. (2001). Novel amyloid precursor protein mutation in an Iowa family with dementia and severe cerebral amyloid angiopathy. *Annals of Neurology*, *49*(6), 697–705. https://doi.org/10.1002/ana.1009

Guo, S.-S., Liu, J., Zhou, X., & Zhang, G. (2022). DeepUMQA: ultrafast shape recognition-based protein model quality assessment using deep learning. *Bioinformatics*, *38*(7), 1895–1903. https://doi.org/10.1093/bioinformatics/btac056

Hardy, J., & Higgins, G. (1992). Alzheimer's disease: the amyloid cascade hypothesis. *Science*, *256*(5054), 184–185. https://doi.org/10.1126/science.1566067

Jones, D. T., & Cozzetto, D. (2014). DISOPRED3: precise disordered region predictions with annotated protein-binding activity. *Bioinformatics*, *31*(6), 857–863. https://doi.org/10.1093/bioinformatics/btu744

Jonsson, T., Atwal, J. K., Steinberg, S., Snaedal, J., Jonsson, P. V., Bjornsson, S., Stefansson, H., Sulem, P., Gudbjartsson, D., Maloney, J., Hoyte, K., Gustafson, A., Liu, Y., Lu, Y., Bhangale, T., Graham, R. R., Huttenlocher, J., Bjornsdottir, G., Andreassen, O. A., & Jönsson, E. G. (2012). A mutation in APP protects against Alzheimer's disease and age-related cognitive decline. *Nature*, *488*(7409), 96–99. https://doi.org/10.1038/nature11283

Jumper, J., Evans, R., Pritzel, A., Green, T., Figurnov, M., Ronneberger, O., Tunyasuvunakool, K., Bates, R., Žídek, A., Potapenko, A., Bridgland, A., Meyer, C., Kohl, S. A. A., Ballard, A. J., Cowie, A., Romera-Paredes, B., Nikolov, S., Jain, R., Adler, J., & Back, T. (2021). Highly accurate protein structure prediction with alphafold. *Nature*, *596*(7873), 583–589. https://doi.org/10.1038/s41586-021-03819-2

Kumar-Singh, S. (2000). Nonfibrillar diffuse amyloid deposition due to a gamma42-secretase site mutation points to an essential role for N-truncated Abeta42 in Alzheimer's disease. *Human Molecular Genetics*, *9*(18), 2589–2598. https://doi.org/10.1093/hmg/9.18.2589

Kwok, J. B., Li, Q. X., Hallupp, M., Whyte, S., Ames, D., Beyreuther, K., Masters, C. L., & Schofield, P. R. (2000). Novel Leu723Pro amyloid precursor protein mutation increases amyloid beta42(43) peptide levels and induces apoptosis. *Annals of Neurology*, *47*(2), 249–253. https://doi.org/10.1002/1531-8249(200002)47:2%3C249::aid-ana18%3E3.0.co;2-8

Landrum, M. J., Lee, J. M., Riley, G. R., Jang, W., Rubinstein, W. S., Church, D. M., & Maglott, D. R. (2014). ClinVar: public archive of relationships among sequence variation and human phenotype. *Nucleic Acids Research*, *42*(Database issue), D980–D985. https://doi.org/10.1093/nar/gkt1113

Levy, E., Carman, M., Fernandez-Madrid, I., Power, M., Lieberburg, I., van Duinen, S., Bots, G., Luyendijk, W., & Frangione, B. (1990). Mutation of the Alzheimer's disease amyloid gene in hereditary cerebral hemorrhage, Dutch type. *Science*, *248*(4959), 1124–1126. https://doi.org/10.1126/science.2111584

Milacic, M., Beavers, D., Conley, P., Gong, C., Gillespie, M., Griss, J., Haw, R., Jassal, B., Matthews, L., May, B., Petryszak, R., Eliot Ragueneau, Rothfels, K., Sevilla, C., Shamovsky, V., Stephan, R., Krishna Kumar Tiwari, Thawfeek Varusai, Weiser, J., & Wright, A. (2023). The Reactome Pathway Knowledgebase 2024. *Nucleic Acids Research*, *52*(D1). https://doi.org/10.1093/nar/gkad1025

Mullan, M., Crawford, F., Axelman, K., Houlden, H., Lilius, L., Winblad, B., & Lannfelt, L. (1992). A pathogenic mutation for probable Alzheimer's disease in the APP gene at the N–terminus of β–amyloid. *Nature Genetics*, *1*(5), 345–347. https://doi.org/10.1038/ng0892-345

Murrell, J. R., Hake, A. M., Quaid, K. A., Farlow, M. R., & Ghetti, B. (2000). Early-Onset Alzheimer Disease Caused by a New Mutation (V717L) in the Amyloid Precursor Protein Gene. *Archives of Neurology*, *57*(6), 885. https://doi.org/10.1001/archneur.57.6.885

Murrell, J., Farlow, M., Ghetti, B., & Benson, M. (1991). A mutation in the amyloid precursor protein associated with hereditary Alzheimer's disease. *Science*, *254*(5028), 97–99. https://doi.org/10.1126/science.1925564

Naruse, S., Igarashi, S., Aoki, K., Kaneko, K., Iihara, K., Miyatake, T., Kobayashi, H., Inuzuka, T., Shimizu, T., Kojima, T., & Tsuji, S. (1991). Mis-sense mutation Val→Ile in exon 17 of amyloid precursor protein

gene in Japanese familial Alzheimer's disease. *The Lancet*, *337*(8747), 978–979. https://doi.org/10.1016/0140-6736(91)91612-x

Nicolas, G., Wallon, D., Charbonnier, C., Quenez, O., Rousseau, S., Richard, A.-C., Rovelet-Lecrux, A., Coutant, S., Le Guennec, K., Bacq, D., Garnier, J.-G., Olaso, R., Boland, A., Meyer, V., Deleuze, J.-F., Munter, H. M., Bourque, G., Auld, D., Montpetit, A., & Lathrop, M. (2015). Screening of dementia genes by whole-exome sequencing in early-onset Alzheimer disease: input and lessons. *European Journal of Human Genetics*, *24*(5), 710–716. https://doi.org/10.1038/ejhg.2015.173

Obici, L., Demarchi, A., Giulia de Rosa, Bellotti, V., Marciano, S., Donadei, S., Arbustini, E., Palladini, G., Diegoli, M., Genovese, E., Ferrari, G., Coverlizza, S., & Merlini, G. (2005). A novelAβPP mutation exclusively associated with cerebral amyloid angiopathy. *Annals of Neurology*, *58*(4), 639–644. https://doi.org/10.1002/ana.20571

Pasalar, P., Najmabadi, H., Noorian, A. R., Moghimi, B., Jannati, A., Soltanzadeh, A., Krefft, T., Crook, R., & Hardy, J. (2002). An Iranian family with Alzheimer's disease caused by a novel APP mutation (Thr714Ala). *Neurology*, *58*(10), 1574–1575. https://doi.org/10.1212/wnl.58.10.1574

Sala Frigerio, C., Lau, P., Troakes, C., Deramecourt, V., Gele, P., Van Loo, P., Voet, T., & De Strooper, B. (2015). On the identification of low allele frequency mosaic mutations in the brains of Alzheimer's disease patients. *Alzheimer's & Dementia*, *11*(11), 1265–1276. https://doi.org/10.1016/j.jalz.2015.02.007

Sassi, C., Guerreiro, R., Gibbs, R., Ding, J., Lupton, M., Troakes, C., Al-Sarraj, S., Niblock, M., Gallo, J.-M., Adnan, J., & Alzheimer's Research UK Consortium. (2014). Investigating the role of rare coding variability in Mendelian dementia genes (APP, PSEN1, PSEN2, GRN, MAPT, and PRNP) in late-onset Alzheimer's disease. *Neurobiology of Aging*, *35*(12), 2881.e1–2881.e6. https://doi.org/10.1016/j.neurobiolaging.2014.06.002

Statistics Kingdom. (2017a). *Kruskal-Wallis test calculator* . Www.statskingdom.com. https://www.statskingdom.com/kruskal-wallis-calculator.html

Statistics Kingdom. (2017b). *One Way ANOVA*. Www.statskingdom.com. https://www.statskingdom.com/180Anova1way.html

Szklarczyk, D., Kirsch, R., Koutrouli, M., Nastou, K., Mehryary, F., Hachilif, R., Gable, A. L., Fang, T., Doncheva, N., Pyysalo, S., Bork, P., Jensen, L., & von Mering, C. (2022). The STRING database in 2023: protein–protein association networks and functional enrichment analyses for any sequenced genome of interest. *Nucleic Acids Research*, *51*(D1), D638–D646. https://doi.org/10.1093/nar/gkac1000

Theuns, J., Marjaux, E., Vandenbulcke, M., Van Laere, K., Kumar-Singh, S., Bormans, G., Brouwers, N., Van den Broeck, M., Vennekens, K., Corsmit, E., Cruts, M., De Strooper, B., Van Broeckhoven, C., & Vandenberghe, R. (2006). Alzheimer dementia caused by a novel mutation located in the APP C-terminal intracytosolic fragment. *Human Mutation*, *27*(9), 888–896. https://doi.org/10.1002/humu.20402

Wishart, D. S., Feunang, Y. D., Guo, A. C., Lo, E. J., Marcu, A., Grant, J. R., Sajed, T., Johnson, D., Li, C., Sayeeda, Z., Assempour, N., Iynkkaran, I., Liu, Y., Maciejewski, A., Gale, N., Wilson, A., Chin, L., Cummings, R., Le, D., & Pon, A. (2018). DrugBank 5.0: a major update to the DrugBank database for 2018. *Nucleic Acids Research*, *46*(D1), D1074–D1082. https://doi.org/10.1093/nar/gkx1037

8.3 Chapter 3

Alba, R. D. (1973). A graph-theoretic definition of a sociometric clique†. *The Journal of Mathematical Sociology*, *3*(1), 113–126. https://doi.org/10.1080/0022250x.1973.9989826

Alexandrescu, A. T. (2005, January 14). *Amyloid accomplices and enforcers*. https://doi.org/10.1110%2Fps.04887005

Bekris, L. M., Yu, C.-E., Bird, T. D., & Tsuang, D. W. (2010). Review Article: Genetics of Alzheimer Disease. *Journal of Geriatric Psychiatry and Neurology*, *23*(4), 213–227. https://doi.org/10.1177/0891988710383571

Cavalcante, S. F. de A., Simas, A. B. C., Barcellos, M. C., de Oliveira, V. G. M., Sousa, R. B., Cabral, P. A. d.M, Kuča, K., & França, T. C. C. (2020, March 7). *Acetylcholinesterase: The "Hub" for Neurodegenerative Diseases and Chemical Weapons Convention*. https://doi.org/10.3390/biom10030414

Chen, G., Xu, T., Yan, Y., Zhou, Y., Jiang, Y., Melcher, K., & Xu, H. E. (2017). Amyloid beta: structure, Biology and structure-based Therapeutic Development. *Acta Pharmacologica Sinica*, *38*(9), 1205–1235. https://doi.org/10.1038/aps.2017.28

Coronel, R., Bernabeu-Zornoza, A., Palmer, C., Muñiz-Moreno, M., Zambrano, A., Cano, E., & Liste, I. (2018). Role of Amyloid Precursor Protein (APP) and Its Derivatives in the Biology and Cell Fate Specification of Neural Stem Cells. *Molecular Neurobiology*, *55*(9), 7107–7117. https://doi.org/10.1007/s12035-018-0914-2

Das, B., & Yan, R. (2019). A Close Look at BACE1 Inhibitors for Alzheimer's Disease Treatment. *CNS Drugs*, *33*(3), 251–263. https://doi.org/10.1007/s40263-019-00613-7

Fazeli, E., Child, D. D., Bucks, S. A., Stovarsky, M., Edwards, G., Rose, S. E., Yu, C.-E., Latimer, C., Kitago, Y., Bird, T., Suman Jayadev, Andersen, O. M., & Young, J. E. (2024). A familial missense variant in the Alzheimer's disease gene SORL1 impairs its maturation and endosomal sorting. *Acta Neuropathologica*, *147*(1). https://doi.org/10.1007/s00401-023-02670-1

Glenner, G. G., & Wong, C. W. (1984). Alzheimer's disease: Initial Report of the Purification and Characterization of a Novel Cerebrovascular Amyloid Protein. *Biochemical and Biophysical Research Communications*, *120*(3), 885–890. https://doi.org/10.1016/s0006-291x(84)80190-4

Hung, C., Tuck, E., Stubbs, V., van der Lee, S. J., Aalfs, C., van Spaendonk, R., Scheltens, P., Hardy, J., Holstege, H., & Livesey, F. J. (2021). SORL1 deficiency in human excitatory neurons causes APP-dependent defects in the endolysosome-autophagy network. *Cell Reports*, *35*(11), 109259. https://doi.org/10.1016/j.celrep.2021.109259

Jupe, S. (2010, October 15). *Reactome | Amyloid fiber formation*. Reactome.org. https://reactome.org/content/detail/R-HSA-977225

Karmouch, J., Delers, P., Semprez, F., Soyed, N., Areias, J., Bélanger, G., Ravel-Chapuis, A., Dobbertin, A., Jasmin, B. J., & Legay, C. (2020). AChR β-Subunit mRNAs Are Stabilized by HuR in a Mouse Model of Congenital Myasthenic Syndrome With Acetylcholinesterase Deficiency. *Frontiers in Molecular Neuroscience*, *13*. https://doi.org/10.3389/fnmol.2020.568171

Mahajan, S. (2008, January 14). *Reactome | AcCho is hydrolyzed to Cho and acetate by ACHE*. Reactome.org. https://reactome.org/content/detail/R-HSA-372519

McLoughlin, D. M., & Miller, C. C. J. (2008). The FE65 proteins and Alzheimer's disease. *Journal of Neuroscience Research*, *86*(4), 744–754. https://doi.org/10.1002/jnr.21532

Mihaylova, V., Müller, J. S., Vilchez, J. J., Salih, M. A., Kabiraj, M. M., D'Amico, A., Bertini, E., Wölfle, J., Schreiner, F., Kurlemann, G., Rasic, V. M., Siskova, D., Colomer, J., Herczegfalvi, A., Fabriciova, K., Weschke, B., Scola, R., Hoellen, F., Schara, U., & Abicht, A. (2008). Clinical and molecular genetic findings in COLQ-mutant congenital myasthenic syndromes. *Brain*, *131*(3), 747–759. https://doi.org/10.1093/brain/awm325

Milacic, M., Beavers, D., Conley, P., Gong, C., Gillespie, M., Griss, J., Haw, R., Jassal, B., Matthews, L., May, B., Petryszak, R., Eliot Ragueneau, Rothfels, K., Sevilla, C., Shamovsky, V., Stephan, R., Krishna Kumar Tiwari, Thawfeek Varusai, Weiser, J., & Wright, A. (2023). The Reactome Pathway Knowledgebase 2024. *Nucleic Acids Research*, *52*(D1). https://doi.org/10.1093/nar/gkad1025

Minopoli, G., Gargiulo, A., Parisi, S., & Russo, T. (2012). Fe65 matters: New light on an old molecule. *IUBMB Life*, *64*(12), 936–942. https://doi.org/10.1002/iub.1094

Pohanka, M. (2014). Inhibitors of Acetylcholinesterase and Butyrylcholinesterase Meet Immunity. *International Journal of Molecular Sciences*, *15*(6), 9809–9825. https://doi.org/10.3390/ijms15069809

Rovelet-Lecrux, A., Feuillette, S., Miguel, L., Schramm, C., Pernet, S., Quenez, O., Ségalas-Milazzo, I., Guilhaudis, L., Rousseau, S., Riou, G., Frébourg, T., Campion, D., Nicolas, G., & Lecourtois, M. (2021). Impaired SorLA maturation and trafficking as a new mechanism for SORL1 missense variants in Alzheimer disease. *Acta Neuropathologica Communications*, *9*(1). https://doi.org/10.1186/s40478-021-01294-4

Szklarczyk, D., Kirsch, R., Koutrouli, M., Nastou, K., Mehryary, F., Hachilif, R., Gable, A. L., Fang, T., Doncheva, N., Pyysalo, S., Bork, P., Jensen, L., & von Mering, C. (2022). The STRING database in 2023: protein–protein association networks and functional enrichment analyses for any sequenced genome of interest. *Nucleic Acids Research*, *51*(D1), D638–D646. https://doi.org/10.1093/nar/gkac1000

Vanhaesebrouck, A. E., & Beeson, D. (2019). The congenital myasthenic syndromes: expanding genetic and phenotypic spectrums and refining treatment strategies. *Current Opinion in Neurology*, *32*(5), 696–703. https://doi.org/10.1097/WCO.0000000000000736

Velan , B., Grosfeld , H., Kronman , C., Leitner , M., Gozes , Y., Lazar , A., Flashner , Y., Marcus , D., Cohen , S., & Shafferman , A. (1991). The effect of elimination of intersubunit disulfide bonds on the activity, assembly, and secretion of recombinant human acetylcholinesterase. Expression of acetylcholinesterase Cys-580----Ala mutant. *The Journal of Biological Chemistry*, *266*(35). https://pubmed.ncbi.nlm.nih.gov/1748670/

Weinstock, M., & Groner, E. (2008). Rational design of a drug for Alzheimer's disease with cholinesterase inhibitory and neuroprotective activity. *Chemico-Biological Interactions*, *175*(1-3), 216–221. https://doi.org/10.1016/j.cbi.2008.03.014

Wishart, D. S., Feunang, Y. D., Guo, A. C., Lo, E. J., Marcu, A., Grant, J. R., Sajed, T., Johnson, D., Li, C., Sayeeda, Z., Assempour, N., Iynkkaran, I., Liu, Y., Maciejewski, A., Gale, N., Wilson, A., Chin, L.,

Cummings, R., Le, D., & Pon, A. (2018). DrugBank 5.0: a major update to the DrugBank database for 2018. *Nucleic Acids Research*, *46*(D1), D1074–D1082. https://doi.org/10.1093/nar/gkx1037

Yamamoto, H., Hagino, Y., Kasai, S., & Ikeda, K. (2015). Specific Roles of NMDA Receptor Subunits in Mental Disorders. *Current Molecular Medicine*, *15*(3), 193–205. https://doi.org/10.2174/1566524015666150330142807

Zhou, D., Zambrano, N., Russo, T., & D'Adamio, L. (2009). Phosphorylation of a Tyrosine in the Amyloid-β Protein Precursor Intracellular Domain Inhibits Fe65 Binding and Signaling. *Journal of Alzheimer's Disease*, *16*(2), 301–307. https://doi.org/10.3233/jad-2009-0970

8.4 Chapter 4

Akdel, M., Pires, D. E. V., Pardo, E. P., Jänes, J., Zalevsky, A. O., Mészáros, B., Bryant, P., Good, L. L., Laskowski, R. A., Pozzati, G., Shenoy, A., Zhu, W., Kundrotas, P., Serra, V. R., Rodrigues, C. H. M., Dunham, A. S., Burke, D., Borkakoti, N., Velankar, S., & Frost, A. (2022). A structural biology community assessment of AlphaFold2 applications. *Nature Structural & Molecular Biology*, *29*(11), 1056–1067. https://doi.org/10.1038/s41594-022-00849-w

Anfinsen, C. B. (1973). Principles that Govern the Folding of Protein Chains. *Science*, *181*(4096), 223–230. https://doi.org/10.1126/science.181.4096.223

APP | ALZFORUM. (n.d.). Www.alzforum.org. Retrieved July 4, 2024, from https://www.alzforum.org/mutations/app

Baek, M., DiMaio, F., Anishchenko, I., Dauparas, J., Ovchinnikov, S., Lee, G. R., Wang, J., Cong, Q., Kinch, L. N., Schaeffer, R. D., Millán, C., Park, H., Adams, C., Glassman, C. R., DeGiovanni, A., Pereira, J. H., Rodrigues, A. V., van Dijk, A. A., Ebrecht, A. C., & Opperman, D. J. (2021). Accurate prediction of protein structures and interactions using a three-track neural network. *Science*, *373*(6557), 871–876. https://doi.org/10.1126/science.abj8754

Barrett, P. M., Song, Y., Van, W. D., Hustedt, E. J., Schafer, J. M., Hadziselimovic, A., Beel, A. J., & Sanders, C. R. (2012). *The Amyloid Precursor Protein Has a Flexible Transmembrane Domain and Binds Cholesterol*. *336*(6085), 1168–1171. https://doi.org/10.1126/science.1219988

Bateman, A., Martin, M.-J., Orchard, S., Magrane, M., Ahmad, S., Alpi, E., Bowler-Barnett, E. H., Britto, R., Bye-A-Jee, H., Cukura, A., Denny, P., Dogan, T., Ebenezer, T., Fan, J., Garmiri, P., da Costa Gonzales, L. J., Hatton-Ellis, E., Hussein, A., Ignatchenko, A., & Insana, G. (2022). UniProt: the Universal Protein Knowledgebase in 2023. *Nucleic Acids Research*, *51*(D1). https://doi.org/10.1093/nar/gkac1052

Biffi, A., & Greenberg, S. M. (2011). Cerebral Amyloid Angiopathy: A Systematic Review. *Journal of Clinical Neurology*, *7*(1), 1. https://doi.org/10.3988/jcn.2011.7.1.1

Buchan, D. W. A., Moffat, L., Lau, A., Kandathil, S., & Jones, D. (2024). Deep learning for the PSIPRED Protein Analysis Workbench. *Nucleic Acids Research*, *52*(W1). https://doi.org/10.1093/nar/gkae328

Bugiani, O., Giaccone, G., Rossi, G., Mangieri, M., Capobianco, R., Morbin, M., Mazzoleni, G., Cupidi, C., Marcon, G., Giovagnoli, A., Bizzi, A., Di Fede, G., Puoti, G., Carella, F., Salmaggi, A., Romorini, A., Patruno, G. M., Magoni, M., Padovani, A., & Tagliavini, F. (2010). Hereditary Cerebral Hemorrhage

With Amyloidosis Associated With the E693K Mutation of APP. *Archives of Neurology*, *67*(8). https://doi.org/10.1001/archneurol.2010.178

Callaway, E. (2020). "It will change everything": DeepMind's AI makes gigantic leap in solving protein structures. *Nature*, *588*. https://doi.org/10.1038/d41586-020-03348-4

Castro-Alvarez, A., Costa, A., & Vilarrasa, J. (2017). The Performance of Several Docking Programs at Reproducing Protein–Macrolide-Like Crystal Structures. *Molecules*, *22*(1), 136. https://doi.org/10.3390/molecules22010136

Chakrabarti, P., & Chakravarty, D. (2022). Intrinsically disordered proteins/regions and insight into their biomolecular interactions. *Biophysical Chemistry*, *283*, 106769. https://doi.org/10.1016/j.bpc.2022.106769

Chen, G., Xu, T., Yan, Y., Zhou, Y., Jiang, Y., Melcher, K., & Xu, H. E. (2017). Amyloid beta: structure, biology and structure-based therapeutic development. *Acta Pharmacologica Sinica*, *38*(9), 1205–1235. https://doi.org/10.1038/aps.2017.28

Chiti, F., & Dobson, C. M. (2006). Protein Misfolding, Functional Amyloid, and Human Disease. *Annual Review of Biochemistry*, *75*(1), 333–366. https://doi.org/10.1146/annurev.biochem.75.101304.123901

Díaz-Villanueva, J., Díaz-Molina, R., & García-González, V. (2015). Protein Folding and Mechanisms of Proteostasis. *International Journal of Molecular Sciences*, *16*(8), 17193–17230. https://doi.org/10.3390/ijms160817193

Dill, K. A., & MacCallum, J. L. (2012). The Protein-Folding Problem, 50 Years On. *Science*, *338*(6110), 1042–1046. https://doi.org/10.1126/science.1219021

Dyson, H. J., Wright, P. E., & Scheraga, H. A. (2006). The role of hydrophobic interactions in initiation and propagation of protein folding. *Proceedings of the National Academy of Sciences*, *103*(35), 13057–13061. https://doi.org/10.1073/pnas.0605504103

Gambardella, G., Notari, S., Cavaterra, D., Iavarone, F., Castagnola, M., Bocedi, A., & Ricci, G. (2022). The Anfinsen Dogma: Intriguing Details Sixty-Five Years Later. *International Journal of Molecular Sciences*, *23*(14), 7759. https://doi.org/10.3390/ijms23147759

Graña-Montes, R., & Ventura, S. (2015). Protein Aggregation and Its Prediction. *NATO Science for Peace and Security Series. A, Chemistry and Biology*, 115–127. https://doi.org/10.1007/978-94-017-9719-1_10

Guo, S.-S., Liu, J., Zhou, X., & Zhang, G. (2022). DeepUMQA: ultrafast shape recognition-based protein model quality assessment using deep learning. *Bioinformatics*, *38*(7), 1895–1903. https://doi.org/10.1093/bioinformatics/btac056

Guyon, A., Rousseau, J., Lamothe, G., & Tremblay, J. P. (2020). The protective mutation A673T in amyloid precursor protein gene decreases Aβ peptides production for 14 forms of Familial Alzheimer's Disease in SH-SY5Y cells. *PLOS ONE*, *15*(12), e0237122. https://doi.org/10.1371/journal.pone.0237122

Hardy, J., & Higgins, G. (1992). Alzheimer's disease: the amyloid cascade hypothesis. *Science*, *256*(5054), 184–185. https://doi.org/10.1126/science.1566067

Jamecna, D., & Antonny, B. (2021). Intrinsically disordered protein regions at membrane contact sites. *Biochimica et Biophysica Acta (BBA) - Molecular and Cell Biology of Lipids*, *1866*(11), 159020–159020. https://doi.org/10.1016/j.bbalip.2021.159020

Johnson, M. S., Sutcliffe, M. J., & Blundell, T. L. (1990). Molecular anatomy: Phyletic relationships derived from three-dimensional structures of proteins. *Journal of Molecular Evolution*, *30*(1), 43–59. https://doi.org/10.1007/bf02102452

Jones, D. T., & Cozzetto, D. (2014). DISOPRED3: precise disordered region predictions with annotated protein-binding activity. *Bioinformatics*, *31*(6), 857–863. https://doi.org/10.1093/bioinformatics/btu744

Jumper, J., Evans, R., Pritzel, A., Green, T., Figurnov, M., Ronneberger, O., Tunyasuvunakool, K., Bates, R., Žídek, A., Potapenko, A., Bridgland, A., Meyer, C., Kohl, S. A. A., Ballard, A. J., Cowie, A., Romera-Paredes, B., Nikolov, S., Jain, R., Adler, J., & Back, T. (2021). Highly accurate protein structure prediction with alphafold. *Nature*, *596*(7873), 583–589. https://doi.org/10.1038/s41586-021-03819-2

Kendrew, J. C., Bodo, G., Dintzis, H. M., Parrish, R. G., Wyckoff, H., & Phillips, D. C. (1958). A Three-Dimensional Model of the Myoglobin Molecule Obtained by X-Ray Analysis. *Nature*, *181*(4610), 662–666. https://doi.org/10.1038/181662a0

Krissinel, E., & Henrick, K. (2004). Secondary-structure matching (SSM), a new tool for fast protein structure alignment in three dimensions. *Acta Crystallographica Section D Biological Crystallography*, *60*(12), 2256–2268. https://doi.org/10.1107/s0907444904026460

Kryshtafovych, A., Schwede, T., Topf, M., Fidelis, K., & Moult, J. (2023). Critical assessment of methods of protein structure prediction (CASP)—Round XV. *Proteins: Structure, Function, and Bioinformatics*, *91*(12), 1539–1549. https://doi.org/10.1002/prot.26617

Kufareva, I., & Abagyan, R. (2012). Methods of protein structure comparison. *Methods in Molecular Biology (Clifton, N.J.)*, *857*, 231–257. https://doi.org/10.1007/978-1-61779-588-6_10

Kuhn, J., & Sharman, T. (2022). *Cerebral Amyloid Angiopathy*. PubMed; StatPearls Publishing. https://www.ncbi.nlm.nih.gov/books/NBK556105/

Landrum, M. J., Lee, J. M., Riley, G. R., Jang, W., Rubinstein, W. S., Church, D. M., & Maglott, D. R. (2014). ClinVar: public archive of relationships among sequence variation and human phenotype. *Nucleic Acids Research*, *42*(Database issue), D980–D985. https://doi.org/10.1093/nar/gkt1113

Levinthal, C. (1968). Are there pathways for protein folding? *Journal de Chimie Physique*, *65*, 44–45. https://doi.org/10.1051/jcp/1968650044

Levy, E., Carman, M., Fernandez-Madrid, I., Power, M., Lieberburg, I., van Duinen, S., Bots, G., Luyendijk, W., & Frangione, B. (1990). Mutation of the Alzheimer's disease amyloid gene in hereditary cerebral hemorrhage, Dutch type. *Science*, *248*(4959), 1124–1126. https://doi.org/10.1126/science.2111584

Maat-Schieman, M., Roos, R., & van Duinen, S. (2005). Hereditary cerebral hemorrhage with amyloidosis-Dutch type. *Neuropathology*, *25*(4), 288–297. https://doi.org/10.1111/j.1440-1789.2005.00631.x

Magana, G., & Kovalevskiy, O. (2024). *AlphaFold: A practical guide*. https://doi.org/10.6019/tol.alphafold-w.2024.00001.1

McGuffin, L. J., Adiyaman, R., Maghrabi, A. H. A., Shuid, A. N., Brackenridge, D. A., Nealon, J. O., & Philomina, L. S. (2019). IntFOLD: an integrated web resource for high performance protein structure and function prediction. *Nucleic Acids Research*, *47*(W1), W408–W413. https://doi.org/10.1093/nar/gkz322

Mirdita, M., Schütze, K., Moriwaki, Y., Heo, L., Ovchinnikov, S., & Steinegger, M. (2022). ColabFold: making protein folding accessible to all. *Nature Methods*, *19*, 1–4. https://doi.org/10.1038/s41592-022-01488-1

Mullan, M., Crawford, F., Axelman, K., Houlden, H., Lilius, L., Winblad, B., & Lannfelt, L. (1992). A pathogenic mutation for probable Alzheimer's disease in the APP gene at the N–terminus of β–amyloid. *Nature Genetics*, *1*(5), 345–347. https://doi.org/10.1038/ng0892-345

Muller, U. C., & Zheng, H. (2011). Physiological Functions of APP Family Proteins. *Cold Spring Harbor Perspectives in Medicine*, *2*(2), a006288–a006288. https://doi.org/10.1101/cshperspect.a006288

Murrell, J., Farlow, M., Ghetti, B., & Benson, M. (1991). A mutation in the amyloid precursor protein associated with hereditary Alzheimer's disease. *Science*, *254*(5028), 97–99. https://doi.org/10.1126/science.1925564

Naruse, S., Igarashi, S., Aoki, K., Kaneko, K., Iihara, K., Miyatake, T., Kobayashi, H., Inuzuka, T., Shimizu, T., Kojima, T., & Tsuji, S. (1991). Mis-sense mutation Val→Ile in exon 17 of amyloid precursor protein gene in Japanese familial Alzheimer's disease. *The Lancet*, *337*(8747), 978–979. https://doi.org/10.1016/0140-6736(91)91612-x

Nassar, R., Dignon, G. L., Razban, R. M., & Dill, K. A. (2021). The protein folding problem: The role of theory. *Journal of Molecular Biology*, 167126. https://doi.org/10.1016/j.jmb.2021.167126

Nelson, D. L., & Cox, M. M. (2013). *Lehninger Principles of Biochemistry* (6th ed.). W. H. Freeman and Company.

Nicolas, G., Wallon, D., Charbonnier, C., Quenez, O., Rousseau, S., Richard, A.-C., Rovelet-Lecrux, A., Coutant, S., Le Guennec, K., Bacq, D., Garnier, J.-G., Olaso, R., Boland, A., Meyer, V., Deleuze, J.-F., Munter, H. M., Bourque, G., Auld, D., Montpetit, A., & Lathrop, M. (2015). Screening of dementia genes by whole-exome sequencing in early-onset Alzheimer disease: input and lessons. *European Journal of Human Genetics*, *24*(5), 710–716. https://doi.org/10.1038/ejhg.2015.173

Parakh, S., & Atkin, J. D. (2016). Protein folding alterations in amyotrophic lateral sclerosis. *Brain Research*, *1648*(Pt B), 633–649. https://doi.org/10.1016/j.brainres.2016.04.010

Pauwels, K., Van Molle, I., Tommassen, J., & Van Gelder, P. (2007). Chaperoning Anfinsen: the steric foldases. *Molecular Microbiology*, *64*(4), 917–922. https://doi.org/10.1111/j.1365-2958.2007.05718.x

Pearce, R., Li, Y., Omenn, G. S., & Zhang, Y. (2022). Fast and accurate Ab Initio Protein structure prediction using deep learning potentials. *PLoS Computational Biology*, *18*(9), e1010539. https://doi.org/10.1371/journal.pcbi.1010539

Perutz, M. F., Rossmann, M. G., Cullis, A. F., Muirhead, H., Will, G., & North, A. C. (1960). Structure of haemoglobin: a three-dimensional Fourier synthesis at 5.5-A. resolution, obtained by X-ray analysis. *Nature*, *185*(4711), 416–422. https://doi.org/10.1038/185416a0

Pettersen, E. F., Goddard, T. D., Huang, C. C., Couch, G. S., Greenblatt, D. M., Meng, E. C., & Ferrin, T. E. (2004). UCSF Chimera--A visualization system for exploratory research and analysis. *Journal of Computational Chemistry*, *25*(13), 1605–1612. https://doi.org/10.1002/jcc.20084

Saito, T., Suemoto, T., Brouwers, N., Sleegers, K., Funamoto, S., Mihira, N., Matsuba, Y., Yamada, K., Nilsson, P., Takano, J., Nishimura, M., Iwata, N., Van Broeckhoven, C., Ihara, Y., & Saido, T. C. (2011). Potent amyloidogenicity and pathogenicity of Aβ43. *Nature Neuroscience*, *14*(8), 1023–1032. https://doi.org/10.1038/nn.2858

Sellal, F., Wallon, D., Martinez-Almoyna, L., Marelli, C., Dhar, A., Oesterlé, H., Rovelet-Lecrux, A., Rousseau, S., Kourkoulis, C. E., Rosand, J., DiPucchio, Z. Y., Frosch, M., Gombert, C., Audoin, B., Miné, M., Riant, F., Frebourg, T., Hannequin, D., Campion, D., & Greenberg, S. M. (2016). APP Mutations in Cerebral Amyloid Angiopathy with or without Cortical Calcifications: Report of Three Families and a Literature Review. *Journal of Alzheimer S Disease*, *56*(1), 37–46. https://doi.org/10.3233/jad-160709

Shen, F., & Sergi, C. (2021). *Biochemistry, Amino Acid Synthesis and Degradation*. PubMed; StatPearls Publishing. https://www.ncbi.nlm.nih.gov/books/NBK559250/

Tunyasuvunakool, K., Adler, J., Wu, Z., Green, T., Zielinski, M., Žídek, A., Bridgland, A., Cowie, A., Meyer, C., Laydon, A., Velankar, S., Kleywegt, G. J., Bateman, A., Evans, R., Pritzel, A., Figurnov, M., Ronneberger, O., Bates, R., Kohl, S. A. A., & Potapenko, A. (2021). Highly accurate protein structure prediction for the human proteome. *Nature*, *596*, 1–9. https://doi.org/10.1038/s41586-021-03828-1

Wang, W., Peng, Z., & Yang, J. (2022). Single-sequence protein structure prediction using supervised transformer protein language models. *Nature Computational Science*, *2*(12), 804–814. https://doi.org/10.1038/s43588-022-00373-3

Waterhouse, A., Bertoni, M., Bienert, S., Studer, G., Tauriello, G., Gumienny, R., Heer, F. T., de Beer, T. A., Rempfer, C., Bordoli, L., Lepore, R., & Schwede, T. (2018). SWISS-MODEL: homology modelling of protein structures and complexes. *Nucleic Acids Research*, *46*(W1), W296–W303. https://academic.oup.com/nar/article/46/W1/W296/5000024

Wright, P. E., & Dyson, H. Jane. (1999). Intrinsically unstructured proteins: re-assessing the protein structure-function paradigm. *Journal of Molecular Biology*, *293*(2), 321–331. https://doi.org/10.1006/jmbi.1999.3110

Yang, J., Anishchenko, I., Park, H., Peng, Z., Ovchinnikov, S., & Baker, D. (2020). Improved protein structure prediction using predicted interresidue orientations. *Proceedings of the National Academy of Sciences*, *117*(3), 1496–1503. https://doi.org/10.1073/pnas.1914677117

8.5 Chapter 5

Amft, M., Ortner, M., Eichenlaub, U., Goldhardt, O., Diehl-Schmid, J., Hedderich, D. M., Yakushev, I., & Grimmer, T. (2022). The cerebrospinal fluid biomarker ratio Aβ42/40 identifies amyloid positron emission tomography positivity better than Aβ42 alone in a heterogeneous memory clinic cohort. Alzheimer's Research & Therapy, 14(1). https://doi.org/10.1186/s13195-022-01003-w

APP | ALZFORUM. (n.d.). Www.alzforum.org. Retrieved July 4, 2024, from https://www.alzforum.org/mutations/app

Berman, H. M. (2000). The Protein Data Bank. Nucleic Acids Research, 28(1), 235–242. https://doi.org/10.1093/nar/28.1.235

Bolduc, D. M., Montagna, D. R., Seghers, M. C., Wolfe, M. S., & Selkoe, D. J. (2016). The amyloid-beta forming tripeptide cleavage mechanism of γ-secretase. ELife, 5. https://doi.org/10.7554/elife.17578

Bukhari, H., Glotzbach, A., Kolbe, K., Leonhardt, G., Loosse, C., & Müller, T. (2017). Small things matter: Implications of APP intracellular domain AICD nuclear signaling in the progression and pathogenesis of Alzheimer's disease. Progress in Neurobiology, 156, 189–213. https://doi.org/10.1016/j.pneurobio.2017.05.005

Chasseigneaux, S., & Allinquant, B. (2011). Functions of Aβ, sAPPα and sAPPβ : similarities and differences. Journal of Neurochemistry, 120, 99–108. https://doi.org/10.1111/j.1471-4159.2011.07584.x

Chen, G., Xu, T., Yan, Y., Zhou, Y., Jiang, Y., Melcher, K., & Xu, H. E. (2017). Amyloid beta: structure, Biology and structure-based Therapeutic Development. Acta Pharmacologica Sinica, 38(9), 1205–1235. https://doi.org/10.1038/aps.2017.28

Chow, V. W., Mattson, M. P., Wong, P. C., & Gleichmann, M. (2009). An Overview of APP Processing Enzymes and Products. NeuroMolecular Medicine, 12(1), 1–12. https://doi.org/10.1007/s12017-009-8104-z

Conidi, M. E., Bernardi, L., Puccio, G., Smirne, N., Muraca, M. G., Curcio, S. A. M., Colao, R., Piscopo, P., Gallo, M., Anfossi, M., Frangipane, F., Clodomiro, A., Mirabelli, M., Vasso, F., Cupidi, C., Torchia, G., Di Lorenzo, R., Mandich, P., Confaloni, A., & Maletta, R. G. (2015). Homozygous carriers of APP A713T mutation in an autosomal dominant Alzheimer disease family. Neurology, 84(22), 2266–2273. https://doi.org/10.1212/wnl.0000000000001648

Coronel, R., Bernabeu-Zornoza, A., Palmer, C., Muñiz-Moreno, M., Zambrano, A., Cano, E., & Liste, I. (2018). Role of Amyloid Precursor Protein (APP) and Its Derivatives in the Biology and Cell Fate Specification of Neural Stem Cells. Molecular Neurobiology, 55(9), 7107–7117. https://doi.org/10.1007/s12035-018-0914-2

De Jonghe, C., Esselens, C., Kumar-Singh, S., Craessaerts, K., Serneels, S., Checler, F., Annaert, W., Van Broeckhoven, C., & De Strooper, B. (2001). Pathogenic APP mutations near the gamma-secretase cleavage site differentially affect Abeta secretion and APP C-terminal fragment stability. Human Molecular Genetics, 10(16), 1665–1671. https://doi.org/10.1093/hmg/10.16.1665

Hur, J.-Y. (2022). γ-Secretase in Alzheimer's disease. Experimental & Molecular Medicine, 54. https://doi.org/10.1038/s12276-022-00754-8

Jonsson, T., Atwal, J. K., Steinberg, S., Snaedal, J., Jonsson, P. V., Bjornsson, S., Stefansson, H., Sulem, P., Gudbjartsson, D., Maloney, J., Hoyte, K., Gustafson, A., Liu, Y., Lu, Y., Bhangale, T., Graham, R. R., Huttenlocher, J., Bjornsdottir, G., Andreassen, O. A., & Jönsson, E. G. (2012). A mutation in APP protects against Alzheimer's disease and age-related cognitive decline. Nature, 488(7409), 96–99. https://doi.org/10.1038/nature11283

Kakuda, N., Funamoto, S., Yagishita, S., Takami, M., Osawa, S., Dohmae, N., & Ihara, Y. (2006). Equimolar Production of Amyloid β-Protein and Amyloid Precursor Protein Intracellular Domain from

β-Carboxyl-terminal Fragment by γ-Secretase. Journal of Biological Chemistry, 281(21), 14776–14786. https://doi.org/10.1074/jbc.m513453200

Kumar-Singh, S., De Jonghe, C., Cruts, M., Kleinert, R., Wang, R., Mercken, M., De Strooper, B., Vanderstichele, H., Lofgren, A., Vanderhoeven, I., Backhovens, H., Vanmechelen, E., Kroisel, P. M., & Van Broeckhoven, C. (2000). Nonfibrillar diffuse amyloid deposition due to a gamma42-secretase site mutation points to an essential role for N-truncated Abeta42 in Alzheimer's disease. Human Molecular Genetics, 9(18), 2589–2598. https://doi.org/10.1093/hmg/9.18.2589

Kuperstein, I., Broersen, K., Benilova, I., Rozenski, J., Jonckheere, W., Debulpaep, M., Vandersteen, A., Segers-Nolten, I., Van Der Werf, K., Subramaniam, V., Braeken, D., Callewaert, G., Bartic, C., D'Hooge, R., Martins, I. C., Rousseau, F., Schymkowitz, J., & De Strooper, B. (2010). Neurotoxicity of Alzheimer's disease Aβ peptides is induced by small changes in the Aβ42 to Aβ40 ratio. The EMBO Journal, 29(19), 3408–3420. https://doi.org/10.1038/emboj.2010.211

Liu, Y., Xiao, X., Liu, H., Liao, X., Zhou, Y., Weng, L., Zhou, L., Liu, X., Bi, X., Xu, T., Zhu, Y., Yang, Q., Zhang, S., Hao, X., Zhang, W., Wang, J., Jiao, B., & Shen, L. (2022). Clinical characteristics and genotype-phenotype correlation analysis of familial Alzheimer's disease patients with pathogenic/likely pathogenic amyloid protein precursor mutations. Frontiers in Aging Neuroscience, 14. https://doi.org/10.3389/fnagi.2022.1013295

Olsson, F., Schmidt, S., Althoff, V., Munter, L. M., Jin, S., Rosqvist, S., Lendahl, U., Multhaup, G., & Lundkvist, J. (2014). Characterization of intermediate steps in amyloid beta (Aβ) production under near-native conditions. The Journal of Biological Chemistry, 289(3), 1540–1550. https://doi.org/10.1074/jbc.M113.498246

Pettersen, E. F., Goddard, T. D., Huang, C. C., Couch, G. S., Greenblatt, D. M., Meng, E. C., & Ferrin, T. E. (2004). UCSF Chimera--A visualization system for exploratory research and analysis. Journal of Computational Chemistry, 25(13), 1605–1612. https://doi.org/10.1002/jcc.20084

Tang, N., & Kepp, K. P. (2018). Aβ42/Aβ40 Ratios of Presenilin 1 Mutations Correlate with Clinical Onset of Alzheimer's Disease. Journal of Alzheimer's Disease, 66(3), 939–945. https://doi.org/10.3233/jad-180829

Van Meer, G., Voelker, D. R., & Feigenson, G. W. (2008). Membrane lipids: Where they are and how they behave. Nature Reviews Molecular Cell Biology, 9(2), 112–124. https://doi.org/10.1038/nrm2330

van der Kant, R., & Goldstein, Lawrence S. B. (2015). Cellular Functions of the Amyloid Precursor Protein from Development to Dementia. Developmental Cell, 32(4), 502–515. https://doi.org/10.1016/j.devcel.2015.01.022

Zhou, R., Yang, G., Guo, X., Zhou, Q., Lei, J., & Shi, Y. (2019). Recognition of the amyloid precursor protein by human γ-secretase. Science, 363(6428), eaaw0930. https://doi.org/10.1126/science.aaw0930

8.6 Chapter 6

Abramson, J., Adler, J., Dunger, J., Evans, R., Green, T., Pritzel, A., Ronneberger, O., Willmore, L., Ballard, A. J., Bambrick, J., Bodenstein, S. W., Evans, D. A., Hung, C.-C., O'Neill, M., Reiman, D.,

Tunyasuvunakool, K., Wu, Z., Žemgulytė, A., Arvaniti, E., & Beattie, C. (2024). Accurate structure prediction of biomolecular interactions with AlphaFold 3. *Nature*, *630*, 1–3. https://doi.org/10.1038/s41586-024-07487-w

Alvarez, A., Alarcón, R., Opazo, C., Campos, E. O., Muñoz, F. J., Calderón, F. H., Dajas, F., Gentry, M. K., Doctor, B. P., De Mello, F. G., & Inestrosa, N. C. (1998). Stable Complexes Involving Acetylcholinesterase and Amyloid-β Peptide Change the Biochemical Properties of the Enzyme and Increase the Neurotoxicity of Alzheimer's Fibrils. *The Journal of Neuroscience*, *18*(9), 3213–3223. https://doi.org/10.1523/jneurosci.18-09-03213.1998

Alvarez, A., Opazo, C., Alarcón, R., Garrido, J., & Inestrosa, N. C. (1997). Acetylcholinesterase promotes the aggregation of amyloid-β-peptide fragments by forming a complex with the growing fibrils11Edited by A. R. Fersht. *Journal of Molecular Biology*, *272*(3), 348–361. https://doi.org/10.1006/jmbi.1997.1245

Barrett, P. M., Song, Y., Van, W. D., Hustedt, E. J., Schafer, J. M., Hadziselimovic, A., Beel, A. J., & Sanders, C. R. (2012). *The Amyloid Precursor Protein Has a Flexible Transmembrane Domain and Binds Cholesterol*. *336*(6085), 1168–1171. https://doi.org/10.1126/science.1219988

Bateman, A., Martin, M.-J., Orchard, S., Magrane, M., Ahmad, S., Alpi, E., Bowler-Barnett, E. H., Britto, R., Bye-A-Jee, H., Cukura, A., Denny, P., Dogan, T., Ebenezer, T., Fan, J., Garmiri, P., da Costa Gonzales, L. J., Hatton-Ellis, E., Hussein, A., Ignatchenko, A., & Insana, G. (2022). UniProt: the Universal Protein Knowledgebase in 2023. *Nucleic Acids Research*, *51*(D1). https://doi.org/10.1093/nar/gkac1052

Berman, H. M. (2000). The Protein Data Bank. *Nucleic Acids Research*, *28*(1), 235–242. https://doi.org/10.1093/nar/28.1.235

Bolduc, D. M., Montagna, D. R., Seghers, M. C., Wolfe, M. S., & Selkoe, D. J. (2016). The amyloid-beta forming tripeptide cleavage mechanism of γ-secretase. *ELife*, *5*. https://doi.org/10.7554/elife.17578

Campanari, M.-L., García-Ayllón, M.-S., Belbin, O., Galcerán, J., Lleó, A., & Sáez-Valero, J. (2014). Acetylcholinesterase Modulates Presenilin-1 Levels and γ-Secretase Activity. *Journal of Alzheimer's Disease*, *41*(3), 911–924. https://doi.org/10.3233/jad-140426

Carvajal, F. J., & Inestrosa, N. C. (2011). Interactions of AChE with A? Aggregates in Alzheimer?s Brain: Therapeutic Relevance of IDN 5706. *Frontiers in Molecular Neuroscience*, *4*. https://doi.org/10.3389/fnmol.2011.00019

Chen, G., Xu, T., Yan, Y., Zhou, Y., Jiang, Y., Melcher, K., & Xu, H. E. (2017). Amyloid beta: structure, Biology and structure-based Therapeutic Development. *Acta Pharmacologica Sinica*, *38*(9), 1205–1235. https://doi.org/10.1038/aps.2017.28

Cottingham, M. G., Hollinshead, M. S., & Vaux, D. J. T. (2002). Amyloid Fibril Formation by a Synthetic Peptide from a Region of Human Acetylcholinesterase that Is Homologous to the Alzheimer's Amyloid-β Peptide. *Biochemistry*, *41*(46), 13539–13547. https://doi.org/10.1021/bi0260334

Dvir, H., Harel, M., Bon, S., Liu, W.-Q., Vidal, M., Garbay, C., Sussman, J. L., Massoulié, J., & Silman, I. (2004). The synaptic acetylcholinesterase tetramer assembles around a polyproline II helix. *The EMBO Journal*, *23*(22), 4394–4405. https://doi.org/10.1038/sj.emboj.7600425

Dym, O., Unger, T., Toker, L., Silman, I., & Sussman, J. L. (2015). *Crystal Structure of Human Acetylcholinesterase*. https://doi.org/10.2210/pdb4pqe/pdb

Evans, R., O'Neill, M., Pritzel, A., Antropova, N., Senior, A., Green, T., Žídek, A., Bates, R., Blackwell, S., Yim, J., Ronneberger, O., Bodenstein, S., Zielinski, M., Bridgland, A., Potapenko, A., Cowie, A., Tunyasuvunakool, K., Jain, R., Clancy, E., & Kohli, P. (2021). Protein complex prediction with AlphaFold-Multimer. *BioRxiv*. https://doi.org/10.1101/2021.10.04.463034

Fishman, E., Siek, G. C., MacCallum, R. C., Bird, E. D., Volicer, L., & Marquis, J. K. (1986). Distribution of the molecular forms of acetylcholinesterase in human brain: Alterations in dementia of the Alzheimer type. *Annals of Neurology*, *19*(3), 246–252. https://doi.org/10.1002/ana.410190305

García-Ayllón, M.-S., Campanari, M.-L., Montenegro, M. F., Cuchillo-Ibañez, I., Belbin, O., Lleó, A., Wah, K., Vidal, C. J., & Sáez-Valero, J. (2014). Presenilin-1 influences processing of the acetylcholinesterase membrane anchor PRiMA. *Neurobiology of Aging*, *35*(7), 1526–1536. https://doi.org/10.1016/j.neurobiolaging.2014.01.147

García-Ayllón, M.-S., Riba-Llena, I., Serra-Basante, C., Alom, J., Boopathy, R., & Sáez-Valero, J. (2010). Altered Levels of Acetylcholinesterase in Alzheimer Plasma. *PLoS ONE*, *5*(1), e8701. https://doi.org/10.1371/journal.pone.0008701

Inestrosa, N., Alvarez, A., Dinamarca, M., Perez-Acle, T., & Colombres, M. (2005). Acetylcholinesterase-Amyloid-β-peptide Interaction: Effect of Congo Red and the Role of the Wnt Pathway. *Current Alzheimer Research*, *2*(3), 301–306. https://doi.org/10.2174/1567205054367928

Jean, L., Thomas, B., Tahiri-Alaoui, A., Shaw, M., & Vaux, D. J. (2007). Heterologous Amyloid Seeding: Revisiting the Role of Acetylcholinesterase in Alzheimer's Disease. *PLoS ONE*, *2*(7), e652. https://doi.org/10.1371/journal.pone.0000652

Luk, W. K. W., Chen, V. P., Choi, R. C. Y., & Tsim, K. W. K. (2012). N-linked glycosylation of dimeric acetylcholinesterase in erythrocytes is essential for enzyme maturation and membrane targeting. *FEBS Journal*, *279*(17), 3229–3239. https://doi.org/10.1111/j.1742-4658.2012.08708.x

Magana, G., & Kovalevskiy, O. (2024). *AlphaFold: A practical guide*. https://doi.org/10.6019/tol.alphafold-w.2024.00001.1

Nalivaeva, N. N., & Turner, A. J. (2016). AChE and the amyloid precursor protein (APP) – Cross-talk in Alzheimer's disease. *Chemico-Biological Interactions*, *259*, 301–306. https://doi.org/10.1016/j.cbi.2016.04.009

Nordberg, A., Darreh-Shori, T., Peskind, E., Soininen, H., Mousavi, M., Eagle, G., & Lane, R. (2009). Different Cholinesterase Inhibitor Effects on CSF Cholinesterases in Alzheimer Patients. *Current Alzheimer Research*, *6*(1), 4–14. https://doi.org/10.2174/156720509787313961

Pettersen, E. F., Goddard, T. D., Huang, C. C., Couch, G. S., Greenblatt, D. M., Meng, E. C., & Ferrin, T. E. (2004). UCSF Chimera--A visualization system for exploratory research and analysis. *Journal of Computational Chemistry*, *25*(13), 1605–1612. https://doi.org/10.1002/jcc.20084

Rees, T., Berson, A., Sklan, E., Younkin, L., Younkin, S., Brimijoin, S., & Soreq, H. (2005). Memory Deficits Correlating with Acetylcholinesterase Splice Shift and Amyloid Burden in Doubly Transgenic Mice. *Current Alzheimer Research*, *2*(3), 291–300. https://doi.org/10.2174/1567205054367847

Rees, T., Hammond, P. I., Soreq, H., Younkin, S., & Brimijoin, S. (2003). Acetylcholinesterase promotes beta-amyloid plaques in cerebral cortex. *Neurobiology of Aging*, *24*(6), 777–787. https://doi.org/10.1016/S0197-4580(02)00230-0

Rosenberry, T. L., Brazzolotto, X., Macdonald, I. R., Wandhammer, M., Trovaslet-Leroy, M., Darvesh, S., & Nachon, F. (2017). Comparison of the Binding of Reversible Inhibitors to Human Butyrylcholinesterase and Acetylcholinesterase: A Crystallographic, Kinetic and Calorimetric Study. *ProQuest*, 2098. https://doi.org/10.3390/molecules22122098

Sáez-Valero, J., Sberna, G., McLean, C. A., & Small, D. H. (2001). Molecular Isoform Distribution and Glycosylation of Acetylcholinesterase Are Altered in Brain and Cerebrospinal Fluid of Patients with Alzheimer's Disease. *Journal of Neurochemistry*, *72*(4), 1600–1608. https://doi.org/10.1046/j.1471-4159.1999.721600.x

Silveyra, M. X., Evin, G., Montenegro, M.-F., Vidal, C. J., Martínez, S., Culvenor, J. G., & Sáez-Valero, J. (2008). Presenilin 1 Interacts with Acetylcholinesterase and Alters Its Enzymatic Activity and Glycosylation. *Molecular and Cellular Biology*, *28*(9), 2908–2919. https://doi.org/10.1128/mcb.02065-07

Silveyra, M.-X., García-Ayllón, M.-S., Serra-Basante, C., Mazzoni, V., García-Gutierrez, M.-S., Manzanares, J., Culvenor, J. G., & Sáez-Valero, J. (2012). Changes in acetylcholinesterase expression are associated with altered presenilin-1 levels. *Neurobiology of Aging*, *33*(3), 627.e27–627.e37. https://doi.org/10.1016/j.neurobiolaging.2011.04.006

Trang, A., & Khandhar, P. B. (2023, January 19). *Physiology, Acetylcholinesterase*. PubMed; StatPearls Publishing. https://www.ncbi.nlm.nih.gov/books/NBK539735/

Velan, B., Kronman, C., Ordentlich, A., Flashner, Y., Leitner, M., Cohen, S., & Shafferman, A. (1993). N-glycosylation of human acetylcholinesterase: effects on activity, stability and biosynthesis. *Biochemical Journal*, *296*(3), 649–656. https://doi.org/10.1042/bj2960649

Xu, M. L., Luk, W. K. W., Lau, K. M., Bi, C. W. C., Cheng, A. W. M., Gong, A. G. W., Lin, H., & Tsim, K. W. K. (2015). Three N-Glycosylation Sites of Human Acetylcholinesterase Shares Similar Glycan Composition. *Journal of Molecular Neuroscience*, *57*(4), 486–491. https://doi.org/10.1007/s12031-015-0629-z

Yang, Y., Arseni, D., Zhang, W., Huang, M., Lövestam, S., Schweighauser, M., Kotecha, A., Murzin, A. G., Peak-Chew, S. Y., Macdonald, J., Lavenir, I., Garringer, H. J., Gelpi, E., Newell, K. L., Kovacs, G. G., Vidal, R., Ghetti, B., Ryskeldi-Falcon, B., Scheres, S. H. W., & Goedert, M. (2022). Cryo-EM structures of amyloid-β 42 filaments from human brains. *Science (New York, N.Y.)*, *375*(6577), 167–172. https://doi.org/10.1126/science.abm7285

Zhang, Y., & Skolnick, J. (2004). Scoring function for automated assessment of protein structure template quality. *Proteins: Structure, Function, and Bioinformatics*, *57*(4), 702–710. https://doi.org/10.1002/prot.20264

Zhou, Y., Wang, S., & Zhang, Y. (2010). Catalytic Reaction Mechanism of Acetylcholinesterase Determined by Born−Oppenheimer Ab Initio QM/MM Molecular Dynamics Simulations. *The Journal of Physical Chemistry B*, *114*(26), 8817–8825. https://doi.org/10.1021/jp104258d

9 Miscellaneous

9.1 Supplementary Figures

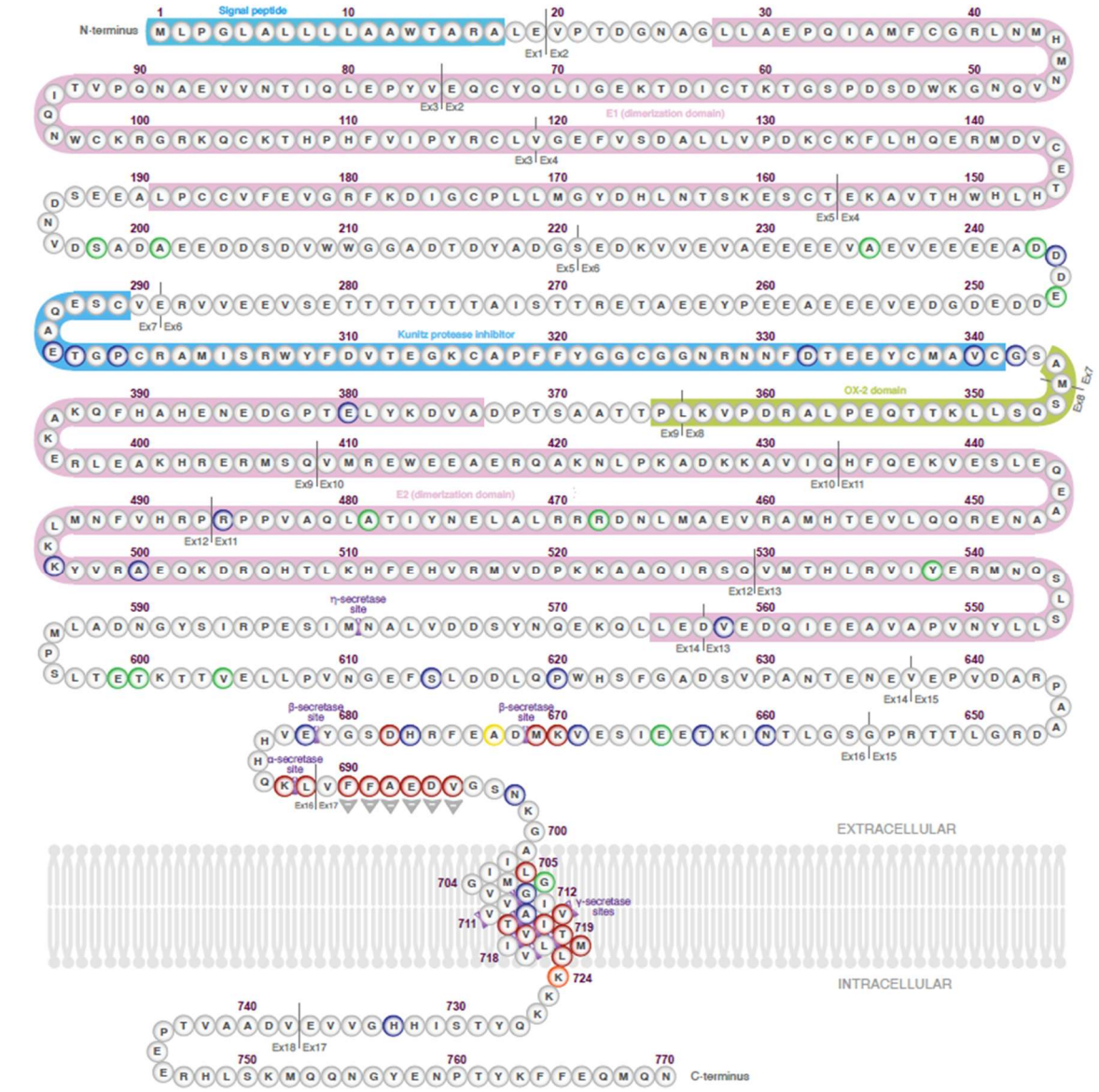

Schematic of APP Protein.
Variants are named according to amino acid positions in isoform 1 (Uniprot: P05067), which has 770 amino acids. Amino acids 290–364, not present in neuronal APP695 isoform.

- Pathogenic
- Likely Pathogenic
- Benign / Likely Benign
- Protective
- Uncertain Significance / Not Classified

(page 115) Figure S9.1 Schematic of APP Protein.
APP770 diagram displaying the amino acid chain, domains and pathogenicity of point mutations. Obtained from (September 2024): https://www.alzforum.org/mutations/app

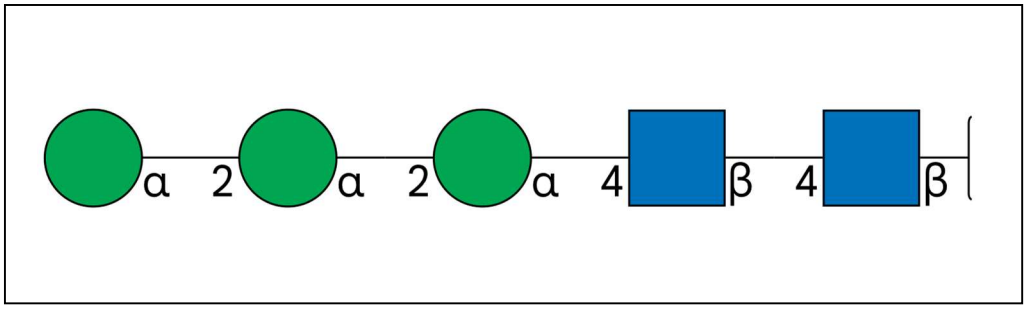

Figure S9.2 High-mannose glycan chain
Glycan chain used to glycosylate ACHE at positions 265, 350 and 464.

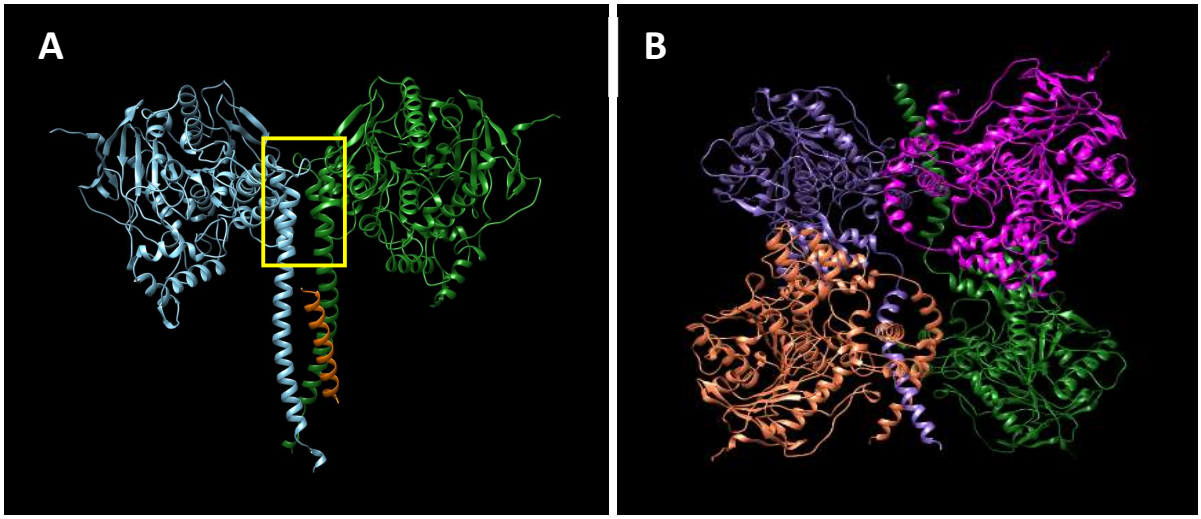

Figure S9.3 Additional predicted ACHE oligomers.
A) Predicted ACHE dimer (light blue and green) alongside APP's TMD (orange). The TMD does not appear to interact with the dimerisation zone (yellow box). B) Predicted ACHE tetramer (each unit a different colour). No clear oligomerisation zone can be found, and its structure does not resemble the tetramerisation domain experimentally obtained (**Figure 6.6D**).